The Small Unmanned Meteorological Observer (SUMO)

Characterization and test of a new measurement system for atmospheric boundary layer research

Master's thesis in meteorology

Marius Opsanger Jonassen

June 2008

UNIVERSITY OF BERGEN
GEOPHYSICAL INSTITUTE

"Þó að æði ógn og hríðir,
aldrei neinu kviða skal.
Alltaf birtir upp um síðir,
aftur kemur vor í dal."

The photo on the frontpage shows the Fun-Jet from Multiplex used as airframe for the prototype of SUMO. The photo was taken by Erik Kolstad under a scientific cruise with KV Svalbard in Storfjorden, spring 2008.

This thesis is written in LaTeX2ϵ, twosided format, 12pt text and reportstyle.

Acknowledgment

Jeg vil først og fremst rette en stor takk til min veileder Joachim Reuder som har ledet meg gjennom denne tiden som mastergradstudent. Han har alltid vært behjelpelig og tatt seg tid til å svare på spørsmål. Samtidig har han gitt meg en veldig spennende oppgave, noe jeg har satt stor pris på!

Jeg vil dernest takke de jeg har vært på feltarbeid med. Dette gjelder spesielt dere jeg deltok med på FLOHOF, sommeren 2007 og som gjorde oppholdet på Island til en opplevelse for livet. I denne sammenheng vil jeg også takke Christan Lindenberg og Martin Müller for at dere gjorde denne masteroppgaven mulig, både gjennom deres UAV-opplæring i Tyskland og senere deltakelse på Island.

En stor takk går også til Norsk Polarinstitutt som gjennom et personlig stipend (ID nr. 356) gjorde en feltkampanje på Svalbard mulig, våren 2008. I den sammenheng vil jeg også takke sikkerhetspilot Michael Kislat for hyggelig samvær under kampanjen. Videre vil jeg takke mine medstudenter på lesesalen ODD for en virkelig trivelig studenttilværelse. Sigrid Bojesen og Christopher Lee leste korrektur på oppgaven, og fortjener begge en stor takk. Sist, men ikke minst, retter jeg en takk til dere der hjemme, min kjære familie, som alltid har vært der for meg.

Marius
Bergen, 01. juni 2008

Contents

1 Introduction **5**

2 The SUMO system **8**
2.1 The airframe 9
2.2 The Paparazzi autopilot system 12
2.2.1 The airborne part 12
2.2.2 Telemetry link 16
2.2.3 The ground based part 16
2.2.4 Safety of operation 20
2.3 Meteorological instrumentation 21
2.3.1 Temperature and humidity sensors 21
2.3.2 Pressure sensor 22
2.4 Operation of SUMO for atmospheric profiling 23
2.4.1 General 23
2.4.2 Principle of operation 23

3 Time-lag correction of temperature and humidity profiles **26**
3.1 Background 26
3.1.1 The effect of time-lag on atmospheric soundings 28
3.1.2 Solutions to the problem of time-lag 30
3.2 The correction method 32
3.3 Time constant estimation 33
3.3.1 Methods 34
3.3.2 Application to the SUMO datasets 35
3.3.3 Estimated sensor time constants 36
3.4 Results of the time-lag correction 38
3.4.1 General 38
3.4.2 Statistics 40
3.5 Discussion of the time-lag correction results 44
3.5.1 Potentials for improvement of the correction scheme 45
3.6 Additional sources of errors 46

3.6.1 Solar radiation 46
3.6.2 Contamination 48

4 Intercomparison **49**
4.1 Intercomparison of SUMO and a radiosonde 49
4.1.1 Experimental setup 49
4.1.2 Results of the intercomparison 52
4.1.3 Discussion and interpretation 55
4.1.4 Summary 57
4.2 Intercomparison of SUMO, a tethersonde and the KALI UAV 58
4.2.1 Experimental setup 58
4.2.2 The platforms used for the intercomparison 60
4.2.3 Results, Hofsjökull North 65
4.2.4 Results, Hofsjökull South 71
4.2.5 Discussion and interpretation 76
4.2.6 Summary 81

5 Potential meteorological applications in the future **82**
5.1 Validation of a numerical model's boundary layer profiles 82
5.1.1 The WRF simulations 82
5.1.2 Results 83
5.1.3 18.08.2007, Ingolfsskáli 83
5.1.4 13.08.2007, Kerlingar 1 85
5.1.5 Future corresponding applications 88
5.2 Future scientific applications 88
5.2.1 Energy exchange over leads, polynyas and in the marginal ice zone 88
5.2.2 The stable (nocturnal) boundary layer (SBL) 89
5.3 Future technical improvements of the SUMO system 89

6 Summary **92**

A Meteorological data, SUMO measurement days **98**

B Tables **109**

C Miscellaneous **112**
C.1 Aeronautics 112
C.2 Statistical methods used in Chapter 3 113
C.3 Parameterization schemes used in the WRF model simulations 113

D Paper **114**

Chapter 1

Introduction

The atmospheric boundary layer (ABL) is the link between the earth's surface, where most exchange of energy, matter and momentum takes place, and the free atmosphere. This part of the atmosphere, with a typical vertical extension of several hundreds of meters to a few kilometers, can be defined as the layer affected by the surface at a time-scale of one hour or below (e.g. Stull, 1988). The corresponding surface-atmosphere exchange strongly depends on the stratification of the boundary layer. The key to the understanding of the related exchange processes is therefore the detailed information on the vertical and horizontal ABL structure, especially with respect to temperature, humidity and wind.

Many of the boundary layer processes are not resolved explicitly in numerical weather prediction and climate models and therefore need to be parameterized. With increasing computational power, the horizontal resolution of the meso-scale models is now reaching one km and even below. Critical to the validation and improvement of the corresponding parameterization schemes, is the availability of measurements with high temporal and spatial resolution. Until now, there is a lack of platforms capable of performing the required measurements. The resulting observational gap is especially evident in the Arctic, where such observations are greatly limited by the lack of infrastructure and the harsh conditions prevailing in the region (Tjernström et al., 2005). In addition, heavy cloud cover often limits the use of satellites (Inoue and Curry, 2004) and manned aircraft operations are often considered too expensive or dangerous in the area. Furthermore, the air-sea-ice interactions characterizing the Arctic region, where sea ice, leads and polynyas are central elements, play a crucial role in the global climate system (e.g. Andreas and Cash, 1999; Wadhams, 2000). Phenomena such as the stable boundary layer (SBL) often occuring there are also of importance and not yet well understood.

Hence, there is a need for a meteorological measurement platform capable of performing the desired measurements. With their unique flexibility, cost efficient performance and unequaled data coverage in space and time, unmanned aerial vehicles (UAVs) are nearly perfect for this purpose.

The history of UAVs in atmospheric research dates back to the early 70's (e.g. Konrad et al., 1970). At that time, the systems were simple remotely piloted model aircrafts equipped with primitive meteorological sensors. A similar example from more modern days is the KALI UAV, which was developed at the University of Munich, Germany in the late 90's. This system has successfully been used in several field campaigns to measure profiles of temperature and relative humidity up to 3 km above ground (e.g. Egger et al., 2002, 2005). The main shortcoming of such systems, is their lack of autonomous capabilities. They need constant guidance from a skilled pilot and are therefore greatly limited, both with respect to range and endurance as well as the number of aircrafts that can be deployed simultaneously.

During the last couple of decades, a substantial progress in the field of miniaturization of electronic components has been achieved. In addition, advanced GPS based navigation systems are now available. Together, these factors have significantly increased the range of applications for this type of platform. As a result, a large variety of UAVs in all kind of shapes, configurations and sizes have been proposed to the atmospheric science community.

In a UAV system, the aircraft size is a central measure and the systems are often classified thereafter. The largest ones are as a rule of thumb those providing highest payload capacity, longest range and thereby also most flexible in terms of potential applications. An example is the Perseus A (Langford and Emanuel, 1993), which at a unit cost of about 4$ million and a payload capacity of 100 kg, is one of the larger in its class. However, in response to the ongoing downsizing and corresponding increase in availability of cost efficient parts, the Aerosonde (Holland et al., 1992) was developed as a much smaller (15 kg, 2.9 m wingspan), significantly lower priced, but yet flexible competitor to its larger counterparts.

The Aerosonde has so far been used in a wide range of applications. *In-situ* measurements of cloud properties, remote sensing of surface temperatures and measurements of atmospheric chemical compounds are just some of its capabilities (Inoue and Curry, 2004). In addition, it has also proven its viability in provision of input data to operational analyses by the National Center for Environmental Prediction (NCEP) and the European Centre for Medium-Range Weather Forecasts (ECMWF) (Curry et al., 2004). The latter type of application is also one of the proposed missions for the corresponding Cryowing UAV, that is developed under a Norwegian initiative at the Northern Research Institute (NORUT, 2008). Additional tasks for this system have been identified in terms of satellite validation, mapping of snow cover and snow water equivalent as well as natural disaster management. Another system, which falls within the same category, is developed at the Technical University of Braunschweig. This system is dedicated to boundary layer research and has already shown promising results from a corresponding measurement campaign on the Brunt Ice Shelf in the Antarctic (Kroonenberg et al., 2007).

For some applications however, even these UAV systems are too large and with a

typical price of 50.000 Euro per unit, too expensive. Therefore, a small, cost efficient and easier to handle meteorological UAV system has been developed at the Geophysical Insititute, University of Bergen. SUMO, the Small Unmanned Meteorological Observer, has been developed as a "recoverable radiosonde" for boundary layer research. During the FLOHOF (Flow over and around Hofsjökull) field campaign on Iceland, July/August 2007 (www.flohof.uib.no), a prototype of the SUMO system successfully performed its first in-field test. Over 30 profiles of temperature and relative humidity were determined up to 3.5 km above ground. In spring 2008, SUMO performed its second field test under a scientific campaign on and around Spitsbergen. During this campaign, SUMO was operated in temperatures down to -20 ^{o}C and winds up to 15 m/s. This latter field campaign is hereafter referred to as "the Svalbard campaign". Before any scientific application of a new *in-situ* measurement system, as described here, the most important step is an assessment of the meteorological data quality. The evaluation and validation of the temperature and relative humidity measurements performed by SUMO so far, is the main topic of this thesis.

In Chapter 2, the SUMO system and its associated autopilot hardware and software is presented. The meteorological instrumentation and the principle of operation for atmospheric profiling are also shortly described. Chapter 3 is dedicated to correction for a prominent measurement error originating from slow sensor response. Also other, less quantifiable sources of error are shortly discussed. Chapter 4 reports on a validation of the SUMO data through a comparison with data from well established measurement systems. Chapter 5 is included to sketch future applications of the system. Lastly, the most important conclusions from the study of this thesis are summarized in Chapter 6.

Chapter 2

The SUMO system

UAVs represent a novel platform for meteorological measurements. For the understanding of the potential and the limitations of such systems, a relatively thorough description of the SUMO system will be presented. This chapter will guide the reader through the general setup of the SUMO system and technical details of the components and sensors in use. A short description of the Paparazzi project, the airborne and ground based parts of SUMO will be given. Finally, a description of the meteorological instrumentation is presented together with the principal of operation for atmospheric profiling. The reader should be aware that SUMO is a system under constant development, and its recent version has to be regarded a successful working prototype. However, if substantial changes are underway or planned, this will be mentioned.

SUMO has been designed as a "recoverable radiosonde" for atmospheric boundary layer research. It is based on a commercially available model aircraft construction kit, equipped with an autopilot system and meteorological sensors for the measurement of temperature, humidity and pressure.

Figure 2.1 illustrates the main components of SUMO in terms of the underlaying Paparazzi autopilot system:

- the airframe equipped with an autopilot controller board and meteorological sensors
- the ground control station (GCS)
- the telemetry link for online data transfer
- a standard remote control (RC) transmitter as safety link

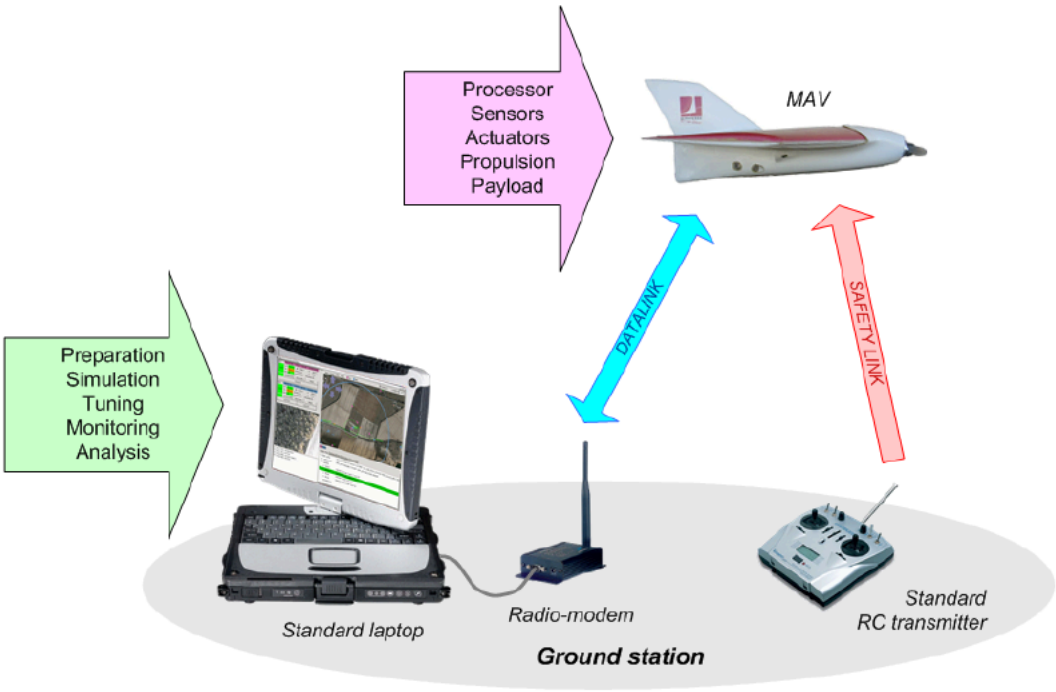

Figure 2.1: *The main parts of the SUMO system (Brisset et al., 2006)*

2.1 The airframe

For the SUMO prototype, the FunJet construction kit from Multiplex is chosen as the airframe. It is a delta-wing, pusher prop jet made of EPP (expanded polypropylen), a light-weight foam material (Multiplex, 2006). The propulsion source is a brushless electrical motor (AXI 2212/26) driving a 9"x 6" propeller, which is powered by a 3 cell Lithium Polymer (LiPo) battery package.

There are several reasons for choosing this specific aircraft as a basis for the SUMO prototype. First, the aircraft's payload area is, with its width of 4.6 cm and length of 50.8 cm, a suitable platform for the Paparazzi avionics package and light meteorological instrumentation. Second, the price is comparably low (below 100 Euro) and the availability of new aircrafts correspondingly high. Third, its flight performance makes it applicable for a wide range of boundary layer conditions. Last, but not least, the construction material is very durable and in the event of small structural damage, repair is done quickly and easily by instant glue and an activator spray. The EPP material is also proven to absorb great amounts of kinetic energy as all on-board electronic parts survived a crash where the aircraft hit the ground at over 130 km/h during FLOHOF.

Concerning vital measurements, the fully equipped FunJet has a total weight of appr.

580 g. For comparison, the propulsion system is about half of this weight. Together with a wing span of 80 cm and a fuselage length (from nose to tail) of 75 cm, these measures put the aircraft into the Micro Aerial Vehicle (MAV) category (Buschmann et al., 2004).

The aircraft is hand launched and does belly landings. It can therefore be operated virtually anywhere. This makes it in particular suitable for scientific missions in difficult topography such as narrow valley systems or densely populated areas. This flexibility was a highly appreciated property during the Svalbard campaign in spring 2008 where the system was operated from the helicopter deck of the Coast Guard vessel KV Svalbard. Compared with larger, long range UAVs such as the Aerosonde (Holland et al., 1992) and the Cryowing (NORUT, 2008) this is a considerable advantage since these require a catapult or bungee for launching and small runways (or larger, flat fields) for landings.

With regard to performance of the current FunJet setup, some of the key figures are listed in Table 2.1. With a typical operational air speed of approximately 15-20 m/s, peaking at a maximum of over 30 m/s, SUMO can operate at wind speeds up to 20 m/s. The maximum ceiling height above ground level (AGL) of about 3.5 km reached under FLOHOF is at the moment limited by the ground antenna used for online telemetry and the LiPo battery capacity. With the use of a stronger gain antenna and further developments in battery technology, flight ceilings up to at least 6 km over ground can be expected.

In this context, it should be pointed out that the battery capacity is critically dependent on temperature. During the Svalbard campaign, where temperatures down to -20 ^{o}C were frequently encountered, the endurance was reduced to around 15 min, limiting soundings to 1500 m above ground. New batteries based on lithium iron phosphate are currently under testing. These will potentially provide enhanced performance and enable operations under even lower temperatures.

Figure 2.2: *The Multiplex FunJet as seen from the helicopter deck of KV Svalbard, East of Spitsbergen. The red color is chosen for maximum visual contrast under Arctic conditions. Courtesy of Erik Kolstad.*

Table 2.1: *Technical details of the FunJet airframe used as SUMO platform.*

length	75 cm
wingspan	80 cm
weight	580 g
average air speed	12-18 m/s
maximum air speed	35 m s/s
average ascent rate	5-10 m/s
maximum ascent rate	15 m/s
maximum altitude above ground	3.5 km
engine run time	up to 30 min

2.2 The Paparazzi autopilot system

For autonomous navigation, SUMO uses the open source Paparazzi autopilot system (Brisset et al., 2006). The corresponding project was founded in 2003 by a team of enthusiastic individuals with the aim to enable inexpensive autonomous UAV operation. Since its start, the project has enjoyed constant growth and is now, in addition to its use by several individual teams around the world, officially being developed at Ecole Nationale de l'Aviation Civile (ENAC), the French National School of Civil Aviation.

From a UAV developer's point of view, the Paparazzi system represents a unique possibility of making a light, robust and fully operational system within a relatively short period of time and at a very favourable price. It can be seen as a "ready-set" where all necessary basic components except the meteorological instrumentation is already implemented. Hundreds, maybe thousands of working hours are therefore saved compared to "from scratch" meteorological UAV projects. In this context, a key factor is the project's use of *open source* technology, which implies that the cost of the system is solely associated with materials and technical support. The use of open source also ensures constant updates from the large Paparazzi user community, both with respect to technical and software related details. Additionally, changes to the system can be done without the permission of the creators.

A comprehensive documentation on the Paparazzi system, the associated hardware parts and software parts is found at http://paparazzi.enac.fr/wiki/index.php/Main Page. Unless otherwise stated, this is the source of the presented facts on the system.

2.2.1 The airborne part

As illustrated in Figure 2.3, the airborne part of the Paparazzi system features conventional model aircraft components as well as components related to autonomous navigation. Including the autopilot controller board, which until recently (March, 2008) was a "do it yourself" part, all these components are now available on a commercial basis.

Since a main goal of the Paparazzi project is to keep the total system cost low and reliability high, the amount of airborne sensors is kept at a minimum level. In addition, due to the aircraft's payload and power supply constraints, each sensor unit has to fulfil strict requirements where weight, size and power consumption are key elements.

The autopilot controller board

The autopilot controller board is the "brain" of the airborne avionics package. Its role is, in simple terms, to gather and process information from peripheral sensors giving information on position, attitude[1] and velocity of the aircraft. On this basis, it controls the motor and servos in order to make the aircraft follow a predefined flight plan.

[1] A definition of an aircraft's attitude is given in Appendix C

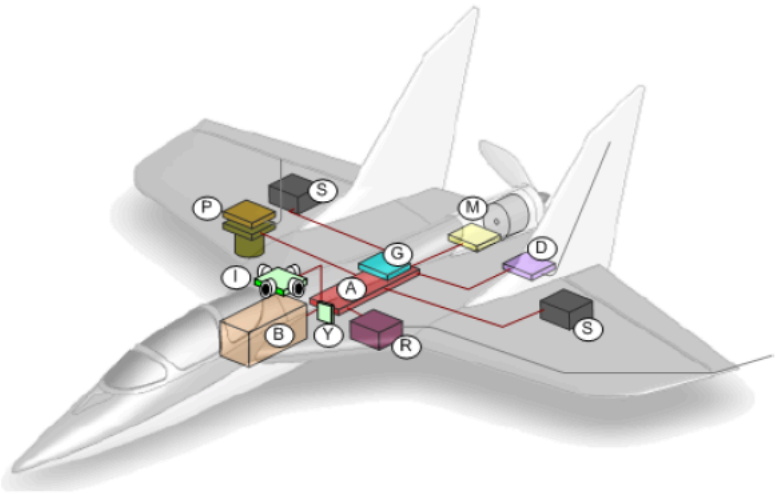

Figure 2.3: *The Paparazzi airborne system components: (A)utopilot Controller Board, (B)attery, (D)atalink Radio-Modem & Antenna, (G)PS Receiver, (I)R Sensors Board,(M)otor & Controller, (R)C Receiver & Antenna, (S)ervos, (P)ayload = e.g. Instrumentation &/or Video Transmitter. (Brisset et al., 2006)*

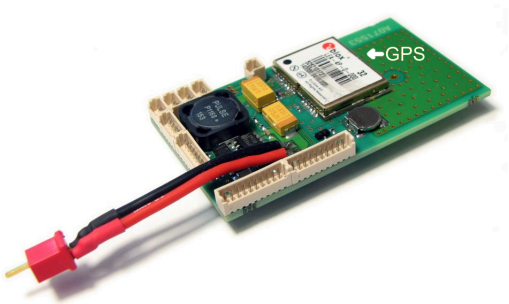

Figure 2.4: *The Tiny v1.1 with GPS from u-blox (Brisset et al., 2006)*

There are several controller boards designed under the Paparazzi project to run the associated autopilot software. The board chosen for SUMO is the Tiny v1.1 as shown in Figure 2.4. The Tiny v1.1 uses a single NXP LPC ARM7 based microcontroller, meaning that one processor is responsible for all on board calculations. In addition to control the navigational related components described above, the board also features controllers for a radio modem and additional payload, e.g. the meteorological instrumentation used for SUMO.

Uploading of software updates and flight plans is quickly and easily done through a

standard Universal Serial Bus (USB) connector situated on the controller board.

Smaller UAV aircrafts such as the FunJet set, as mentioned, high requirements for the size and weight of the on board hardware. With a weight of only 25 g and a size of 63 x 35 mm, the Tiny meets these requirements with excellence. In addition to the navigational sensors currently in use, the controller board features support for a full set of inertial and magnetic sensors (potentially used in the future).

Several peripheral components are attached to this controller board. In addition to the engine and servos, the most important of these are the attitude and positional sensing units. For retrieval of positional information, the Paparazzi setup relies on a minituarized GPS unit which is described in the following subsection.

The GPS unit

The main role of the GPS unit is to supply the autopilot with information on the aircraft's position, heading and ground speed. The positional information is given in terms of the three geodetic coordinates latitude, longitude and altitude and the velocity is obtained through doppler shift. The aircraft heading, which is related to one of the aircraft's three orientational angles (yaw), is derived from the flight trajectory as the aircraft moves.

The GPS unit chosen for the SUMO setup is a 16-channel LEA-4P from u-blox. As shown in Figure 2.4, this unit is small enough to be directly soldered on to the Tiny controller board. The unit features a 4 Hz update rate, support for active or passive antennas and classic GPS augmentations such as Differential GPS (DGPS).

The information obtained by the use of an on-board GPS is not only necessary for autonomous navigation, it also represents a major advantage of SUMO over non-GPS equipped meteorological UAVs. It associates meteorological measurements with spatial coordinates and an exact time stamp. In addition, the information on ground speed and heading allows for an indirect wind estimation method as shortly described in Section 2.4.2.

Having the aircraft's position, velocity and heading, the orientational information with respect to pitch and roll still remains. This is taken care of by a set of horizon sensing infrared thermopiles which are depictured in Figure 2.5 and presented in the following subsection.

The infrared thermopiles

The sensors themselves are mounted into the aircraft fuselage and arranged in oppositional pointing pairs, measuring the temperature contrasts of the surroundings in the aircraft's x and y directions. As illustrated in Figure 2.6, the theory is that at zero roll and pitch angle (i.e. the sensors point to the horizon), the measured temperature contrast between the pairs should be zero and at 90 degrees it should be maximum

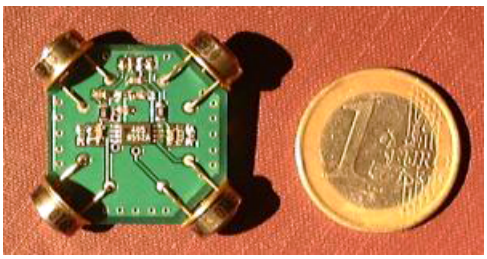

Figure 2.5: *The FMA Direct MLX90247, Infrared Thermopile.(Brisset et al., 2006)*

(pointing to the ground and the sky). An additional, z pointing pair of infrared (IR) sensors gives an update of the maximum temperature contrast (the contrast between earth and sky). They remove the need to calibrate before each flight and make it much easier to recalibrate during flight as the cloud and the surface temperatures change.

In comparison to more expensive inertial navigation systems (INS), these IR sensors represent a more robust, less computer demanding and simpler way of determining the attitude of an aircraft.

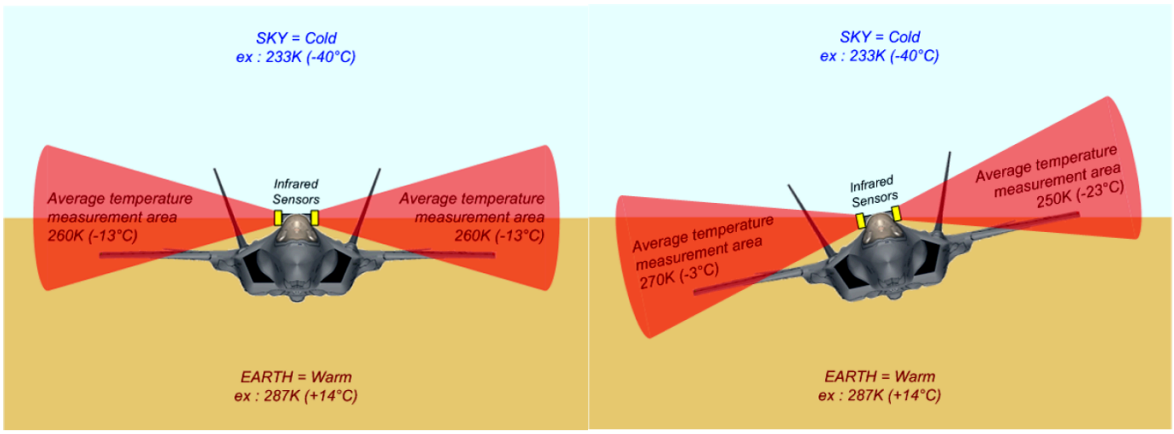

(a) Measured temperature contrast at zero roll and pitch

(b) Measured temperature at 15° roll and zero pitch

Figure 2.6: *IR sensor principle (Brisset et al., 2006)*

Since the sensors measure infrared radiation emitted in a range between 7-13.5 micrometers (corresponding to -75 to +85 ^{o}C), they are not dependent nor affected by sunlight. They can therefore operate during the day as well as the night. The IR sensors' reliability has been proven by both the GFI and the Paparazzi teams through operations during rain, at high altitudes, over open ocean, near large mountains or structures, in temperatures ranging from -20 to +48 ^{o}C and across vastly different terrain

transitions such as asphalt to water.

Despite this performance, one limitation remains, namely reduced or even no functionality under conditions with low measurable radiation temperature contrast between earth and sky. Such conditions may appear e.g. when flying in heavy rain, or in clouds or thick fog ($<$ 200 m visibility). There are currently plans of implementing advanced digital IR-sensors to the FunJet. These have the potential to decrease the critical radiation temperature contrast limit between ground and sky (currently around 10 K).

2.2.2 Telemetry link

The role of the telemetry link is to handle the communication between the aircraft and the ground station. This communication is made at 2.4 GHz, which is the common frequency for wire-less networking. With the aid of a strong gain antenna, the described link provided over 3.5 km vertical and 4.5 km horizontal range during the FLOHOF campaign.

The link ifself consists of two modems, one airborne and one at the ground. In principle, no such link is needed for autonomous UAV operation. However, a contiunous bi-directional connection has several advantages. First of all, it lets the GCS monitor the complete UAV status such as position, velocity, motor status and battery voltage. Secondly, it allows for inflight-tuning of aircraft parameters and changes of the flight plan. Atmospheric sampling can therefore be optimized, as the operator can immediately recognize interesting atmospheric structures (e.g. inversions) and modify the flight plan correspondingly.

The meteorological data sent to the ground station are stored there. For future applications however, it is also desirable to store the meteorological data on on-board. This can provide redundancy and a more secure/robust data storage in case of telemetry failure.

2.2.3 The ground based part

Ground Control Station (GCS)

The GCS functions as a control and monitoring unit for one or more UAVs. It consists of a standard laptop computer and the Paparazzi software package.

This section describes the GCS with its related components, the associated architecture of these, and the graphical user interface (GUI).

Architecture

The Paparazzi GCS software is developed to run on the Debian GNU/linux operating system (www.debian.org) and utilizes a so called distributed architecture. This flexible architecture, which is also known as a server/client structure, allows for simultaneous

(a) XBee Pro USB Stand-alone Modem

(b) XBee Pro OEM Modem

Figure 2.7: *The ground stationed (a) and airborne (b) modems.*

operation of several UAVs as illustrated in Figure 2.8. This possibility has not yet been used for meteorological SUMO missions, but will be implemented in near future.

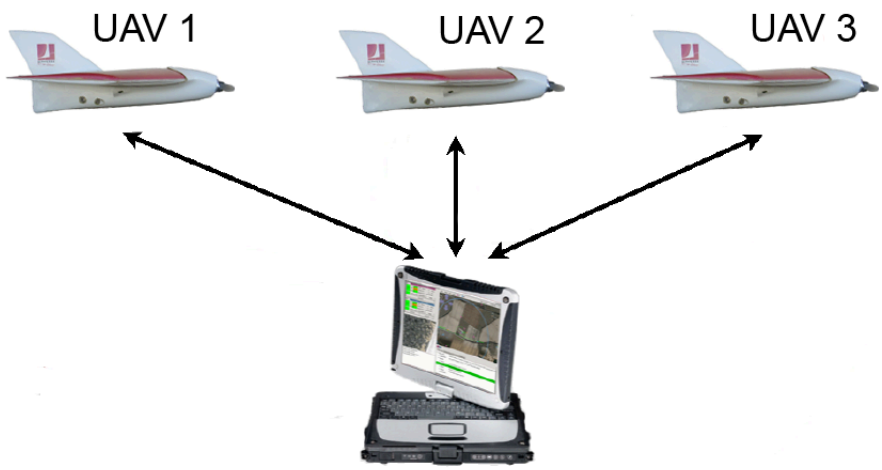

Figure 2.8: *An illustration of a simultaneous operation of several UAVs*

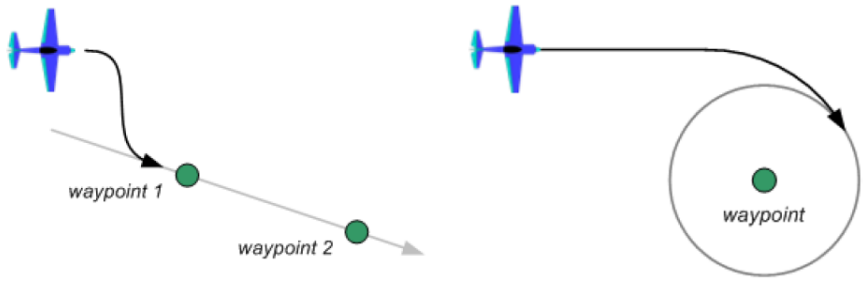

(a) Follow mode (b) Circle mode

Figure 2.9: *Example of waypoint actions in a flight plan.*

Flight plan language

The Paparazzi software contains a powerful flight plan language with possibilities to make a variety of autonomous flight missions. The associated software is easy to use and resembles to a close extent that of a GPS route planner. Similar to such planners, the navigation is done by way points. Each of these points is defined individually in 3D space and associated with tasks for the aircraft to perform. The aircraft can e.g. be programmed to follow way points in a certain order or circle around the way points themselves (Figure 2.9.). These examples are the most basic way point actions in the Paparazzi flight plan and if combined, they give rise to endless possibilities (horizontal surveys, boxes, lines etc.).

The properties (e.g. 3D position) of each way point can also be altered during flight. Whenever a new flight plan is designed, it is easily uploaded to the Tiny controller board as described above. A typical flight plan for atmospheric soundings is described in Section 2.4.2.

Graphical User Interface (GUI)

The Paparazzi GUI is specially developed for ease of use and maximum of control. It looks more like a command centre than a pilot's cockpit since the operator wants to monitor the autonomous aircraft, not to fly it.

The GUI is highly configurable, meaning that the operator decides exactly what to monitor and when to monitor it. A screen shot of a typical GUI setup is shown in Figure 2.10. This setup is divided into four main windows. In the bottom left window, information such as the aircraft's altitude, ground speed, battery capacity, flight mode and mission time are displayed. In the same window, underneath the aforementioned information, the so called hot-keys are found. These are shortcuts to important commands embedded in the flight plan such as home-mode, standby, start sounding, end

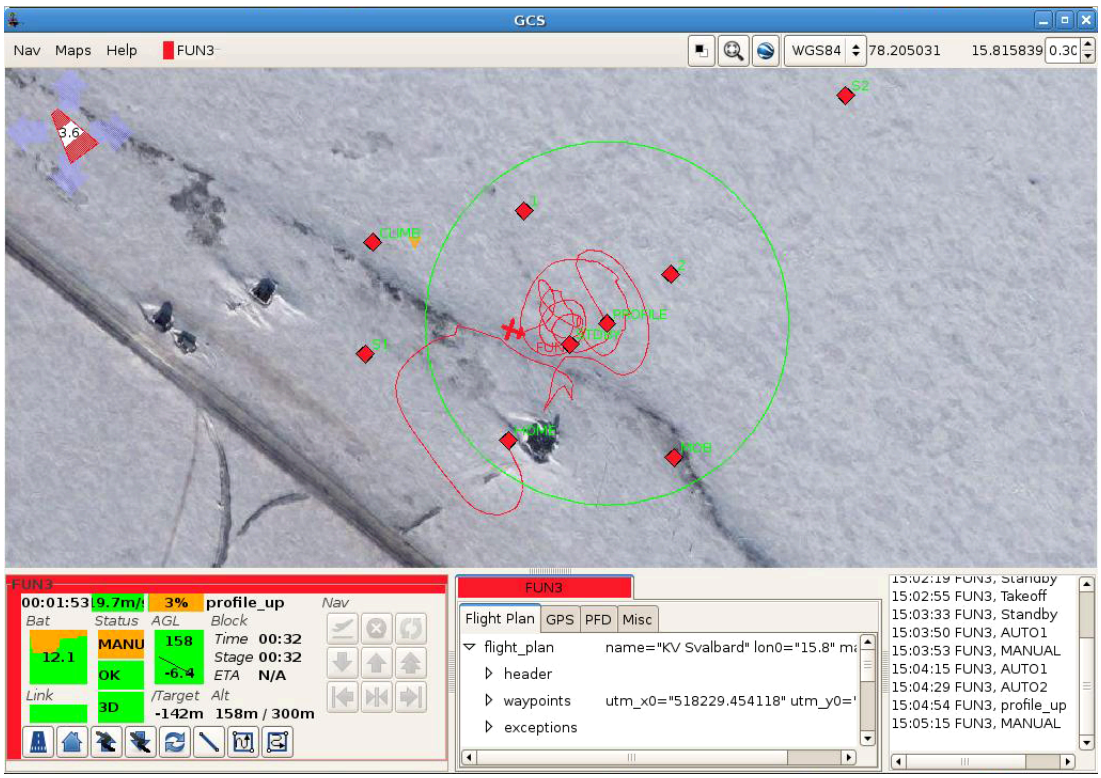

Figure 2.10: *A typical Paparazzi GUI setup. The shown example is from a mission in Adventdalen under the Svalbard campaign. The old Auroral Station is seen right below the center of the background map.*

sounding, start survey etc. In the bottom middle window, there are four main tabs that can be displayed. The tab shown in this example is the flight plan tab which basically gives the operator a list of the commands in the flight plan. These are clickable and can be used to give new commands to the aircraft. In the next tab, important GPS information such as connectivety etc. is shown. Thereafter, the tab for an artificial horizon is situated and at the end a misc. tab gives possibilites of in-flight tuning of the aircraft. The bottom right window shows a message log where every command to the aircraft is confirmed by a line of text. In addition, warnings on low battery or ground proximity for example, are issued in this window. The main window displays the aircraft's current position with the 2D track trajectory (red line), the way points (red squares) and in the background a digital map over the mission area. This map is downloaded automatically from google maps (maps.google.com). Where internet is not available, it is also possible to download and store a google map in advance, or to manually scan and calibrate ones own map. Having a map has several advantages as it gives a reference for the aircraft position with respect to the environment. Together with the live feed of meteorological

data, this also gives a possibility of identifying special conditions with respect to e.g. humidity and temperature when performing horizontal surveys over different types of underlaying surfaces. In case of loss of an aircraft, it can easily be recovered by its last sent GPS position and the map.

To further increase user friendliness, this interface includes support for a touch-screen. This was a highly appreciated option during the Svalbard campaign where low temperatures necessitated the use of thick gloves under operation. Moreover, if a camera is mounted on the aircraft (not installed on SUMO at the moment), a window showing live video feed can be added.

2.2.4 Safety of operation

Since any aircraft out of control creates a potential risk of damage to material and/or humans, safety is and has always been a first priority in the Paparazzi project. This section lists the key elements that are included in the system to enhance the safety of operation.

Flight plan simulation/replay

Prior to every flight, a new flight plan should successfully pass a simulation procedure. A specific simulation interface has been designed to uncover flaws in the flight plans. Eventual errors will thus be detected and accidents caused by e.g. erroneous placement of way points can be avoided. Every flight is replayable in the same simulation environment. This enables error tracking and trouble-shooting in case of problems or accidents.

Alarms

During flight, the status of the aircraft is under constant surveillance by the GCS. In case of too low a battery, if the aircraft is flying too far away from the predefined limit or if the aircraft is flying too close to the ground, a warning will be issued in form of an audiovisual alarm.

Automatic safety actions (fail safe)

Under special circumstances, it might be desirable to let the aircraft itself take action in order to avoid, or at least minimize, the impact of an eventual accident. Some examples of such situations are:

- If the aircraft is displaced too far from its origin or in case of data link loss:

  The aircraft returns to, and circles around a predefined way point, typically back to where it was launched.

- If the GPS temporarily fails:

  The aircraft performs a predefined action, e.g. circling with constant throttle.

- If the aircraft is not able to return (e.g. due to continuous loss of GPS signal):

  The engine is stopped, and the aircraft starts a slow, spiraling descent to avoid further displacement away from the operator and to minimize impact when hitting the ground.

In addition, if the aircraft is within visual range, the safety pilot can at any time switch the aircraft from autonomous to manual mode and guide the aircraft back.

2.3 Meteorological instrumentation

An important task under the development of SUMO has been the selection of appropriate meteorological instrumentation for measuring temperature, relative humidity and pressure. During this selection process, many requirements had to be taken into consideration. First, the sensors should have a short enough response time appropriate for in-flight measurements. Second, the vital measures such as weight, size, power consumption and data exchange interface could not exceed the limits and specifications set by the aircraft and the airborne hardware. Last, but not least, the price should be within reasonable limits to make an eventual loss of instrumentation bearable for the SUMO budget. The sensors that are found to fulfill these strict requirements and that are used for SUMO, are presented in the following section.

2.3.1 Temperature and humidity sensors

So far, two combined temperature and humidity sensors have been adapted to the SUMO system. The first one is the DigiPicco™Basic I2C, from Innovative Sensor Technology (IST). It combines a capacitive relative humidity sensor (P14 SMD) with a PT 1000 temperature element. The sensor is mounted inside a thin tube, covered in front by a protective fibre-layer and placed underneath the wing of the FunJet. This position was chosen in order to give sufficient ventilation and to protect the sensor from being affected by solar radiation. In addition to providing extra shielding from radiation, the tube protects the sensors from objects in the air such as insects and from being damaged under rough landings.

As it turned out, this sensor suffered from a relative long response time. It was therefore chosen to implement an additional, smaller and faster temperature and humidity sensor for the Svalbard campaign. The SHT75, manufactured by Sensirion, was mounted underneath the other wing of the FunJet. Technical details of the sensors are listed in Table 2.2.

Table 2.2: *Specifications of the temperature and humidity sensors used on SUMO. *The response times are "ideal" manufacturer values and not specifically given for atmospheric measurements.*

sensor	DigiPicco		SHT	
parameter	RH	T	RH	T
resolution	0.003 %	0.005 K	0.03 %	0.01 K
range	0-100 %	-40 - 50 ^{o}C	0-100 %	-40 - 124 ^{o}C
abs. accuracy	$<$ 3 %	±0.5 K	±1.8 %	±0.5 K
rel. accuracy	N/A	N/A	±0.1 %	±0.1 K
response time*	5 s	N/A	6 s	5 s

The analysis of the performance of both sensors with respect to atmospheric measurements is a central task of this thesis and will be a main topic in both Chapter 3 and Chapter 4.

2.3.2 Pressure sensor

Two different pressure sensors are tested for SUMO. The first one, used during FLOHOF, showed out to give erroneous data. Therefore, it was substituted by a SCP1000 Absolute Pressure Sensor from VTI Technologies for the Svalbard campaign. This minituarized sensor, which has the size of only 6.1 · 1.7 mm (diameter · height), is not dependent on direct measurements of the atmospheric flow as the other SUMO sensors. Consequently, it is mounted inside the FunJet fuselage where it is directly coupled with the autopilot controller board. Its measurement range covers 300 to 1200 hPa with a resolution of 0.015 hPa and an absolute pressure accuracy of 1.5 hPa in the range 600-1200 hPa. The relative pressure accuracy relevant for atmospheric profiling is 0.5 hPa. In addition to its pressure sensing element, it also comprises an on-board temperature sensor providing information on the temperature inside the aircraft fuselage. This information is valuable for e.g. the estimation of the aircraft battery capacity (which decreases with lower temperatures), especially when profiling the atmosphere under cold conditions such as in the Arctic.

2.4 Operation of SUMO for atmospheric profiling

2.4.1 General

During operation, the Paparazzi based SUMO system requires two people. One GCS operator for preparing and controlling the autonomous missions and one safety pilot. During FLOHOF, the operation of SUMO was taken care of by group members of Paparazzi (Figure 2.11). During the Svalbard campaign, GCS operations were for the first time performed exclusively by scientists.

Figure 2.11: *The Paparazzi team members operating SUMO during the FLOHOF campaign. Christian Lindenberg (left) acted as safety pilot while Martin Müller (right) operated the GCS.*

2.4.2 Principle of operation

Although the Paparazzi system is capable of doing autonomous take-offs and landings, at least under calm conditions and in flat, open terrain, the standard way of operating the SUMO system so far has been to do both take-offs and landings manually by the safety pilot. The following favourable routine of operation has been developed after numerous meteorological soundings.

After a manual take-off, the aircraft is sent into autonomous standby mode, i.e, it circles at a predefined altitude of typically 150 m. This allows the meteorological sensors

to adjust to the environmental conditions. At the same time, the aircraft is checked for proper functionality. Thereafter, the aircraft is ready for atmospheric profiling in autonomous mode. It is sent to a user defined, in-flight variable, altitude. Pitch and throttle are held constant during this stage of the flight. When the desired altitude is reached, the engine is shut down and the pitch is set to a constant, negative value to begin the spiraling descent. When the aircraft has again reached a predefined safety altitude (typically 150 m), it is automatically switched back to the standby mode, and the safety pilot can guide the aircraft home.

The resulting, typical helical flight pattern for boundary layer profiling, is depictured in Figure 2.12. Green and black dots are used for the ascent and descent parts of the flight track and the x and y values indicate the relative horizontal distance of SUMO to the launch site. In this example, a maximum altitude of 2567 m was reached after 8 minutes. The overall flight duration was 16 minutes.

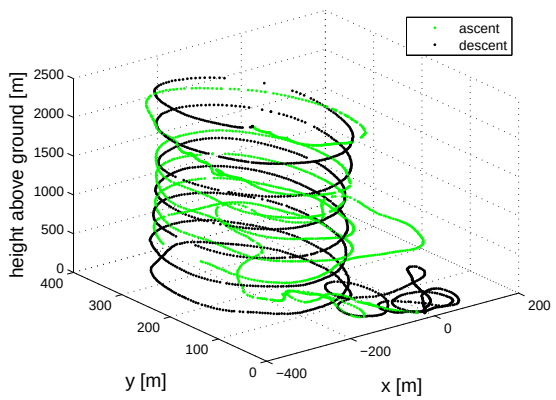

Figure 2.12: *An example of a typical flight pattern from the FLOHOF campaign on Iceland. The ascent starts at 17:56 UTC on 18.08.2007.*

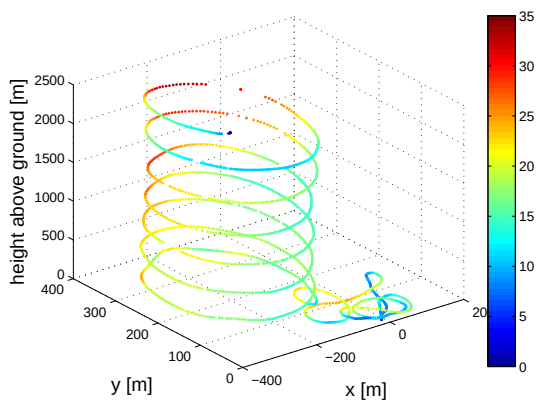

Figure 2.13: *As in Figure 2.12, but only descent. The colors indicate the ground speed of the aircraft given in m/s.*

Estimation of wind speed and direction

Even though the analysis of wind data from SUMO is beyond the scope of this thesis, the ability of determinating wind speed and direction is an important feature of the system and is therefore shortly explained. The employed principle is best illustrated by examining the flight information given by Figure 2.13. This figure shows the descent part of the flight pattern just described, where the ground speed measured by GPS is indicated by the colors on the trajectory. The constant setting of throttle and pitch during ascent and descent results in a nearly constant speed of the aircraft with respect

to the surrounding air (true air speed). By assuming a constant true air speed, it is possible to derive wind information from the ground speed data. Where the ground speed is highest, the aircraft is flying *downwind* and where the ground speed is lowest, *upwind*. By using this difference together with information on the associated positioning, profiles of both wind speed and wind direction can be estimated. Intercomparisons with radiosonde data from the Svalbard campaign and PiBal ascents from FLOHOF, have shown that the SUMO wind data have an accuracy close to these well established measurement techniques (Reuder et al., 2008).

Chapter 3

Time-lag correction of temperature and humidity profiles

A small, airborne platform for meteorological measurements represents many technical challenges. This is especially evident for the choice of instrumentation, where a compromise between weight, size and technical specifications has to be made. Consequently, the meteorolological measurements are potentially subjects to several sensor related sources of error. Among the identified error sources, a relative slow sensor response is found to be the most prominent in the SUMO data. Due to its deterministic character, the associated time-lag *error can to a large extent be corrected for. A numerical correction scheme based on digital filters is suggested for this purpose. In this chapter, the method is presented and thereafter applied to the SUMO datasets from FLOHOF and Svalbard. Central results of the correction are presented and discussed. In addition, non-systematic errors are also shortly discussed.*

3.1 Background

Time-lag errors in atmospheric measurements are well known e.g. from radiosonde profiles and were already described by Badgley (1957). The nature of this error is related to an inherent property of most temperature and humidity sensors and can be explained as follows.

In general, temperature and humidity sensors need a certain time in order to reach equilibrium with their ambient environment. Consequently, their output signal appears as lagged in time when a sudden parameter change is measured. The corresponding response time is characterized by the sensor time constant τ_s, typically defined as the time it takes the sensor to reach 63.2% of an instantaneous change in the measured parameter (Miloshevich et al., 2004, hereafter "M04"). As illustrated in Figure 3.1, the sensor response has an exponential character. A sensor following this ideal curve, will

be able to reproduce 90 % of the parameter change after $2.3 \cdot \tau_s$ or 99 % after $4.6 \cdot \tau_s$.

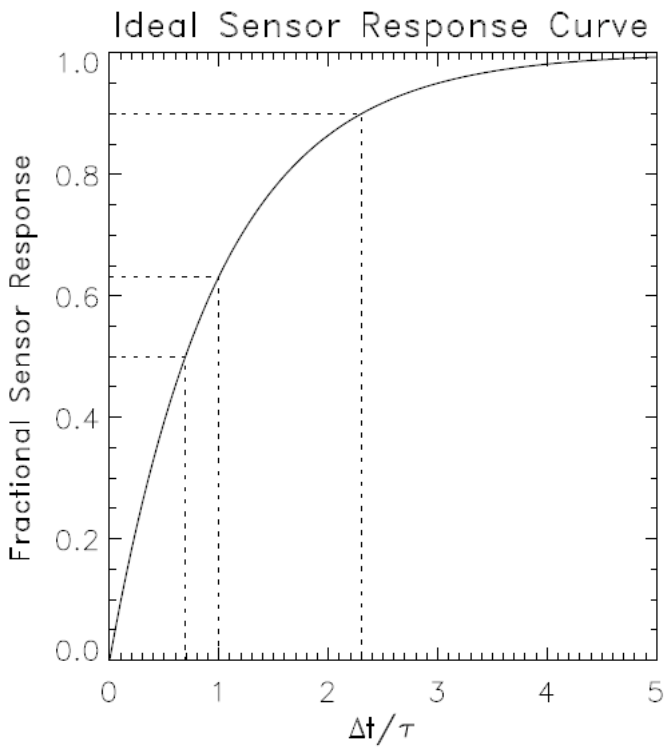

Figure 3.1: *Fractional response of an ideal sensor as a function of time in units of the time constant τ_s, given by 1-exp(-dt/τ_s) (M04)*

Slow sensor response introduces a measurement error often referred to as a "time-lag error". For atmospheric soundings, this error is described by Connell and Miller (1995, hereafter "C95") to be a function of the sensor time constant, the ascent/descent rate of the instrument platform and the vertical gradient of the measured parameter (i.e. temperature or humidity). The magnitude of the time-lag error can thus be described by the following equation:

$$x - y = -\tau_s \cdot V \cdot \frac{dy}{dz} \tag{3.1}$$

Where x is the *true ambient* parameter value, y the *measured* parameter value, τ_s the sensor time constant, V the ascent/descent rate and $\frac{dy}{dz}$ is the vertical parameter gradient.

The sensor time constant is not the same for all atmospheric conditions. For temperature sensors, the sensor time constant is found (e.g. C95) to be primarily dependent on the atmospheric pressure (air density) and the ventilation of the sensor. For relative

humidity sensors, the sensor time constant is additionally a function of absolute temperature and water vapor content. A decrease in temperature and atmospheric pressure leads to increased sensor response times, and so does a lack of ventilation and low water vapor content.

3.1.1 The effect of time-lag on atmospheric soundings

Errors induced by time-lag are commonly observed as systematic deviations between corresponding ascent and descent profiles as e.g. obtained by co-located radio- and dropsonde measurements (Skony et al., 1994; Wang, 2004). When the instrumentation of these platforms is the same, these measurements are analog to the ascent and descent profiles constituting each SUMO sounding.

An example from the SUMO data illustrating the time-lag error can be seen in Figure 3.2, where a set of profiles of temperature and relative humidity from the FLOHOF campaign is shown.

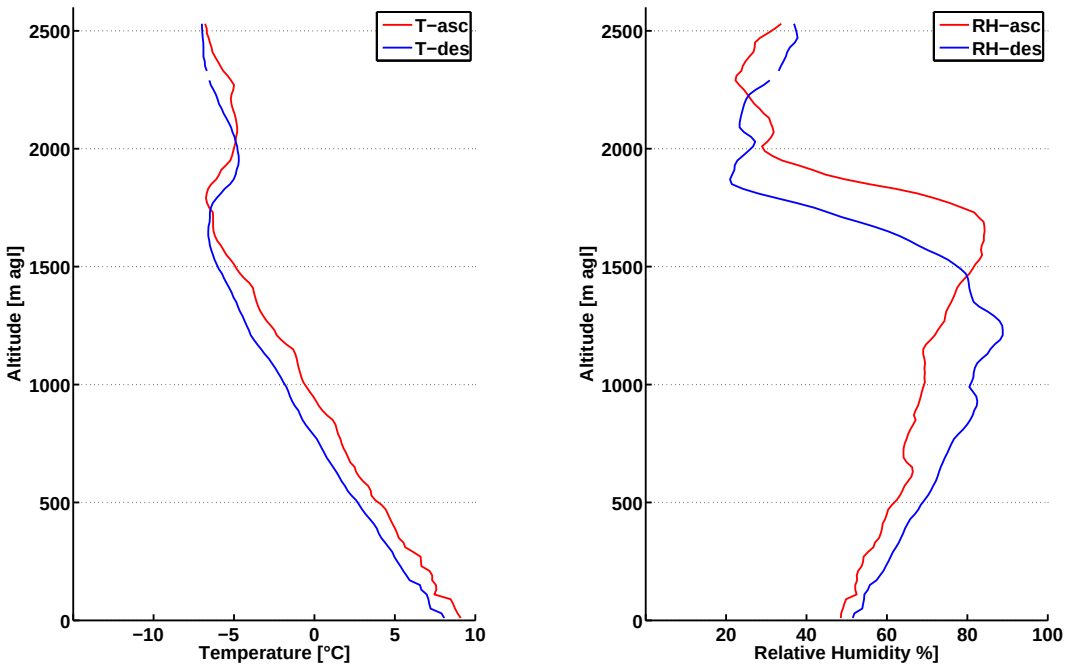

(a) (b)

Figure 3.2: *Ascent and descent profiles of temperature (a) and relative humidity (b). The measurements are performed by SUMO North of Hofsjökull during the FLOHOF campaign on Iceland, 18.08.2007 17:56 UTC.*

For the temperature profiles, the effect of the time-lag can be seen as a general warm bias in ascent data and a cold bias in descent data. In the profiles of relative humidity,

the effect is a corresponding dry bias in ascent data and humid bias in descent data. Thus, the time-lag can also be depictured as a sensor "memory". The measured value of a parameter at a certain height, is "remembered" by the sensor when it comes to the next height of measurement. I.e., the time-lag error has in general a different sign for the ascent and descent profiles. Some authors, e.g. Leiterer et al. (2004), term the time-lag effect "hysteresis" as it induces a certain height displacement between corresponding ascent and descent profiles.

The magnitude of the time-lag error and its importance to interpretation of boundary layer profiles

Because of the characteristics of the time-lag, a statistical quantity such as the mean absolute difference (defined in Appendix C) between corresponding ascent and descent profiles can be used to give a measure of the associated error. For the SUMO profiles in Figure 3.2, this difference has a magnitude of 1 K and 11 % for temperature and relative humidity, respectively. These values are not the same as would be obtained by a direct application of Equation 3.1, but can rather be seen as the mean total time-lag error for both the ascent and descent profiles. Moreover, the corresponding height shift between the presented ascent and descent profiles is in average approximately 150 m and 200 m for both temperature and relative humidity. This height shift is especially evident around the inversion at 1600-2000 m. Similar height shifts are found around inversions in the raw data of almost all profiles measured by SUMO. It is also around these atmospheric features the largest time-lag related errors are found. When considering the relationship expressed by Equation 3.1, this finding is not surprising since inversions are often characterized by steep parameter gradients.

Since inversions often indicate the height of the ABL, the time-lag error may lead to corresponding misinterpretations (e.g. Skony et al., 1994). In the literature, significant time-lag induced temperature and humidity errors are also found in radiosonde profiles of the Arctic (C95) and Antarctic (Mahesh et al., 1997) ABL where strong surface inversions are frequent throughout the year. In these cases, downward longwave radiation fluxes and calculations of vertically integrated water vapor content (VIWVC) were performed, and found to be markedly influenced by time-lag.

Referring to Equation 3.1, it is evident that also high ascent/descent rates can have a potentially significant time-lag error enhancing effect. In contrast to radiosondes, that have relative stable ascent rates of about 3-5 m/s (Mahesh et al., 1997), the SUMO aircraft is typically operated at higher and more variable ascent/descent rates in the range of 5-10 m/s. This factor further complicates the time-lag error in the SUMO profiles and also introduces differing errors between ascent and descent profiles as the ascent rate typically differs from the descent rate.

The importance of accurate radiosonde measurements, and the analog to this study.

Radiosondes have many important roles in modern atmospheric science. Some of these are also intended future applications of SUMO such as evaluation of numerical weather and climate models and validation of remote sensing (C95).

These important roles call for an action in order to minimize observed systematic errors such as those induced by time-lag. Several papers are written on the topic (e.g. M04; Miloshevich et al., 2006; Leiterer et al., 2004) and the main solutions for the problem of time-lag are reported as improvement of the sensors themselves and numerical correction of the measured profiles. The investigated solutions for the SUMO data are presented in the following subsection.

3.1.2 Solutions to the problem of time-lag

Improved sensors

An intuitive way of overcoming the problem of slow sensors is to improve or change the sensors themselves. As sensor technology moves further, faster sensors become available. Such improvements have been especially evident within instrumentation for radiosondes the last 10-20 years as described by e.g. M04. Weight/size reduction and a corresponding decrease in heat capacity of the sensing element was found to be a key to faster sensor response /a shorter time constant.

For the SUMO setup, a second, smaller and lighter sensor (SHT) was found and installed for the Svalbard campaign. As the results of this chapter will show, this sensor did certainly respond faster than the old one (DigiPicco) used under FLOHOF. However, this sensor also has a response time induced error of a significant magnitude.

Change in flight pattern

A second way of overcoming the mentioned problem was found through the autonomous capabilities of the SUMO aircraft.

The principle can be explained as follows. The flight pattern for the sounding is divided into e.g. 200 m intervals at which the aircraft is sent into stationary circles (vertical speed appr. zero). By this procedure, the sensors are given enough time to adjust to their environment. This technique has shown promising results as it successfully gathers the ascent and descent profiles at the levels of the stationary circles. However, a major draw back is a reduction of the maximum flight ceiling caused by energy related issues (i.e. battery capacity). Moreover, the improvement gained by this technique does only yield the height of the stationary circles. The remaining parts of the profiles are therefore still affected by time-lag.

Numerical correction

As the two mentioned methods have not proven satisfactory results, a third, numerical method is found to be the better solution to correct the SUMO data for sensor time-lag. Such a correction is possible because of the error's systematic character and the fact that the ambient information is contained in the sensor output signal, but appears as smoothed in time. Most corresponding work has been performed in connection to radiosonde soundings and several correction schemes have been developed (e.g. M04; Wang et al., 2002; Miloshevich et al., 2001; Mahesh et al., 1997) and in some cases also used operationally (e.g. Leiterer et al., 2004).

A corresponding numerical correction scheme based on digital filters is applied to the SUMO data. The method was originally developed by Jan Schween and the presented theory is based on personal communication with him. Similar to the method of M04, it is a numerical inversion algorithm that calculates the "true" ambient temperature and humidity profiles based on an estimation of the sensor time constant. The estimation of the sensor time constants of the SUMO instrumentation is thus a central part of this chapter. Since the methods used for this estimation are partly based on the correction method itself, the correction method is presented first and the estimation of the time constants thereafter.

Data base

A total of 20 SUMO soundings from FLOHOF and 15 from the Svalbard campaign are used in this study. The response time of the temperature and humidity sensors typically differs. Also, different sensor types do in general not have the same response time.

Moreover, the sensor time constants are known to have certain dependencies as described above (e.g. on temperature). The SUMO data base is therefore divided into 6 separate datasets in the study of this chapter; two main sets for each campaign (temperature, humidity) and one subset for each sensor used under the Svalbard campaign. The profiles from each campaign included in the data sets are marked correspondingly in Table B.1 and B.2 (Appendix B).

3.2 The correction method

Background theory

The basic assumption for the correction method is that the change in the sensor output signal with time is proportional to the difference between the instantanous *measured* parameter value (y) and the *true ambient* parameter value (x) as stated by Equation (3.2).

$$\frac{dy}{dt} = -\frac{1}{\tau_s}(x - y) \tag{3.2}$$

Where τ_s is the sensor time constant. This equation basically expresses the same relationship as Equation 3.1, but time is used as abscissa instead of height ($dt = dz/V$).

For a step change in temperature, as illustrated in Figure 3.1 (x remains unchanged after the first value is set), Equation 3.2 can be shown to yield:

$$y(t) = x + (y_0 - x) \cdot exp(-t/\tau_s) \tag{3.3}$$

Where y_0 and y(t) refers to the initial and final sensor output of the step change, respectively.

The correction equation

In the natural atmospheric environment however, there are no ideal parameter step changes. Thus, for the correction of the SUMO soundings, the general solution of Equation (3.2) is needed. This is a first order differential equation and the solution can be obtained through a Laplace transformation which gives the following low pass filter.

$$y(t) = \frac{1}{\tau_s} \int_{-\infty}^{t} x(s) \cdot exp\left(\frac{s-t}{\tau_s}\right) ds \tag{3.4}$$

The utilized correction method is based on Equation (3.4), which is approximated by a digital recursive filter as stated by the following equation:

$$y(t) \simeq q_s \cdot y(t - \Delta t) + (1 - q_s) \cdot x(t) \tag{3.5}$$
$$\text{where: } q_s = exp(-\Delta t/\tau_s)$$

If solved for the ambient value x(t), Equation (3.5) gives the final reconstruction equation:

$$x(t) = \frac{y(t) - q_s \cdot y(t - \Delta t)}{1 - q_s} \tag{3.6}$$

Which is a digital recursive filter that reconstructs the ambient signal with only two subsequent measured values y(t) and y(t-Δt).

Ideally, Equation (3.6) should provide with everything needed for a reconstruction of the sensor signal. However, since this reconstruction involves a time derivation of the sensor output signal ($\frac{dy}{dt}$), eventual abrupt (unphysical) changes will be enhanced. Such changes can e.g. be introduced by sensor noise. Therefore, as also pointed out by M04, the original datasets need to be smoothed before applying the correction equation. This smoothing can be done by various techniques. The technique utilized here is to apply Equation (3.5) to the original dataset, which functions as a recursive smoothing filter with a time constant τ_f:

$$xf(t) = qf \cdot xf(t - \Delta t) + (1 - qf) \cdot xs(t) \qquad (3.7)$$
$$\text{where: } qf = exp(-\Delta t/\tau_f)$$

Where xs is the original dataset, xf the new, smoothed/filtered dataset and Δt the datasampling interval.

Application to data

After the dataset has been smoothed, it is ready for correction by Equation (3.6), where the correction time constant (τ_x) is equal to:

$$\tau_x^2 = 1/2 \cdot (a + \sqrt{a^2 + 4 * b})$$
$$\text{where: } a = \tau_s^2 + \tau_f^2 \text{ and } b = \tau_s^2 \cdot \tau_f^2$$

3.3 Time constant estimation

Critical to the success of the presented correction method, is an accurate determination of the sensor time constant, τ_s. For sensors used in operational atmospheric measurements such as radiosonde sensors, this information is derived through laboratory experiments (M04). In such experiments, the sensors are tested for several step changes (as described by Equation 3.3) that are made under conditions representative for the true atmosphere.

For the SUMO sensors however, that are not specifically made for atmospheric measurements, only a limited set of manufacturer data exist. However, alternate methods for the time constant estimation are available. Those investigated in this study, are based on the difference between the ascent and descent profile pairs consituting each SUMO sounding. The basic assumption in this respect is that appropriate estimates of

the sensor time constants should make the correction scheme match these profile pairs as closely as possible.

3.3.1 Methods

A total of three methods are investigated for the estimation of the SUMO sensor time constants. Two of these are inspired by Leiterer et al. (2004) and Mahesh et al. (1997) while the third is a manual version of the latter one.

Method 1 (Leiterer et al., 2004)

The effect of the time-lag is, as stated earlier, seen to introduce a certain height shift between the pairs of ascent and descent profiles. If a vertical layer between these profiles is found where both the parameter gradients and the vertical platform speeds are approximately constant, Equation (3.1) can be shown to yield:

$$\Delta H_{asc-des} = \tau_s \cdot (V_{asc} - V_{des}) \tag{3.8}$$

Where $\Delta H_{asc-des}$ is the height of the vertical layer and V_{asc}, V_{des} are the vertical ascent and descent speeds within this layer. Equation (3.8) is then trivially solved for the time constant, τ_s. This method can be said to form a basis for an empirical, rough estimate of the time constant and will in this study serve as a "reality check" of the other methods.

The next two methods are basically variations over the same principle and can both be termed "inverse methods".

Method 2

The correction scheme is run (by a Matlab script) for different combinations of the τ_s and τ_f time constants. The combination giving the lowest visual difference between the ascent and descent profiles are the proper one and are used for correcting the profiles.

This is a rather unsophisticated method that gives in every case a subjective result. It is also fairly time consuming when applied to numerous profiles. The method inspired by Mahesh et al. (1997) is based on the same principle, but is done by a numerical routine which minimizes a statistical quantity to determine the best constant combination. The method is applied in the following manner.

Method 3 (Mahesh et al., 1997)

A numerical routine (in this study a Matlab script) is run for the correction scheme to correct the profiles with all different combinations of τ_s and τ_f in a certain range and with a certain step in between. The constants giving the lowest root mean square

difference (RMSD, defined in Appendix C) between the corrected pairs of ascent and descent profiles is the appropriate combination.

In terms of effectiveness, this is the favourable method as it can be applied to numerous profiles in a relatively short period of time. It also provides a more objective result than method 1 and 2 since it is based on a statistical quantity. A potential drawback of this method however, is that a single statistical quantity does not in itself reveal eventual weaknesses of the correction scheme (e.g. in connection to special atmospheric features). This fact is addressed by the chosen method approach as described in the next section.

3.3.2 Application to the SUMO datasets

In order to make the corresponding ascent/descent profiles directly comparable, they were averaged in 20 m vertical intervals. This was necessery with respect to the RMSD calculations of method 3. These 20 m are then the practical vertical resolution of the datasets.

In addition, the lower 200 meters of every profile were excluded from the calculations in order to avoid the influence of an observed ground heating effect on this part of the ascent profiles. The associated, positive temperature and dry humidity bias is an extreme form for time-lag and is also described for radiosondes by several papers (Mahesh et al., 1997; Schwartz and Doswell, 1991; Hudson et al., 2004). In contrast to the time-lag effect in the remaining profile parts, the effect on these lower levels is of a more irregular character and can therefore not properly be corrected by the numerical correction scheme. This extreme time-lag occurs when the sensors are either heated by the sun on the ground before ascent or suffer from residual heat when the instruments are brought from e.g. a warm cabin to the colder environment outside. Both these effects are evident in the SUMO data where the latter one is especially evident in the Svalbard dataset. As the instruments are well ventilated during ascent, this effect disappears rather fast, where 200 m is found empirically to be a sufficient height limit. In addition, most profiles were run manually by the safety pilot below 200 m. The flight pattern in manual mode is in general unfavourable for atmospheric measurements as it often introduces irregularities in the profiles. This is another reason to avoid basing the time constant estimation on profile parts that are below this height limit. Examples showing the biases introduced by both the ground heating and the manual flight mode are given in Chapter 4 (Figure 4.3a).

Method

With background in the comments to the described time constant estimation methods, a combined method approach was developed. The corresponding procedure can be summarized as follows.

1. Run method 3 with all possible combinations of the time constants (τ_s and τ_f) in the range of 0 to 40 seconds, and a spacing of 1 second. If reasonable constants are derived, use them for correction and move to point 2. If not, stop here and use method 2. Thereafter, if possible, jump to point 3
2. Adjust the outcome with method 2
3. Use method 1 as a reality check

For simplicity, the following assumptions were made. A fixed value for each time constant was chosen, i.e. the constants were assumed to be the same within each dataset and for each sensor. No dependency factor of temperature, atmospheric pressure or ventilation was applied.

The potential implications of the described assumptions are discussed in the later discussion section. Moreover, an underestimation is favoured over an overestimation to avoid implausible variations in the corrected data by over correction. A similar precaution is also made by M04 and Leiterer et al. (2004).

3.3.3 Estimated sensor time constants

The results of the time constant estimation is summarized in Table 3.1 where estimated time constants for the SUMO temperature and relative humidity sensors are presented. Both the mean and standard deviation of the time constant estimations are given for the results of method 1 and 3. The time constants derived by method 3 are those giving the lowest mean RMS temperature/relative humidity difference between the corrected ascent and descent profile pairs of each dataset.

FLOHOF dataset

Method 3 proved successful for the temperature data from FLOHOF. Only a slight adjustment of the smoothing filter time constant (τ_f) from 6 to 5 s for temperature was made after the correction method was investigated by method 2. This adjustment was done in order to preserve more details in the original profiles. In addition, τ_s was rounded down to 12 s to avoid over correction of some profiles. The "reality check" of method 1 suggested a mean time constant of 9.4 seconds, which is somewhat lower than for the two other methods but still a close match conserning the ideal assumptions it is based on.

For relative humidity, method 3 produced somewhat questionable results that needed significant adjustments after the visual inspection by method 2. The amount of smoothing (τ_f) was lowered from 7.7 s to 1 s in order to preserve more details in the profiles. Furthermore, τ_s was reduced from 12.4 s to 11 s to avoid over correction of some profiles.

Table 3.1: *Time constants for the SUMO temperature and humidity sensors. Constants used for correction are marked as red boldface numbers.*

	Temperature				**Relative humidity**			
	FLOHOF			SVALBARD	FLOHOF			SVALBARD
method	1	2	3	2	1	2	3	2
DigiPicco								
$\tau_s(s)$	9.4 (3)	**12**	12.8 (3.2)	**12**	N/A	**11**	12.4 (7.7)	**30**
$\tau_f(s)$	N/A	**5**	6 (3.6)	**5**	N/A	**1**	7.7 (4.2)	**1**
SHT								
$\tau_s(s)$				**5**				**18**
$\tau_f(s)$				**2**				**1**

Svalbard datasets

In contrast to the FLOHOF datasets, method 3 failed to give reasonable results when applied to all Svalbard datasets. The reason for this failure is believed to be related to the relative finer-scale structures of the associated profiles. In addition, these structures made it impossible to get a real estimate through method 1 and therefore only method 2 could be applied to these datasets. The most notable result when comparing the corresponding time constant values from FLOHOF and Svalbard is the increase in response time for the DigiPicco relative humidity sensor. From 11 s for FLOHOF, this constant is increased by almost a factor of 3 (30 s) when compared to the Svalbard dataset. The differing ground temperatures might be the reason for this difference as distinctly higher ground temperatures were recorded under FLOHOF (typically +10 ^{o}C) than on Svalbard (typically -15 ^{o}C). The time constant of capacitive humidity sensors, as used for SUMO, is known to feature a certain dependency on temperature (e.g. M04; C95; Wang et al., 2002). Moreover, the new sensor (SHT) shows a significant improvement over the older one (DigiPicco) for the sensor response time.

3.4 Results of the time-lag correction

3.4.1 General

The main impressions of the time-lag correction are found to be well illustrated by Figure 3.3, showing the corrected and uncorrected FLOHOF profiles as presented in Section 3.1.1.

The numerical correction scheme's effectiveness can be seen by both its ability to bring the profiles closer together and by positioning the inversion heights for relative humidity and temperature to the same level. Secondly, the scheme can also be seen to reveal more vertical details as it e.g. sharpens the parameter gradients. Another important impact is seen as a corresponding narrowing in the thickness of the inversions.

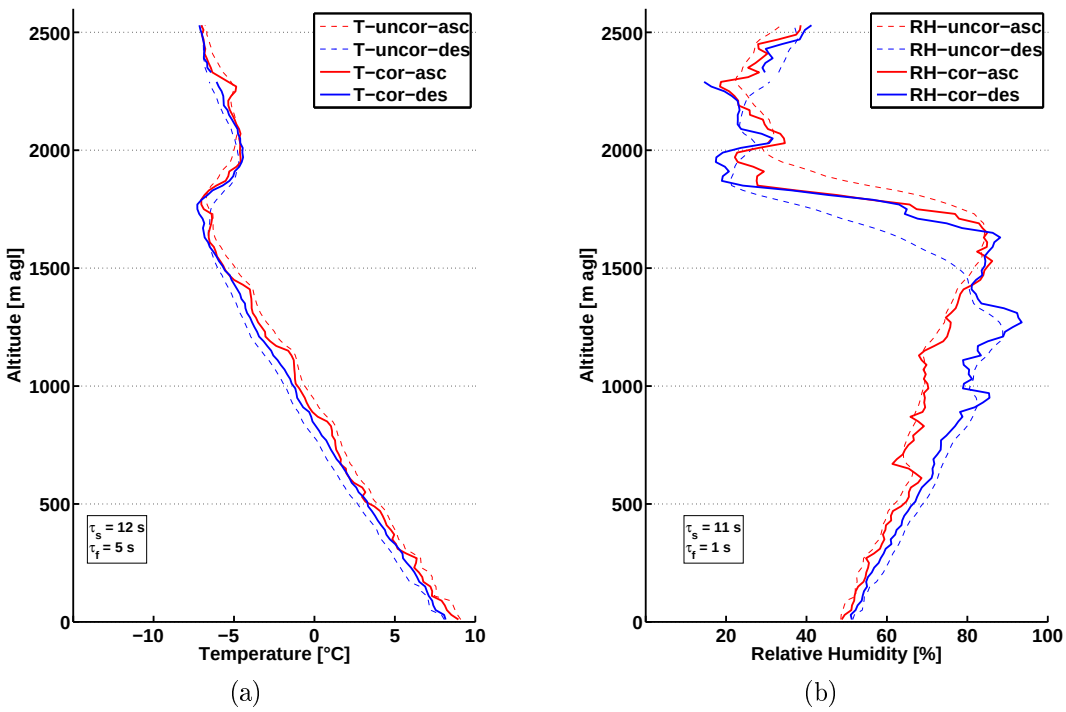

Figure 3.3: *Uncorrected and corrected profiles of temperature (a) and relative humidity (b). The measurements are performed North of Hofsjökull during the FLOHOF campaign on Iceland, 18.08.2007 17:56 UTC.*

The latter mentioned feature can be connected to the tendency of the sensor time-lag to smooth smaller scale vertical structures. This smoothing is especially evident for the Svalbard relative humidity profiles where relatively slow sensor responses (long/high time constants) come along with the fine scale atmospheric moisture structures in the marginal ice zone. An example from this dataset is given in Figure 3.4, showing uncor-

rected and corrected relative humidity profiles measured by SUMO using both the old (DigiPicco) and the new (SHT) sensor, East of Spitsbergen, 28.02.2008.

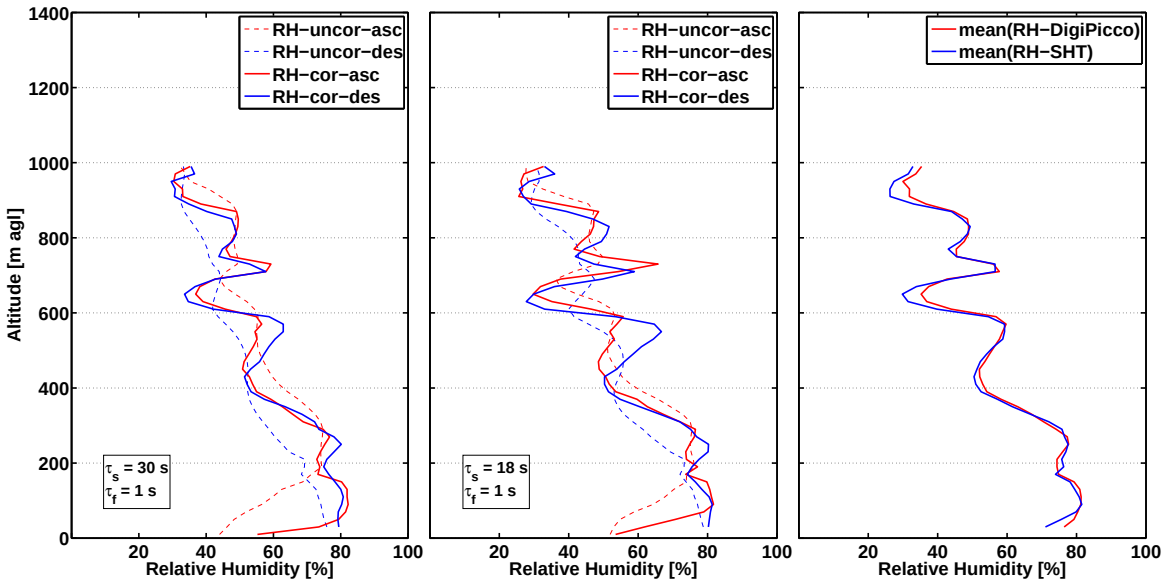

(a) Old sensor (DigiPicco) (b) New sensor (SHT) (c) mean(asc,des)

Figure 3.4: *Uncorrected and corrected profiles of relative humidity measured by SUMO from the helicopter deck of the Norwegian Coast Guard vessel KV Svalbard at 76.74 °N and 18.25 °E in the marginal ice zone on 28.02.2008 15:11 UTC.*

Even more clearly than in Figure 3.3, the correction scheme reconstructs the vertical structures and brings fine scale patterns in the profiles to the same level. In addition, the faster response time of the SHT sensor can be seen by its ability to resolve more of the vertical structure in the uncorrected profiles than the DigiPicco sensor. For the corrected profiles however, both sensors seem to have a similar degree of improvement. This impression is further confirmed by the close agreement seen in Figure 3.3 (c), where the mean of each sensor's ascent and descent data are plotted. This close agreement indicates the general reliability of the used correction method.

Residual discrepancies

Even though the overall results of the correction seem to be quite successful, the correction scheme does not completely gather all parts of the ascent/descent profiles. These residual discrepancies are especially evident in the relative humidity profiles (e.g. Figure 3.3 (b)).

Another intriguing feature is a wave-like, vertically repeating, warm bias in the temperature ascent data of Figure 3.3 (a). Similar biases are also found in other SUMO

profiles from FLOHOF and Svalbard. Neither of these are corrected properly for by the correction scheme and in some cases, they are even enhanced. Further investigations, presented in detail in Section 3.6.1, indicate that this feature is related to solar irradiance.

3.4.2 Statistics

In order to get a more objective measure of the correction results, the differences for each ascent and descent pairs were calculated at every 20 m interval and thereafter averaged over each dataset. For this purpose, the mean bias difference, as defined in Appendix C, is used. The absolute values in Kelvin are used for temperature. The associated plots are shown in Figure 3.5 and 3.6. All profiles did not reach the same height above ground. Thus, large deviations between single profile pairs have potentially larger impacts on the statistics on higher altitude levels than at lower levels. Therefore, the number of profiles reaching a certain height interval is indicated in the mentioned figures (every 500 m for FLOHOF and 200 m for Svalbard). The residual differences after correction, are then used to give an estimate of the quality of the described correction.

Temperature

From the plotted statistics, the most evident improvement by the time-lag correction is found in the temperature profiles from the FLOHOF campaign. The improvement varies with height, but only one altitude level shows an enhancement in difference after correction. This is found around 2700 m and constitutes a negative difference of around -0.3 K. Another interesting feature is the positive peak of 0.5 K around 2000 m, where there is almost no improvement for the corrected profiles.

For the Svalbard profiles, the improvements by the correction are generally less evident (lower magnitude than for FLOHOF). The improvement is moderate for the DigiPicco sensor and only marginal for the SHT sensor. Notable in this context is the smoother curve for the uncorrected versus the corrected differences in the DigiPicco sensor data. This finding reflects the correction's sharpening of gradients connected to smaller scale features that dominate the Svalbard profiles. For the SHT sensor, these fine scale features are seen for the entire vertical columns of both the uncorrected and the corrected profiles, indicating the faster response time of this sensor.

Relative humidity

For relative humidity, the differences between the ascent and descent profiles follow the trend of the example profiles from the previous section. The differences are not only more evident than for temperature, they also show larger variations with height. Looking at the FLOHOF data (Figure 3.6a), the described difference has a distinct

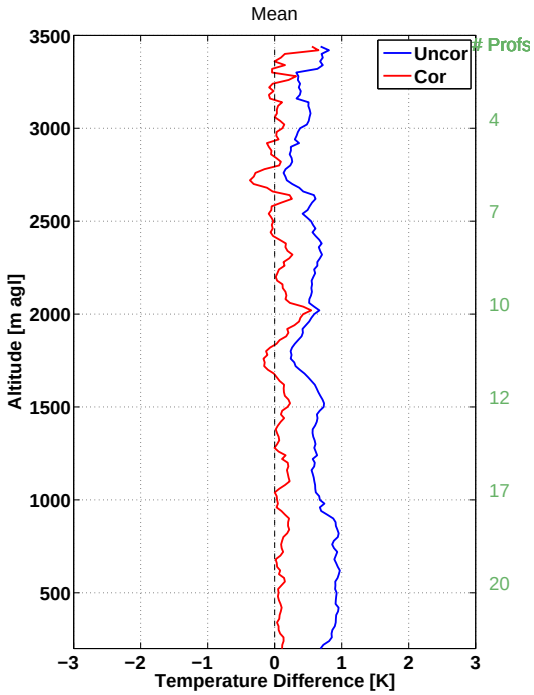

(a) FLOHOF, DigiPicco

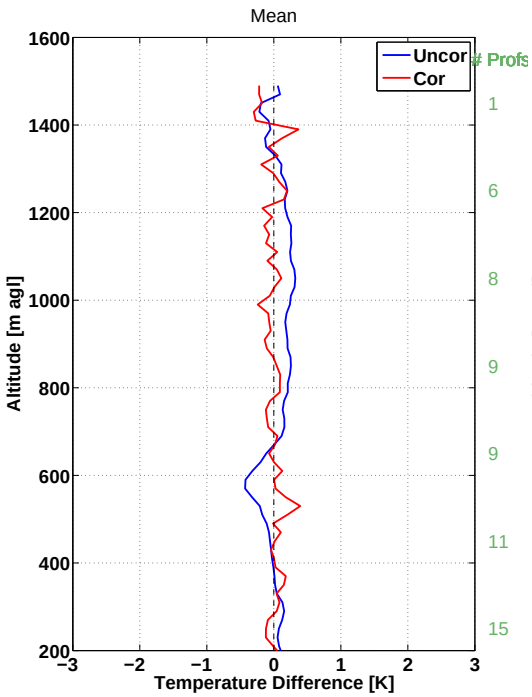

(b) Svalbard, DigiPicco

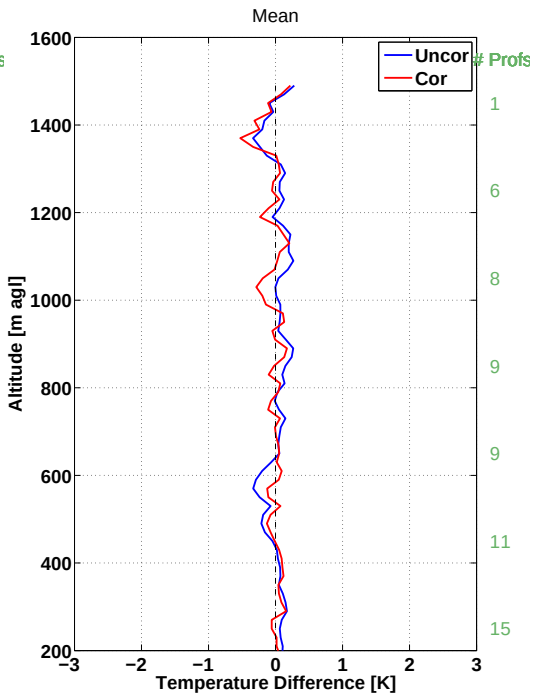

(c) Svalbard, SHT

Figure 3.5: *Mean temperature differences between pairs of ascent and descent profiles of each dataset as a function of height (20 m intervals).*

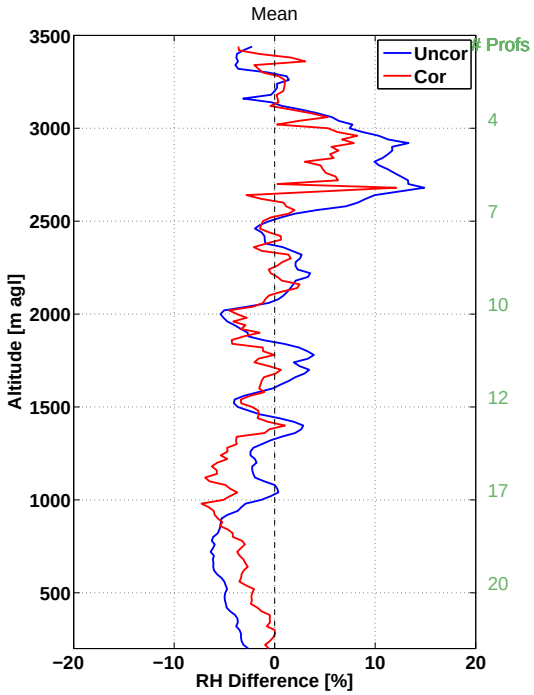

(a) FLOHOF, DigiPicco

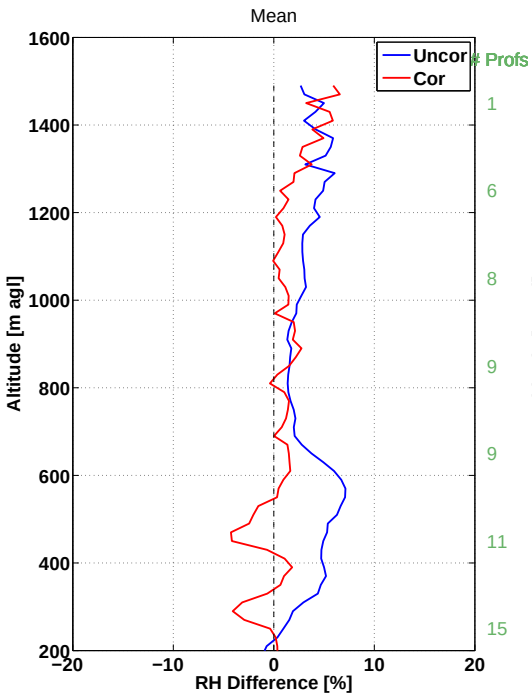

(b) Svalbard, DigiPicco

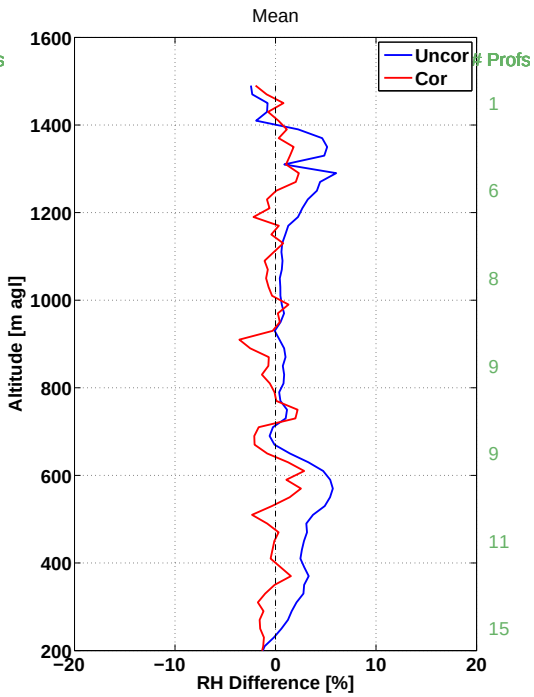

(c) Svalbard, SHT

Figure 3.6: *As in Figure 3.5, but for relative humidity.*

peak of close to 15 % at around 2500-3000 m. In contrast to the values of the lower heights, this higher level peak has a positive sign. For the Svalbard DigiPicco dataset, such positive differences dominate the entire vertical column of mean relative humidity differences. A closer inspection of these profiles reveals a trend where the difference for certain height intervals is increasingly positive with height (e.g. 200-600 m). Though, it should be mentioned that this trend is largely reduced by the correction scheme.

In order to get an overview of the total impact of the correction, the mean absolute differences were calculated for and averaged over each corrected and uncorrected dataset.

Table 3.2: *Mean absolute difference (ascent-descent) averaged for each corrected and uncorrected dataset in addition to the corresponding % reduction in this difference done by the correction scheme. Standard deviations are given in parantheses.*

dataset	**FLOHOF**		**SVALBARD**			
sensor	**DigiPicco**		**DigiPicco**		**SHT**	
param.	T(K)	RH(%)	T(K)	RH(%)	T(K)	RH(%)
uncor.	0.72 (0.17)	6.21 (2.65)	0.26 (0.10)	4.87 (2.84)	0.21 (0.08)	3.79 (2.26)
cor.	0.27 (0.09)	4.38 (2.00)	0.24 (0.09)	2.90 (2.42)	0.25 (0.08)	3.04 (1.16)
% red.	62.5	29	8	40	-19	20

Also by this quantity, the largest reduction in difference between ascent and descent data is found for the FLOHOF temperature profiles. The correction reduces in this case the difference by 62.5 %, from 0.72 to 0.26 K with standard deviations of 0.17 and 0.09, respectively. It is also interesting to find that the difference is increased for the temperature profiles measured by the SHT sensor on Svalbard. However, the corresponding mean absolute differences of 0.21 and 0.25 K are relatively small and in the order of the sensor accuracy.

3.5 Discussion of the time-lag correction results

In general, the presented time-lag correction is seen to largely reduce the differences between ascent and descent data. Inversions and smaller scale features are brought into far better consistency. However, even after correction, there still exist discrepancies. These are mainly found for relative humidity, but are also to some extent present in the temperature profiles.

The understanding of the residual discrepancies requires a closer look into each corrected profile and the general trends in these. Such an investigation revealed that the largest discrepancies coincide with inversions that are not brought totally into consistency by the correction scheme. For temperature, the remaining height shift of inversions explain virtually all of the residual discrepancies. The most extreme examples coincide with the observed positive peak at 2000 m for the FLOHOF data in Figure 3.5. For relative humidity, the peak at 2500-3000 m also coincides with the height of inversions. However, other parts of the relative humidity profiles also show relatively large deviations (e.g. Figure 3.3). Possible reasons for the residual discrepancies are discussed in the following subsections.

Sensor response time dependency

As stated in Section 3.3.2, an assumption of no sensor response time dependency is made and fixed values of the sensor time constants are therefore used for the correction. Deviations from this assumption may e.g. involve the different dependency factors listed in Section 3.1, i.e. ventilation and atmospheric pressure for temperature in addition to temperature and water vapor content, for relative humidity.

Of these variables, the least predictable is ventilation. However, this should be sufficiently ensured since SUMO has a rather high air speed and the assumption of this being fairly constant has shown to be valid for the wind estimation algorithm used for SUMO. Still, there are no real in-situ airflow measurements made for the sensor positions on the aircraft. Lack of ventilation under e.g. sudden aircraft attitude changing maneuvers (roll/pitch/yaw-ing), can therefore not be totally ruled out.

The SUMO measurements are mainly confined to the lower troposphere, and therefore also effects induced by atmospheric pressure should be of a minimum influence. There are no signs of a systematic increase in the time-lag bias with height for temperature as there should be if this dependency was significant.

For the temperature dependency of the relative humidity measurements however, the results are somewhat contradictory. On one hand, the lapse rate of several of the FLOHOF profiles implies that measurements are performed in down to -15 C^o, which is a typical temperature for the measurements on Svalbard. If there really was a significant temperature dependency, this should be indicated by systematic larger ascent/descent differences with height. As mentioned above, increasing differences are found with height

in some of the datasets, but this trend is largely reduced by the correction. On the other hand, significant longer response times are calculated for the Svalbard dataset indicating a time constant dependency on temperature.

In order to further investigate the temperature dependency, tests with a temperature dependent time constant for relative humidity were performed. Similar to methods used by Miloshevich et al. (2004) and C95, an exponential dependency was chosen according to:

$$\tau_s \cdot exp(T \cdot C) \tag{3.9}$$

Where T is temperature and C is the dependency constant. The correction scheme did however not improve the correction results for any dependency constant C.

Natural variations

Although the corresponding ascent/descent profiles are taken within least possible temporal and spatial limits, natural variations will always cause a certain variability. Such variations can be expected to depend on the meteorological situation and the parameter of interest. In general, humidity is known to show higher variability than e.g. temperature (C95). Humidity profiles during the whole FLOHOF campaign, taken by the remotely controlled aircraft KALI and by a tethersonde, have documented a large spatial and temporal variability of relative humidity in the measurement region. In addition, measurements taken by both SUMO and radiosonde soundings during the Svalbard campaign have shown similar variabilities. Enhanced variability will also be encountered in case of highly dynamic boundary layers due to thermally or mechanically induced turbulence or waves (Stull, 1988). Natural variations are also likely to contribute to the observed residual height shift between inversions in ascent/descent data. Corresponding height shifts are found and will be further discussed in Chapter 4.

The described natural variatons can not be corrected for, and should of course not, by a numerical correction scheme. Nevertheless, they still appear as "error sources" in the presented correction statistics.

3.5.1 Potentials for improvement of the correction scheme

As described in Section 3.4.1, some SUMO profiles show repeating warm biases. These are in general not corrected for by the utilized scheme and for some profiles, even enhanced. Also, some of the profiles of relative humidity have signs of over correction of certain sharp profile gradients. This latter observation is especially evident in some of the FLOHOF profiles.

To avoid enhancing such "noisy" features is a challenging task as two contradictory wishes meet as one corrects profiles. On one side, it is desirable to enhance/reconstruct smoothed features of the original profile such as inversions. On the other side, features

causing abrupt changes in the measured parameter such as sensor noise or the described repeating warm biases are desirable to be removed/smoothed out. Thus, when reconstructing a profile both dominated by smoothing due to sensor's inertia and biases as those described, a compromise has to be made when choosing the smoothing time constant τ_f.

A not yet included, but possible solution to this problem is described in connection to a similar correction method by M04. The key principle applied in that study is to make the smoothing filter set constraints to the gradients in the corrected dataset and thereby provide an extra smoothing of abrupt (unphysical) changes. Implementation of such a principle could be desirable to include in future work for the described correction scheme.

3.6 Additional sources of errors

As mentioned in the introduction of this chapter, measurements made by small, airborne platforms are potentially exposed to several sources of sensor related errors. After time-lag, the sources suggested to have the largest impact on the SUMO data are those of solar radiation and sensor contamination. These sources of error are shortly described in the following subsections.

3.6.1 Solar radiation

A further investigation of the repeating warm biases of 0.5-1 ^{o}C revealed a relative strong correlation between the aircraft's heading at the corresponding heights of the biases and the solar azimuth angle.

Radiosondes serve as a good analog since the measurements of these platforms also are found to be affected by this source of error. The error induced by solar radiation is reported by e.g. Luers (1997) and C95 to be mainly dependent on the orientation of the sensor relative to the sun, which coincides with the finding in this study. Both here and by the above mentioned authors, the solar elevation angle is observed to play a lesser role.

In the SUMO profiles, the described error occurs at an offset angle of approximately -40° ($\pm$ 5 ^{o}) for the heading of the aircraft with respect to the sun's azimuth. As the aircraft has a clock wise helical flight pattern, this implies that the sun must hit the aircraft at the right side of its fuselage when the error occurs (the sun heats the sensing temperature element and/or the protective tube). This coincides with the placement of the DigiPicco temperature sensor, which is situated underneath the leading edge of the aircraft's right wing. Furthermore, the effect is seen to have a significantly lesser impact on the descent data than the ascent data. Differing pitch angle between the descent (negative pitch) and ascent (positive pitch) profiling might be a reason.

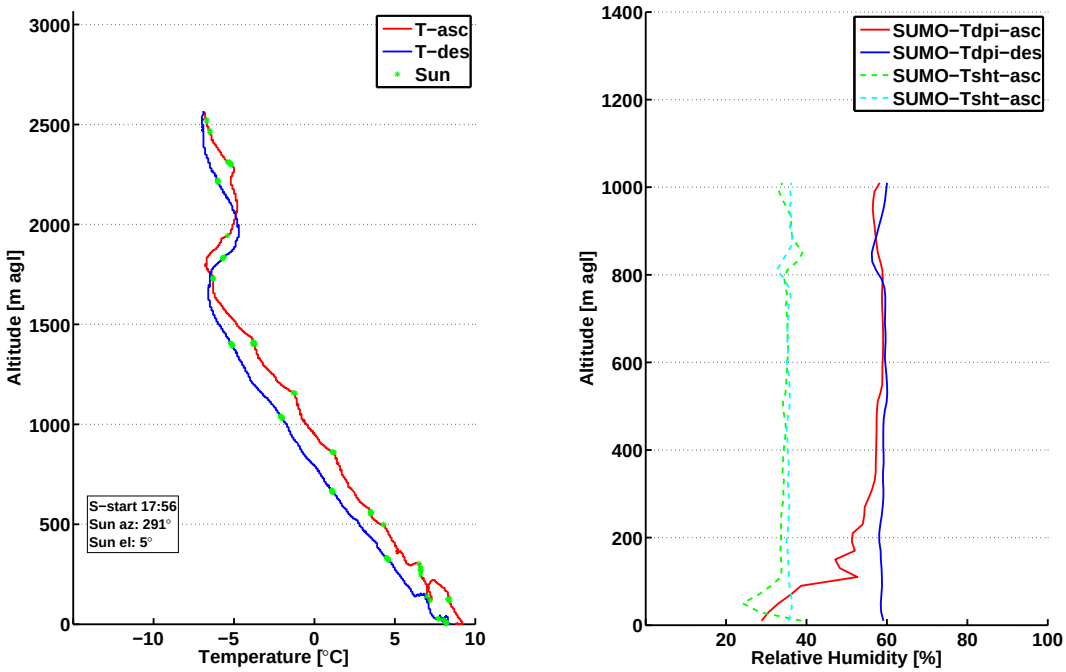

(a) Solar radiation (b) Contamination

Figure 3.7: *Example profiles from the FLOHOF and Svalbard campaigns showing (a) the effect of solar radiation and (b) the effect of contamination, respectively. The green dots mark the height at which the aircraft's heading is at a -40° offset angle with respect to the sun's azimuth, as described in the text.*

Figure 3.7 (a) illustrates the correlation between the solar azimuth angle and the described, repeating warm bias. This is the same SUMO profile as shown in Figure 3.2.

For radiosondes, errors induced by solar radiation are to a large extent corrected for by numerical methods (Luers, 1997). However, before this can be done for the SUMO data, a further investigation is necessary.

Therefore, a more active approach is desirable at first. A better placement of the sensor with respect to shielding from direct solar radiation will be sought. In addition, also the protective sensor housing must be replaced or modified to further reduce the impact of solar radiation. Before implementation of such improvements, the temperature profiles measured during descent should be favoured under sunny conditions.

3.6.2 Contamination

Some of the profiles of relative humidity from the Svalbard campaign show a sudden dry-bias in the relative humidity measured by the new SHT sensor compared to the old DigiPicco sensor. The transition happened from one day to the other. This error is suspected to be caused by sensor contamination. An example profile showing the described effect is given in Figure 3.7 (b).

Contamination is a known error inducing factor in e.g. radiosonde relative humidity data (e.g. M04; Wang et al., 2002; Guichard et al., 2000) and arises when non-water molecules stick to the sensing element of the relative humidity sensor. These molecules take the place of water molecules, and the result is a dry bias. For radiosondes, this error has mainly been attributed to plastic in the package material which new sondes come in. For the SHT sensor however, the situation is quite different. As mentioned previously, the SHT sensor was mounted without a protective tube. It is therefore not unlikely that the sensor has been touched by the operator's fingers at take-off and thereby contaminated the sensor. This source of contamination is pointed out by e.g. Soddell et al. (2004). For future applications, greater care must therefore be taken when operating the aircraft and also a better protection for the sensor itself has to be considered. A smaller and improved version of the protective tube used for the old sensor could be a solution.

Chapter 4

Intercomparison

SUMO is a new meteorological platform with instrumentation not before tested for airborne measurements. A validation of the measurement system is therefore crucial prior to any scientific application. In-field operations where SUMO is compared to well established sounding systems represent an appropriate method for this purpose. The corresponding study of this chapter was made possible through a simultaneous operation of SUMO and a radiosonde during the Svalbard campaign, spring 2008. In addition, a several day long co-located operation of SUMO, and two established profiling systems in the form of a tethersonde and the remotely controlled KALI UAV was conducted under the FLOHOF campaign on Iceland, August 2007. The analysis of the measurements from these two comparison datasets is the topic of this chapter. Special weight will be put on SUMO's ability to resolve phenomena typical for the atmospheric boundary layer such as inversions. The radiosonde measurements provide the better reference data in this context, and the results from the Svalbard campaign are therefore presented first.

4.1 Intercomparison of SUMO and a radiosonde

4.1.1 Experimental setup

The measurements of this intercomparison were performed in the marginal ice zone during a scientific cruise to Storfjorden with the Norwegian Coast Guard vessel KV Svalbard, late February 2008. During this cruise, several radiosondes were launched in connection to the International IPY[1]-THORPEX[2] campaign. One of these radiosondes was timed with the operation of SUMO and thereby formed the basis for this intercomparison.

[1] www.ipy.org
[2] www.wmo.ch/pages/prog/arep/thorpex/

As indicated in Figure 4.1, the geographical position of the measurements was situated in the vicinity of East-Spitsbergen. A more detailed information on both time and location of the described measurements is given in Table 4.1.

Table 4.1: *Details on the compared SUMO and radiosonde profiles. The end time of the radiosonde profile indicates its time to reach the maximum height of the SUMO profile.*

			SUMO		radiosonde	
coordinates ^{o}N	^{o}E	date (local time)	start time (UTC)	end time (UTC)	start time (UTC)	end time (UTC)
76.74	18.25	28.02.2008	15:11	15:22	15:15	15:19

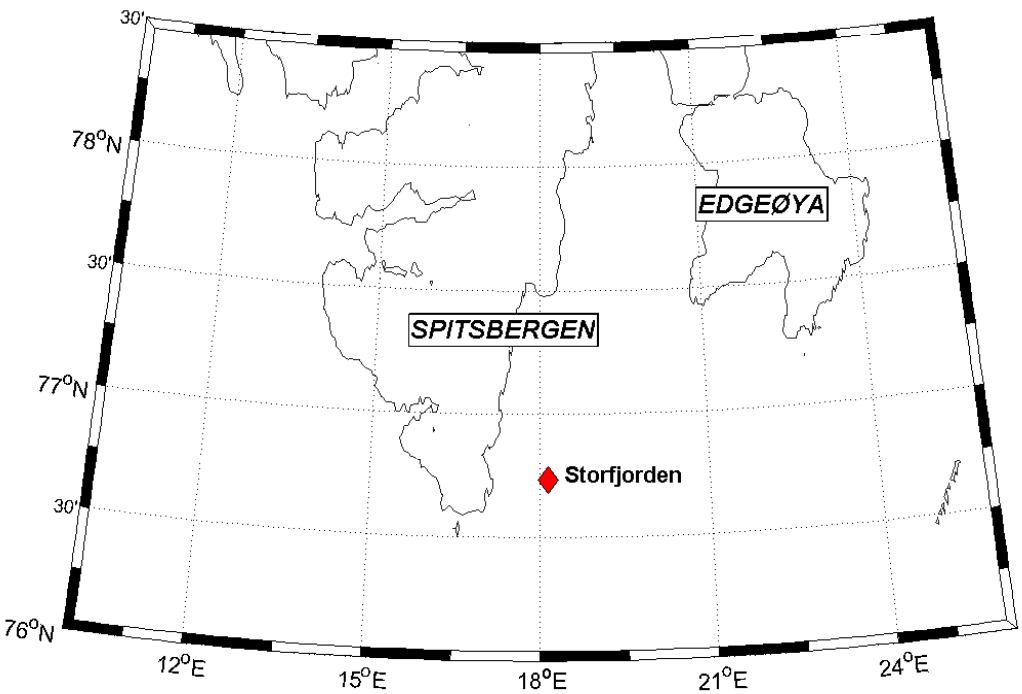

Figure 4.1: *Map showing the location of the measurement site in Storfjorden.*

The Vaisala RS92 radiosonde

For the radiosonde observation, a standard helium filled weather balloon was equipped with a RS92 GPS Vaisala radiosonde, measuring temperature, relative humidity, pressure and wind. The meteorological data were sampled and telemetred to the ground at a 2 second interval. The technical specifications of the RS92 sensors relevant for this study are the accuracies of the temperature and relative humidity measurements. During an atmospheric sounding, these are according to Vaisala (2006) $\pm$ 0.5 K and $\pm$ 5 %, respectively. Studies by e.g. M04 and Miloshevich et al. (2006) have estimated an associated sensor time constant of 2 seconds for relative humidity (at -20 ^{o}C) and a "negligible" short magnitude for the temperature sensor. Thus, no time-lag correction of the radiosonde data is made for this intercomparison.

Figure 4.2: *A radiosonde being released from the helicopter deck of KV Svalbard.*

As illustrated in Figure 4.2, the radiosonde was released by hand from the helicopter deck of KV Svalbard. This was also the position used for the manual take-offs and landings of SUMO.

Method of data analysis and experimental uncertainties

Only few corresponding, comparative studies of radiosonde and meteorological UAV observations have been made. One such study is reported by Soddell et al. (2004) where the Aerosonde (Holland et al., 1992), another metorological UAV, was compared to Vaisala radiosondes. These authors found the differences between the two platforms' measurements mainly to be related to platform related differences as e.g. airflow around the instruments, spatial and temporal dislocation and the instrumentation such as calibration, response time and sensor type. These factors are also present in this study and must be regarded as potential uncertainties in the evaluation of the SUMO data accuracy when using the radiosonde as reference.

No calibration of the SUMO instrumentation was done before the soundings. However, the radiosonde was calibrated by standard Vaisala methods. In addition, 20 m temperature and humidity data from the vessel are available for intercomparison. It is therefore possible to get indications of eventual offsets in the SUMO data e.g. caused by calibration errors.

Moreover, the SUMO profiles of this intercomparison are the same as the profiles shown in Figure 3.4 of Chapter 3. Therefore, the presented comparison serves as both an evaluation of the utilized correction scheme and the accuracy of the SUMO data.

In the beginning of the following result section, some general notes on the weather during the intercomparison is given. Such information might contain additional reasons for high atmospheric variability. Furthermore, to show the impact of the standard SUMO data treatment, the uncorrected SUMO data are presented in full resolution, while the corrected data are averaged in 20 m height intervals.

4.1.2 Results of the intercomparison

Fair weather and almost clear skies dominated the day of measurements, February 28, 2008. The radiosonde and SUMO wind data show North-Northeasterly winds of variable speed at a mean of 15 m/s close to the ground, turning with height to East and decreasing from 15 m/s at 1200 m to 5 m/s at 1600 m.

The SUMO and radiosonde profiles of this intercomparison are presented in Figure 4.3 (a)-(d), both for SUMO raw and time-lag corrected data.

The temperature differences for the altitudes above 200 m are all within the instrumentation accuracy of $\pm$ 0.5 K given by Vaisala. Only a slight improvement is seen for the corrected over the uncorrected temperature profiles. For the relative humidity profiles however, the improvement gained by the time-lag correction is substantial. These corrected SUMO profiles show an evidently closer agreement with the radiosonde profile, especially with respect to the smaller scale vertical structures dominating these profiles.

Under 200 m however, there are two prominent differences. The most evident of these are confined to the ascent data, and shows as a distinct warm bias in the uncorrected

profiles of both SUMO sensors, peaking at over +7 K for the DigiPicco sensor. In the corrected ascent profiles, there is a corresponding negative bias. Again, the DigiPicco sensor shows the larger difference of around -6 K. A dry bias corresponding to the mentioned lower level temperature bias is observed in the SUMO relative humidity profiles. The sign of this bias is negative both before and after correction. Furthermore, this bias is seen to be reduced from a maximum of nearly 40 % before correction to 20 % after. The DigiPicco sensor shows the larger humidity deviations before correction. After correction however, these are found for the SHT sensor.

A second prominent difference can be seen as a profile irregularity around 150-200 m altitude. This irregularity, which constitutes a difference of 1-2 K, is seen for both the uncorrected ascent and descent profiles of the two SUMO sensors. A similar difference is found in the corrected profiles, but smoothed out by the 20 m averaging and constituting a more constant bias of about -1-2 K for the descent and +1 K for the ascent profiles. A corresponding, but less quantifiable irregularity is seen at the same height in relative humidity.

In the following, only the corrected relative humidity profiles will be considered. The average difference in relative humidity is in the order of 5-10 %, with the SUMO profiles being consistently drier in the parts below 400 m. This might suggest a dry bias, but is still close to the accuracy of the radiosonde instrumentation of ±5 %.

For the profile parts over 200 m, the largest variability in relative humidity between the radiosonde and SUMO profiles are mainly confined to the heights between 400 and 800 m. This variability has a two-fold character. In the range from 400 to 600 m, it is larger for the descent (5-10 %) than for the ascent data (10-20 %). From 600 to 800 m however, the variability is approximately the same for both ascent and descent data and ranging between 10 and 20 %.

In comparison to the vessel data, the radiosonde reports slightly drier/warmer 20 m values (around +0.3 K and -1 %). These are both within the accuracy of the platform's instrumentation which thereby indicate the reliability of its measurements, at least for the lower altitude levels.

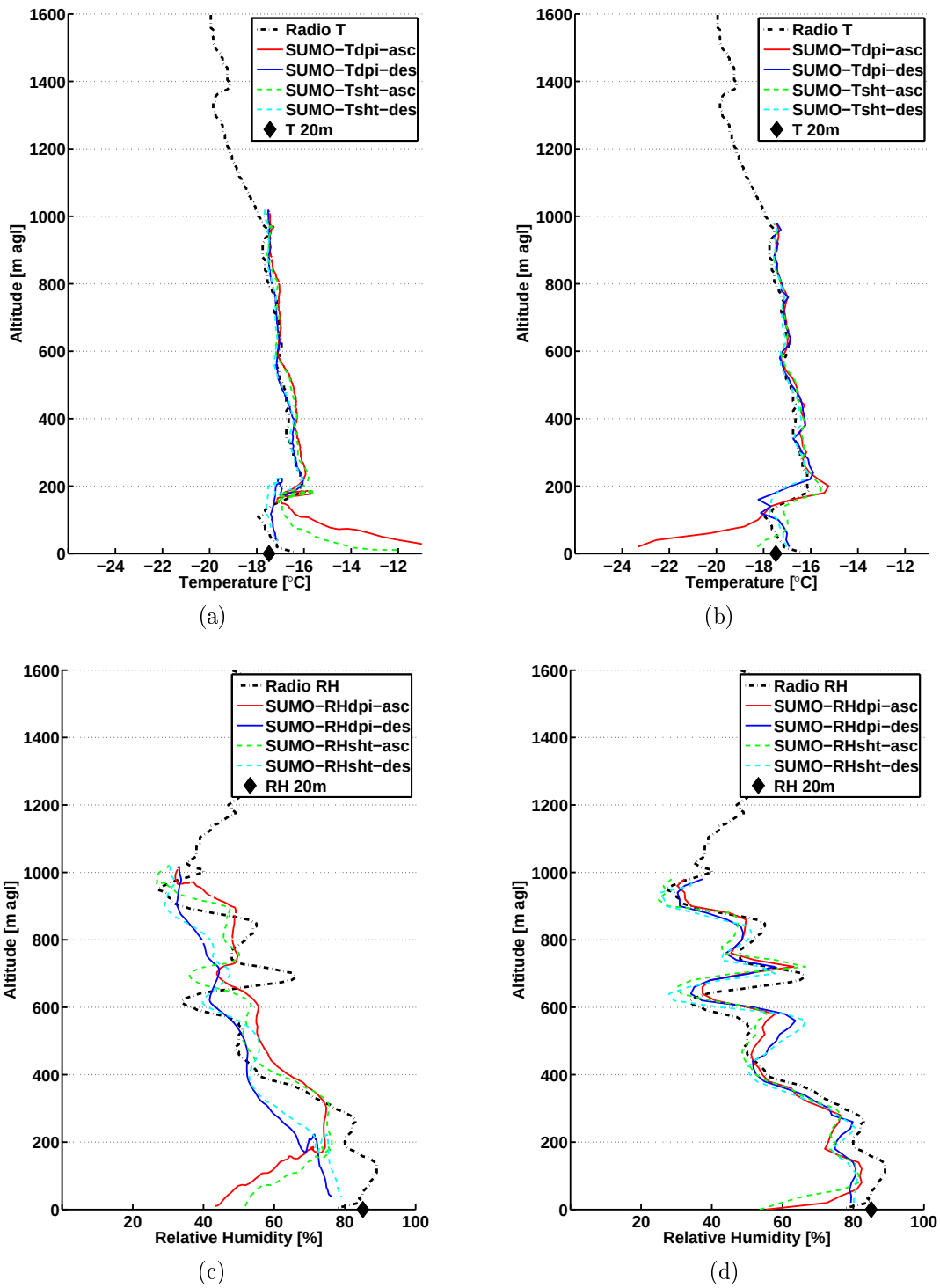

Figure 4.3: *Uncorrected and corrected profiles of temperature (a and b) and relative humidity (c and d). The measurements are performed from the helicopter deck of the Norwegian Coast Guard vessel KV Svalbard at 76.74 °N and 18.25 °E in the marginal ice zone on 28.02.2008. (Take-off SUMO: 15:11; launch of radiosonde: 15:15 UTC). Averaged 20 m data from the vessel measured during the operation of SUMO are indicated by black dots.*

4.1.3 Discussion and interpretation

The three main sources of differences between SUMO and the radiosonde are potentially related to 1) the platforms themselves, 2) the instrumentation of these and 3) spatial and temporal atmospheric variability.

From these factors, some are rather obvious and some more complicated. Temporal and spatial variability belongs in the latter category. In order to get a clearer picture of this factor for the measurement day, three radiosonde soundings are plotted in Figure 4.4 (b) and (c), showing temperature and relative humidity profiles of the lowest 2000 m above sea level. The associated geographical positions are shown in Figure 4.4 (a). This figure shows an evidently higher variability for relative humidity than temperature over 150 m, both with respect to location and time. Below this level however, the relative humidity is fairly constant. Notable is the relatively warm and moist profile of the 11:23 UTC radiosonde sounding. This was performed over the open sea, while the others were observed in the marginal ice zone. Meteorological data from the vessel show a corresponding decrease in temperature at around 12:00 UTC (Figure A.6, Appendix A). The relative humidity, that is measured at 20 m above sea level, is fairly constant also in the vessel data.

The most prominent differences between SUMO and the radiosonde, are found underneath 150 m, and can thus most likely not be explained by atmospheric variability. However, as mentioned in Chapter 3 and by references therein, a high temperature contrast between the preparing room and the measurement environment can lead to a warm bias in the lower ascent profile parts. At KV Svalbard, this temperature contrast was close to 40 K and thus probably explains the observed warm bias in this part of the uncorrected ascent profiles. For the corrected profiles however, a corresponding cold bias is observed. Though, this is also explainable by findings in Chapter 3, as correction of very steep parameter gradients as the described one tend to be over corrected for by the utilized correction scheme.

Sources for platform related differences are the radiosonde's and SUMO's substantially different sounding techniques. While the radiosonde has a fairly stable ascent rate and calm motion through the air, SUMO typically has a more unstable ascent rate and also a faster air speed. In the shown example, a direct impact of this difference is seen in the form of profile irregularities in the SUMO sounding around 150-200 m. Short term ascending/descending motion of the aircraft during the switch between autonomous and manual mode have been observed to cause such irregularities. Similar irregularities are also found under FLOHOF and by Egger et al. (2002) in the lower altitudes of temperature and humidity profiles from the remotely piloted KALI UAV. These irregularities are seen to introduce constant offsets when the profiles are corrected and averaged. For future applications, it is therefore desirable to remove such irregularitites before the described data treatment.

Another factor, which can be set in relation to the different measurement techniques,

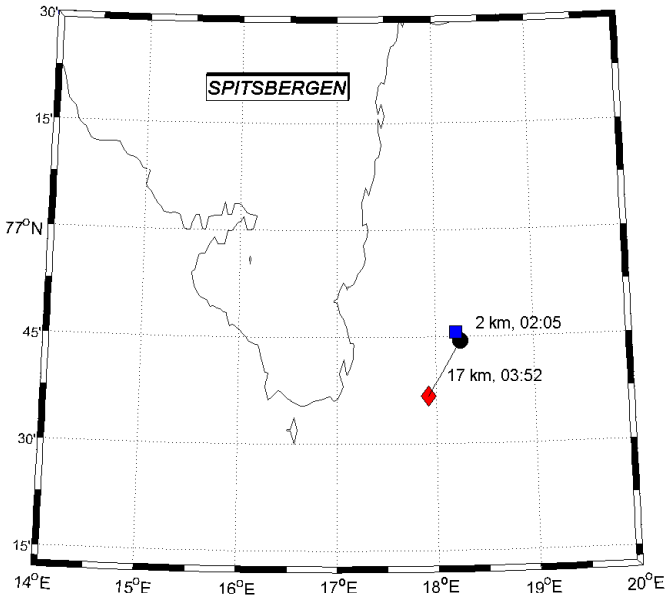

(a) Radiosonde launch locations

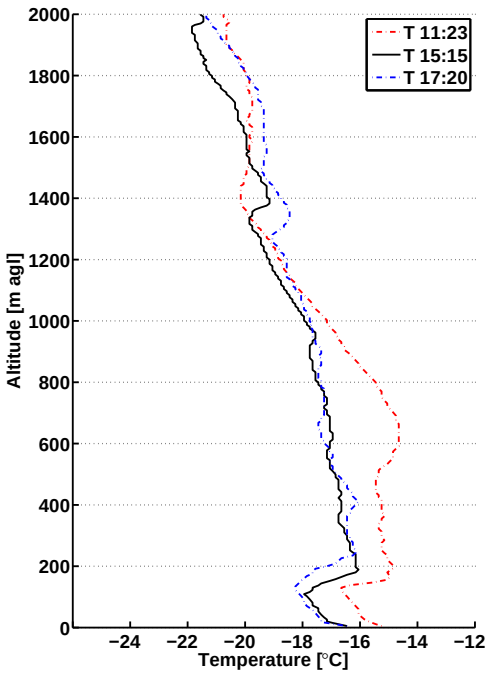

(b)

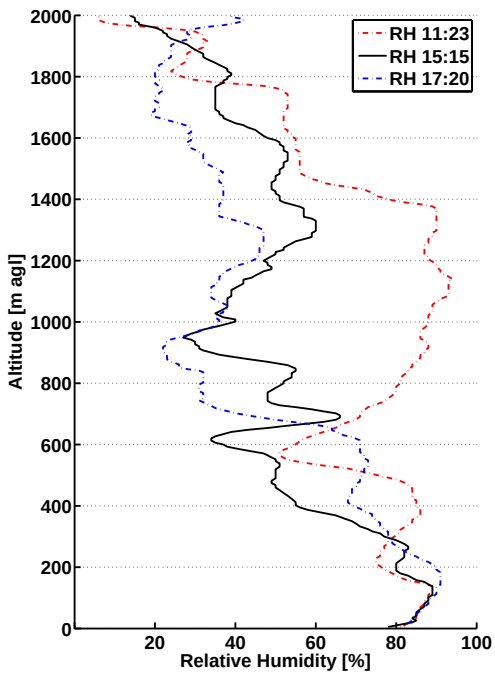

(c)

Figure 4.4: *Illustration of temporal and spatial variability of temperature (b) and relative humidity (c) measured by radiosondes, 28.02.2008, East of Spitsbergen. The launch times (UTC) are indicated in the figure legends. The sounding of this intercomparison is marked in black. The geograhical positions of the launch locations are marked by corresponding colors in (a) and the distances in time (hh:mm) and space (km) between them are indicated as well.*

is atmospheric spatial and temporal variability. After being released, the radiosonde drifts horizontally with the prevailing wind. SUMO however, circles over a more or less fixed point, which in this situation was a ship. The drift of the radiosonde may lead to sampling of different air compared to SUMO. This factor is potentially enhanced in regions with large spatial and temporal atmospheric variability such as documented here.

The close agreement between SUMO ascent and descent data for the relative humidity SUMO/radiosonde differences between 600 and 800 m, suggests that these SUMO profile parts represent the physical truth. Moreover, the height of these coincide with relatively sharp humidity gradients in both platforms' soundings. These descripancies are therefore not unlikely to be caused by the spatial and temporal dislocation between the two platforms.

For the relative humidity differences found between 400 and 600 m, the situation is another. In these profile parts, the deviations relative to the radiosonde are variable between the SUMO ascent and descent data. These SUMO profile parts have a character similar to time-lag induced differences between such profiles as described by (Soddell et al., 2004; Skony et al., 1994) and in Chapter 3. These deviations are thus probably related to time-lag errors not corrected properly for by the utilized correction scheme.

4.1.4 Summary

Although the two platforms of this intercomparison have very different sounding techniques, only marginal temperature differences below 0.5 K occur for altitudes above ca. 150 m. The corresponding differences in relative humidity are somewhat larger (around 5-10 %), but still close to the absolute accuracy limits given by the manufacturers of the humidity sensors. Consequently, the results indicate a SUMO data accuracy comparable to that of the latest and well-established radiosonde systems.

Larger deviations are evident below 150 m. A technical solution for these problems will be suggested in Chapter 6 and a solution to the described over correction is proposed in Chapter 3. Furthermore, some of the observed differences in relative humidity indicate signs of spatial and temporal dislocation. Measurements by radiosondes have documented a large humidity variability in the measurement region. Remaining descripancies resemble the character of time-lag between ascent and descent profiles and are thus probably caused by unsatisfactory profile correction.

4.2 Intercomparison of SUMO, a tethersonde and the KALI UAV

4.2.1 Experimental setup

The measurements of this intercomparison were performed during FLOHOF in the near vicinitiy of Hofsjökull, the main area of research for this campaign. Two of these locations were situated South West of Hofsjökull, near Kerlingarfjöll (1477 m), and are named thereafter (Kerlingar 1 and 2), whereas the last measurements took place at the position of FLOHOF's main base at Ingolfsskáli, North of Hofsjökull. Figure 4.5 indicates the geographical locations of all three sites.

Thanks to the Icelandic Meteorological Office, Veðurstofa Íslands, it was possible to use an abandoned weather station at Hveravellir as a base for the southern part of the experiment. From this location, the measurement sites near Kerlingarfjöll were relatively easy to reach by an hour and a half 4WD-car driving.

The decribed measurements were confined to the six day period from 13th to 18th of August, 2007. During this period of time, a total of 31 SUMO soundings were made. The corresponding numbers for each day and each platform of this intercomparison are listed in Table 4.2 together with more detailed information on time and measurement locations.

Table 4.2: *Summary of measurement days with associated locations, coordinates, height above sea level and number of soundings for each platform*

date	location	[m] asl	coordinates ^{o}N	^{o}W	# SUMO	# KALI	# TETH
13.08.2007	Kerlingar 1	773	64.67	19.23	8	5	7
14.08.2007	Kerlingar 2	676	64.69	19.29	4	6	0
15.08.2007	Ingolfsskáli	840	65.01	18.89	1	3	0
16.08.2007	"	"	"	"	2	0	0
17.08.2007	"	"	"	"	7	5	6
18.08.2007	"	"	"	"	9	5	4

As can be seen in Table 4.2, very few measurements were performed the 15th and 16th of August and these days are therefore left out of this study. The low number of soundings was in general caused by unfavourable measurement weather characterized by repeated rain showers and strong winds. Moreover, an accident on the 14th of August

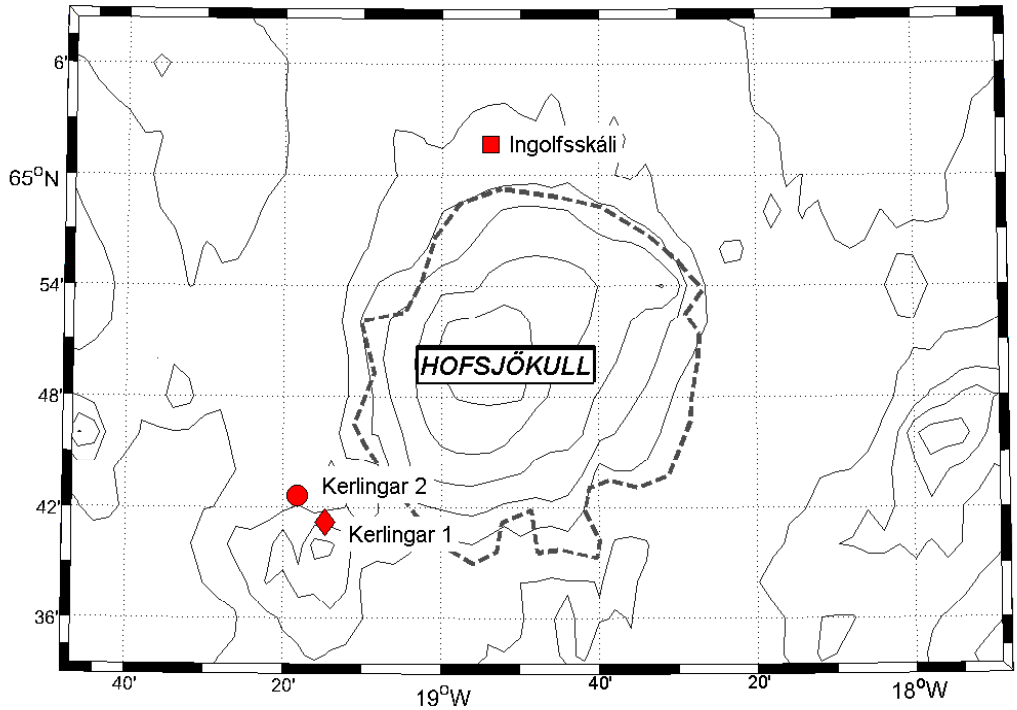

Figure 4.5: *Map showing the locations of the FLOHOF measurement sites. Kerlingar 1 and 2 are situated South West of Hofsjökull, near Kerlingarfjöll, and Ingolfsskáli, the main base during FLOHOF, is located in the North. The glacier edge is indicated by a grey, dashed line (- -).*

caused the loss of a SUMO aircraft (FUN2) and thereby set an early stop for the SUMO measurements this day. A similar event happened the day after where a KALI aircraft was lost and limited the measurements with this system the 16th. No tethersonde measurements were performed the 14th of August due to strong winds of over 10 m/s.

Thus, only the results from the first two and last couple of measurement days will be presented here. The North-South separation of the measurement sites are kept within the later result presentation. The North section is presented first because these measurements were performed with the same SUMO aircraft (FUN3) as those on Svalbard. In addition, as will be shown later, the meteorological situation on the southern side turned out to be very interesting, but quite complicated for intercomparison purposes.

4.2.2 The platforms used for the intercomparison

The main foundation for this intercomparison is the three platforms' common ability of measuring atmospheric profiles of temperature and relative humidity. In addition, the tethersonde measures pressure, wind and wet-bulb temperature whereas SUMO also measures wind and pressure (the latter not working during FLOHOF). However, because of the focus of this thesis, only profiles of temperature and relative humidity are considered in this intercomparison.

Each of the utilized platforms has both similaritites and differences compared to SUMO. The platform most equal to SUMO is without doubt KALI, which is depictured in Figure 4.6 and shortly presented in the following subsection.

KALI

KALI is an already well established platform and has, in addition to its participation in FLOHOF, successfully contributed to international field campaigns in the past, e.g. in Nepal (Egger et al., 2002) and Bolivia (Egger et al., 2005). Similar to SUMO, KALI is an electrically powered meteorological micro-UAV. The aircraft has a weight of 3 kg, a wing span of 2.10 m and length of 1.20 m. In terms of operation, the KALI performs soundings including both ascent and descent in a total of about 15 min. The associated flight velocities are between 10 and 40 m/s and the climb rate is in the order of 4-5 m/s (Egger et al., 2002).

The main shortcoming of KALI is the lack of autonomous flight capabilities, it must therefore be operated continously by an experienced pilot. With the aid of small binoculars mounted on a pair of glasses, the pilots were able to reach an average operating flight ceiling of 1500-2000 m during FLOHOF.

Technical details on KALI's two on-board temperature and humidity sensor packages are listed in Table 4.3. For this intercomparison, data from sensor package 1 are used for temperature and from sensor package 2 for relative humidity. This choice was taken with background in a discovered error in relative humidity data from sensor package 1, and a larger calibration offset for temperatures from package 2. All measurements, both at the northern and southern locations, were taken by the same instrumentation. Height information from KALI is obtained by an on-board pressure sensor.

KALI was the only platform that carried out soundings during the entire FLOHOF campaign. In addition and in contrast to the operation of SUMO (that performed its first environmental test), its soundings were of a regular character with about 1-2 hours in between every sounding during daytime when the conditions were sufficient for measurements.

Figure 4.6: *Rafael Kühnel holding the KALI aircraft. The picture is taken at the position of Ingolfsskáli, looking southwards with Hofsjökull in the background. The landscape is representative for the Icelandic highlands where FLOHOF was conducted. Courtesy of Markus Garhammer.*

Tethersonde

For the tethersonde measurements, a system from AIR was used (Figure 4.7). The basic configuration of the tethersonde is quite different from those of the meteorological UAVs. It shares many similiarities with radiosondes, as both systems consist of an instrument package attached to a helium (/hydrogen) filled balloon. However, in contrast to radiosondes that fly freely up to several kilometers, tethersondes are primarily made for boundary layer research and are also recoverable as they are tied to and controlled by a winch on the ground. This principle of operation makes tethersondes capable of performing continous soundings of pressure, dry and wet-bulb temperature, wind speed and direction.

Similar to meteorological UAVs, the tethersondes are quite flexible platforms in the sense that they can carry various types of instrumentation. But they have one significant limitation as they are not controllable in other than the vertical direction and their flight ceilings are limited by the length of the winch cable. For the system utilized here, the cable length was about 1000 m. In addition, these systems are limited to wind speeds below around 10 m/s.

During operation, the tethersonde ascent and descent speeds can be chosen arbitrarily by the winch operator. For this intercomparison, speeds in the range of 0.3 to 0.5 m/s were chosen. When operative, the tethersonde system was in this intercomparison session utilized more or less continously with appr. 1 hours in between the start of every ascent.

Technical details on the tethersonde instrumentation package are given in Table 4.3.

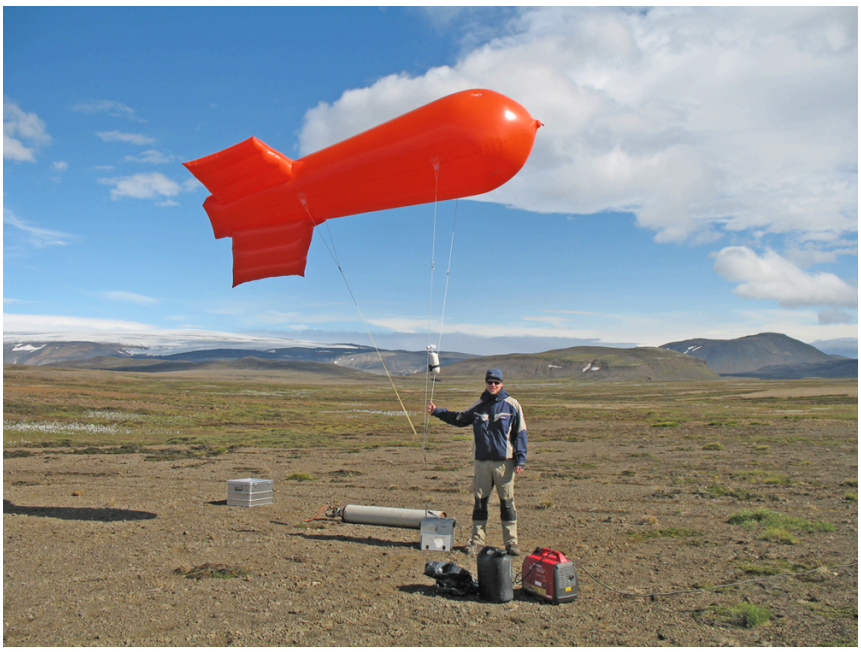

Figure 4.7: *The tethersonde with its helium filled balloon, instrument package underneath and the winch on the ground. The picture is taken at Kerlingar 1, looking northwards with Hofsjökull in the background and Kerlingarfjöll some 500 m behind the photographer.*

Method of data analysis

The data sampling interval, vertical speeds and thereby the vertical resolution of the utilized platforms' measurements vary. Therefore, all soundings were averaged over 20 m height intervals to make them directly comparable.

A total of 40 soundings were matched by a Matlab routine where 60 minutes was set as the maximum time difference. In some cases, this procedure matched one sounding of one platform with two or even three soundings from another platform. From these time matches, a certain number of matches between SUMO and KALI, and where available, also the tethersonde, are picked out on a daily basis. Each of these matches was found to be characteristic for its respective day and is given a comparison ID and listed together with the associated time details in Table 4.4.

Table 4.3: *Specifications of the temperature and humidity sensors used on KALI and the tethersonde.*

sensor	Tethersonde		KALI	
parameter	RH	T	RH	T
resolution	0.1 %	0.01 K	0.6 %	0.2 K
range	3-100 %	-70-50 ^{o}C	0-100 %	-20-30 ^{o}C
abs. Accuracy	5 %	0.5 K	N/A	N/A

Table 4.4: *Details on SUMO, KALI and tethersonde profiles that are matched in time and location. Some profiles appear twice, indicating that two profiles of one platform match the other within the same 60 minute time interval.*

		SUMO		KALI		Tethersonde	
Comp-ID	Date (local time)	start time (UTC)	end time (UTC)	start time (UTC)	end time (UTC)	start time (UTC)	end time (UTC)
N1	17.08.2007	09:57	10:19	09:07	09:18	09:36	11:04
N2	17.08.2007	11:03	11:28	11:04	11:16	11:06	12:45
N3	17.08.2007	12:09	12:32	13:01	13:15	11:06	12:45
N4	17.08.2007	15:34	15:58	15:01	15:13	15:18	16:48
N5	18.08.2007	08:16	08:39	09:04	09:18	-	-
N6	18.08.2007	08:53	09:14	09:04	09:18	09:57	11:11
N7	18.08.2007	10:04	10:27	11:04	11:17	09:57	11:11
N8	18.08.2007	15:22	15:40	15:05	15:24	14:00	14:45
S1	13.08.2007	12:04	12:21	11:22	11:46	11:47	12:48
S2	13.08.2007	13:11	13:28	12:35	13:09	11:47	12:48
S3	13.08.2007	13:48	14:10	14:23	15:03	12:51	13:48
S4	13.08.2007	17:25	17:49	18:17	18:35	17:15	18:13
S5	14.08.2007	12:47	13:09	13:09	13:20	-	-
S6	14.08.2007	13:46	14:22	13:09	13:20	-	-

Experimental uncertainties

In principle, the same platform and instrumentation related uncertainties apply for this intercomparison as for that between SUMO and the radiosonde. Smaller platform related differences are expected between SUMO and KALI and larger between the tethersonde and the two other platforms. In addition, there was a change of SUMO aircraft from FUN2 at the southern location to FUN3 at the northern locations. This change might also introduce intervariability in the SUMO measurements caused by e.g. calibration related offsets. Though, both SUMO aircrafts should in principle be identical.

Sensor response time is potentially a large uncertainty factor. All presented SUMO temperature and humidity profiles are corrected in accordance with the correction method described in Chapter 3. The same procedure was also applied to the KALI relative humidity data, which showed clear signs of a very slow sensor response (τ_s = 45 s, τ_f = 1 s). A corresponding correction was not applied to the remaining KALI and tethersonde data since these did not show the same systematic disagreements between ascent and descent profiles as the other profiles did. As presented in Chapter 3, the utilized correction scheme has shown to be very effective for profiles of temperature. Therefore, the corresponding pairs of SUMO ascent and descent data are, if not otherwise mentioned, treated as one single profile in the description of the results. The same applies for the KALI temperature profiles. For the relative humidity data however, several SUMO and KALI soundings still showed significant deviations between ascent and descent data, even after correction. Therefore, only ascent profiles of relative humidity will be considered in the following section.

Furthermore, a problem concerning the tethersonde data was discovered during the preparatory data treatment. It showed out that almost all tethersonde profiles are dominated by an irregular warm/ dry, probably solar radiation induced bias. As a consequence, the tethersonde data are presented as scatterplots, and only the mean gradient of the colder/ more humid values will be used for comparison. These observed errors are further discussed in the later discussion section.

Neither of the platforms' instruments were calibrated before the soundings, making a direct comparison of relative differences between the matched profiles difficult. However, measurements of temperature and relative humidity were taken on the ground at the northern measurement location by an automatic weather station (AWS N3b) at the position of Ingolfsskáli. Data from these ground measurements are averaged over the time period of each comparison ID and used as a reference in order to give an estimate of eventual offsets in the measurements from these platforms. Also data from other FLOHOF AWSs will be used in the later discussion. The geographical positions of these stations are indicated in Appendix A (Figure A.3).

In the following subsections, the intercomparison results from the North and South of Hofsjökull are presented on a daily basis. General weather information collected at site of direct or indirect importance to the intercomparison results will be shortly

commented in the start of the presentation of each day's results. If otherwise not stated, the sources of this information are Piloted balloon (PiBal) soundings on the northern side, SUMO wind measurements, FLOHOF AWSs and in-field observations done by the author and other FLOHOF campaign participants. Furthermore, synoptic charts (found in Appendix A) will be used to describe the large scale meteorological situation.

4.2.3 Results, Hofsjökull North

17.08.2007, Ingolfsskáli

A weak high pressure ridge forming to the South East of Greenland dominated this day's weather situation. Light winds of less than 5 m/s throughout the lowest 2000 m above ground were observed, turning towards South West during the course of the day. In addition, there was sun through an Altocumulus layer from noon to around 14:00. In the evening, a growing Stratocumulus cloud cover resulted in evening showers, which made a shut down of the tethersonde system necessary at 17:30. The profiles of temperature and relative humidity are presented in Figure 4.8 and 4.9.

The SUMO temperature profiles show a very close agreement of better than 0.5 K when compared to the KALI profiles of these comparisons. The improvement gained by using the correction scheme is also clearly seen as e.g. the temperature profile inversions in N2 match perfectly. An exception to the close agreement however, is found below 400 m in N1, where KALI reports 1-2 K lower temperatures than SUMO.

Most parts of the corresponding tethersonde temperature profiles of N1-3 show an irregular warm bias, but the colder values fit rather well with the SUMO and KALI profiles. Interestingly, the tethersonde profile in N4 does not have any signs of the described bias and all platform profiles fit within the given instrument accuracies in this comparison.

For the relative humidity profiles, an average difference between SUMO and KALI in the order of 5-10 % is observed, SUMO being the drier. The KALI profiles have a slightly steeper vertical gradient than those of SUMO, causing the differences between them to increase with height. Also for relative humidity, the largest differences are found below 400 m in N1. In that profile part, KALI reports 25 % higher values than SUMO. Looking at N4, the agreement is not quite as good as for temperature, but still no irregular bias is seen in the tethersonde data. The average difference there is in the order of 10-20 %, the tethersonde profile being the more humid. The remaining tethersonde profiles though, are not that conclusive and generally hard to interpret.

Considering the ground data, the temperatures of these measurements are in average 1-2 K warmer than the lower parts of the airborne platforms' profiles. Correspondingly, slightly drier relative humidity values are in average recorded at the ground. In this context, the SUMO profiles show the closer match as its profiles match nearly perfect with the ground relative humidity data.

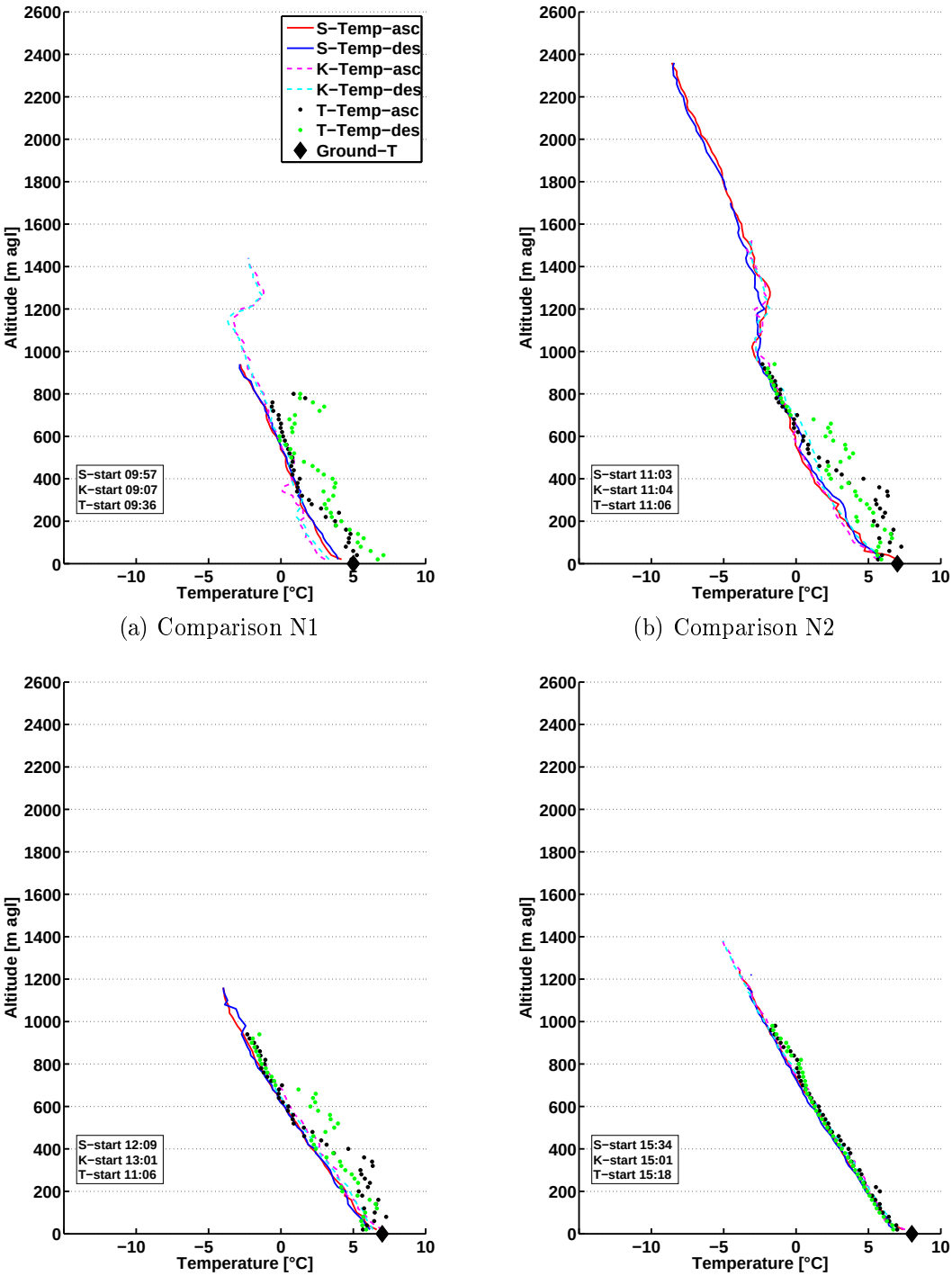

(a) Comparison N1 (b) Comparison N2

(c) Comparison N3 (d) Comparison N4

Figure 4.8: *SUMO, KALI and tethersonde temperature profiles of comparison N1-4, 17.08.2007, North of Hofsjökull.*

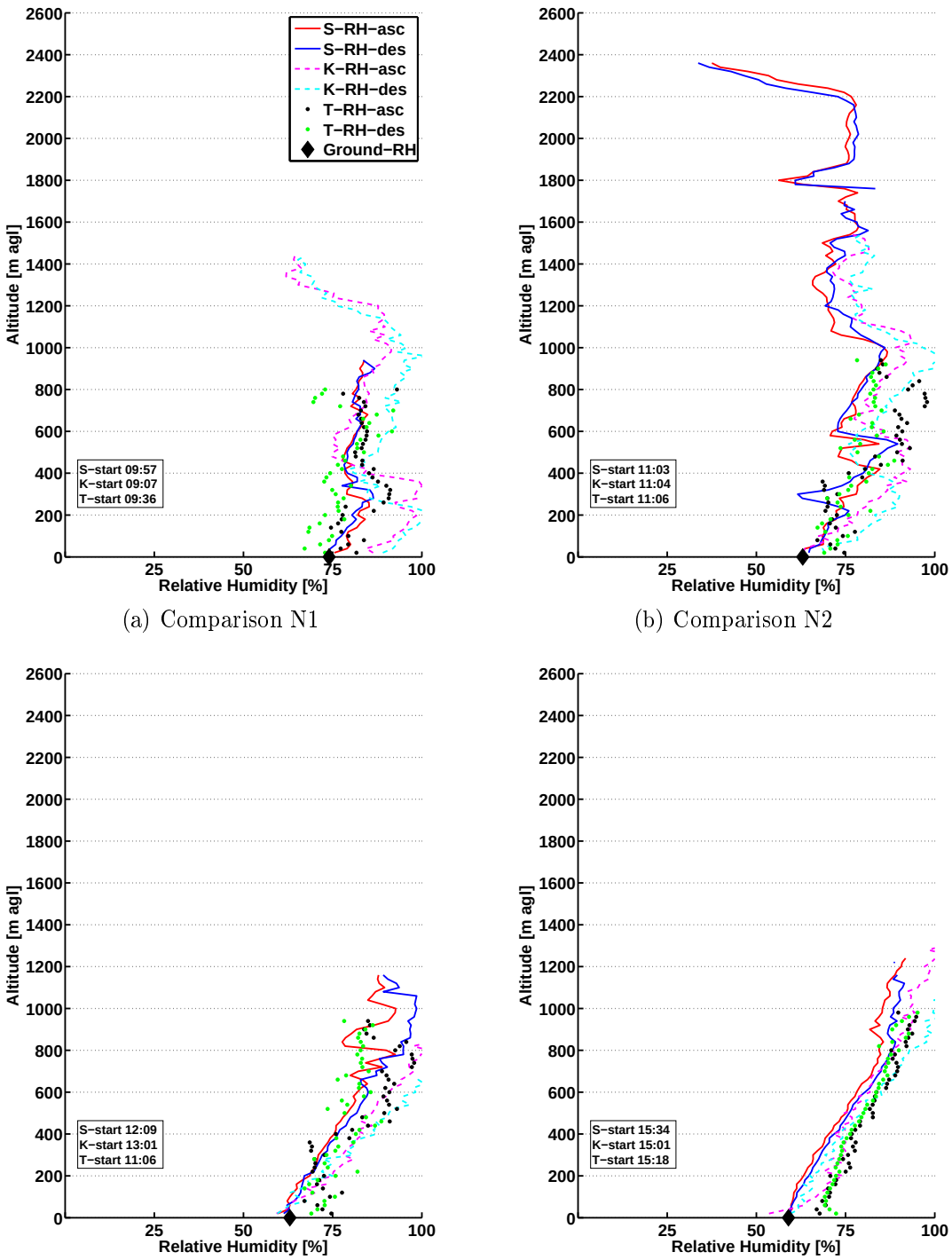

(a) Comparison N1

(b) Comparison N2

(c) Comparison N3

(d) Comparison N4

Figure 4.9: *As in Figure 4.8 but for relative humidity*

18.08.2007, Ingolfsskáli

With exception of a slight strengthening of the high pressure ridge, the synoptic situation was similar to the day before. More northerly winds and longer periods with sun was observed from the measurement site. Again, evening showers caused an early shut down of the tethersonde system, this day at 14:45.

As for the 17th, this day's profiles are presented in Figure 4.10 and Figure 4.11.

In general, the KALI and SUMO temperature profiles show the same close agreement as for the previous day. The most notable difference is found in N7 where the boundary layer height (marked by an inversion) is placed around 150-200 m higher in the KALI profile than in the corresponding SUMO profile. While this difference is in the order of 1-2 K for temperature, the relative humidity shows a disagreement of close to 25 % at the same height. Relative humidity differences in the same order are also found between SUMO and KALI above 600 m in N8. With an hour in between the SUMO and KALI start times, N7 has the longest time difference between the SUMO and KALI profiles of these comparisons.

Looking at the tethersonde temperature profiles, the parts not affected by the irregular bias are in very good agreement with both KALI and SUMO. Only slightly warmer values are recorded when compared to the two other platforms. The exception is N7, where the KALI profile is the warmer. The corresponding relative humidity profiles are also this day generally hard to interpret, but the values recored are in slightly better agreement with SUMO than KALI.

The ground temperatures are warmer also for this day compared to the airborne platforms, but at a difference of only 0.5-1 K. The corresponding relative humidity values are in better consistency with SUMO (5-10 %), slightly less with Kali and least with the tethersonde at a difference between 10 and 20 %.

It should be mentioned that the SUMO ascent profiles of N5-7 have marks of the solar radiation induced bias as described in Chapter 3. This can be seen as a 1-2 K difference between the ascent and descent profiles at 300-400 m height intervals.

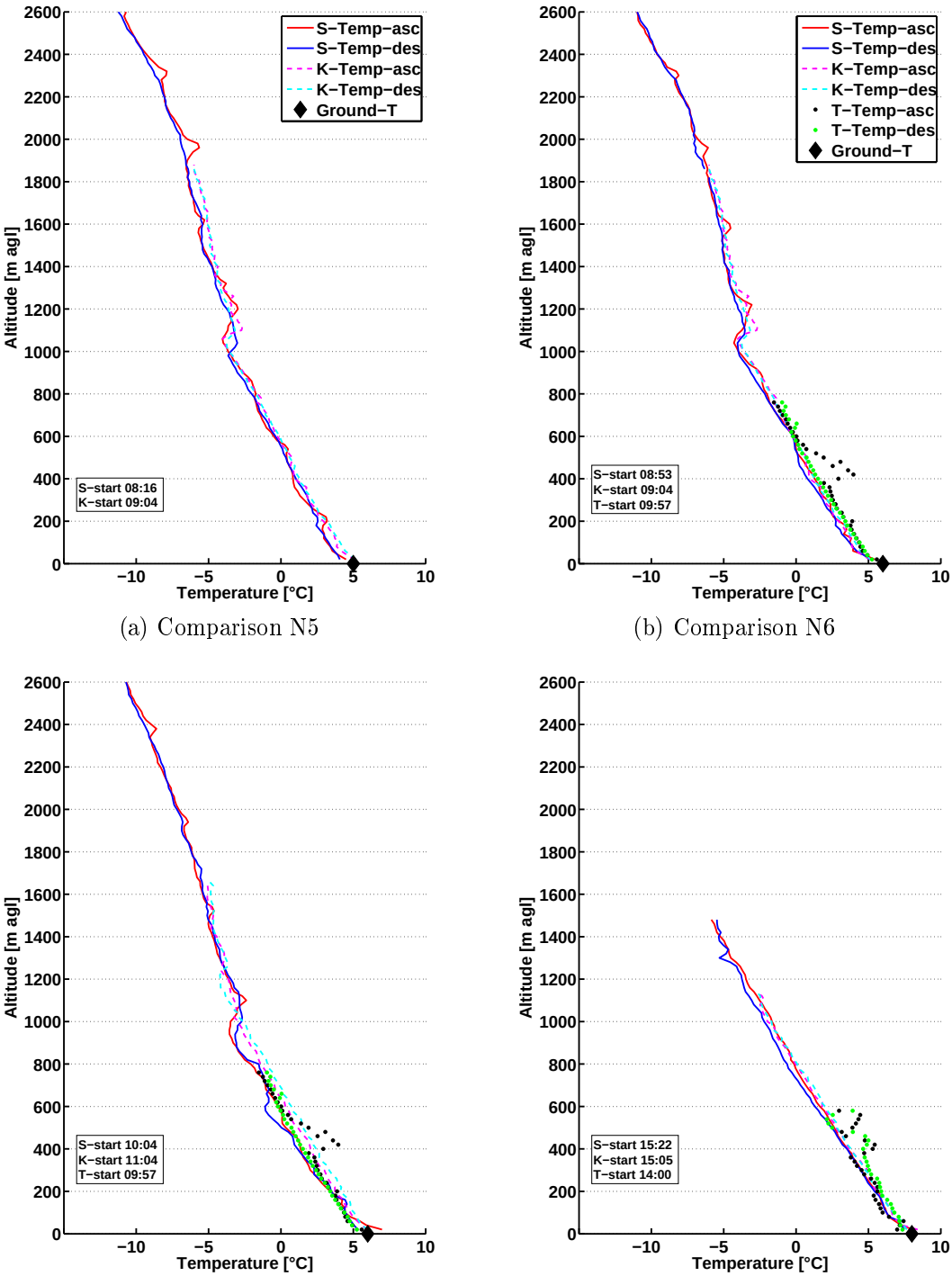

(a) Comparison N5 (b) Comparison N6

(c) Comparison N7 (d) Comparison N8

Figure 4.10: *SUMO, KALI and tethersonde temperature profiles of comparison N5-8, 18.08.2007, North of Hofsjökull.*

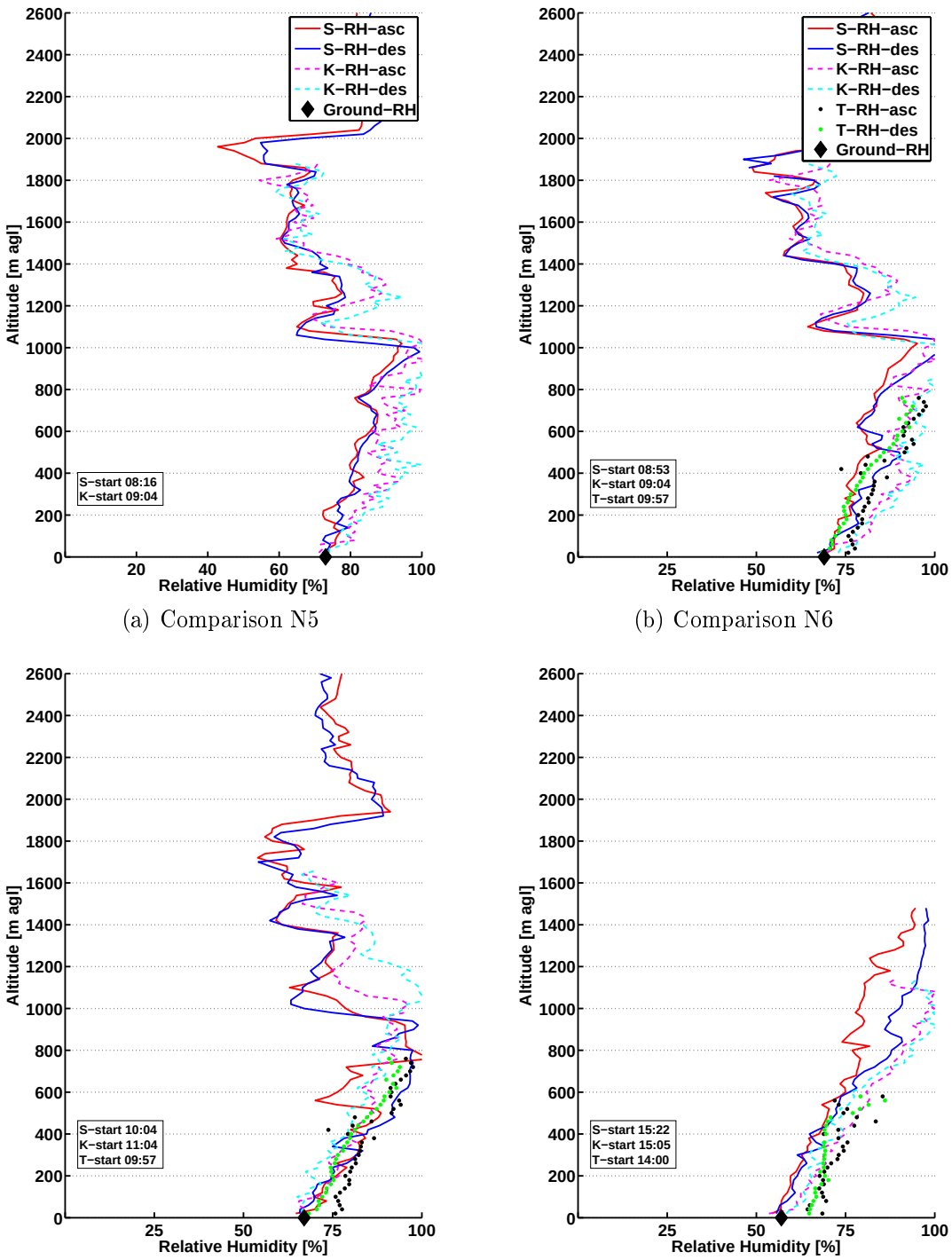

(a) Comparison N5

(b) Comparison N6

(c) Comparison N7

(d) Comparison N8

Figure 4.11: *As in Figure 4.10, but for relative humidity.*

4.2.4 Results, Hofsjökull South

13.08.2007, Kerlingar 1

A low pressure system situated directly to the South East of Iceland set up a larger scale flow from North East this day. The observed wind direction coincided with this flow from around 2000 m at a speed of 10 m/s. Weaker winds of around 5 m/s were observed at the ground. The wind direction at the ground variated during the course of the day, but was mainly from the East. Furthermore, Altocumulus lenticularis clouds were observed in the East/ North East, indicating waves in the atmosphere.

The profiles of this day's comparisons are presented in Figure 4.12 and Figure 4.13.

In average, the KALI profiles are 1-2 K warmer than those of SUMO and the tethersonde profiles agree evidently closer with SUMO than KALI. For relative humidity, the situation is somewhat different. The SUMO profiles are in general 20-25 % drier than the KALI profiles and the tethersonde profiles are 10-20 % moister than those of KALI.

In addition to these more or less constant offsets, the most prominent mismatches between SUMO and KALI are found in connection to inversions. The most evident of these are situated between 1600 and 2000 m altitude in S2. At this height, the SUMO ascent/descent profiles themselves disagree by as much as 3 K at +150 m height difference (ascent-descent) making a direct comparison with the corresponding KALI profile difficult. The closest match between KALI and SUMO is in those profiles found for the SUMO ascent profile, which is also measured closer in time with the KALI profiles. Still, the KALI profiles at this height show a significantly less steep gradient than the SUMO profiles. Taken the time between these soundings into consideration (2 min), the observed differences are relatively large.

A similar mismatch between SUMO ascent/descent data is found in the inversion at 2000 m for comparison S4, where the difference in height is close to -100 m. This corresponds to differences of up to 5 K and as much as 50 % for temperature and relative humidity within this inversion layer. Compared to this SUMO ascent profile, the corresponding KALI profile inversion differs with 200 m, KALI being the lower. These KALI and SUMO profile inversions have approximately the same steep parameter gradients, both with respect to temperature and relative humidity.

A closer inspection of the KALI and SUMO profiles of S2-4 reveals a lower level temperature inversion, situated between 1000 and 1200 m. This inversion corresponds, at least in height, to the more prominent inversions of the SUMO and Kali profiles in comparison S1. Also for this inversion, there are differences in height between the two platforms. Again this seems to be most evident for S2, especially in relative humidity where the SUMO and KALI profiles have significantly different vertical structures. Interestingly, the difference between the KALI and SUMO profiles of S2 is higher below than above the lower level inversion. Another interesting difference between the SUMO and KALI profiles is the evidently steeper lapse rate in the SUMO profile of S3.

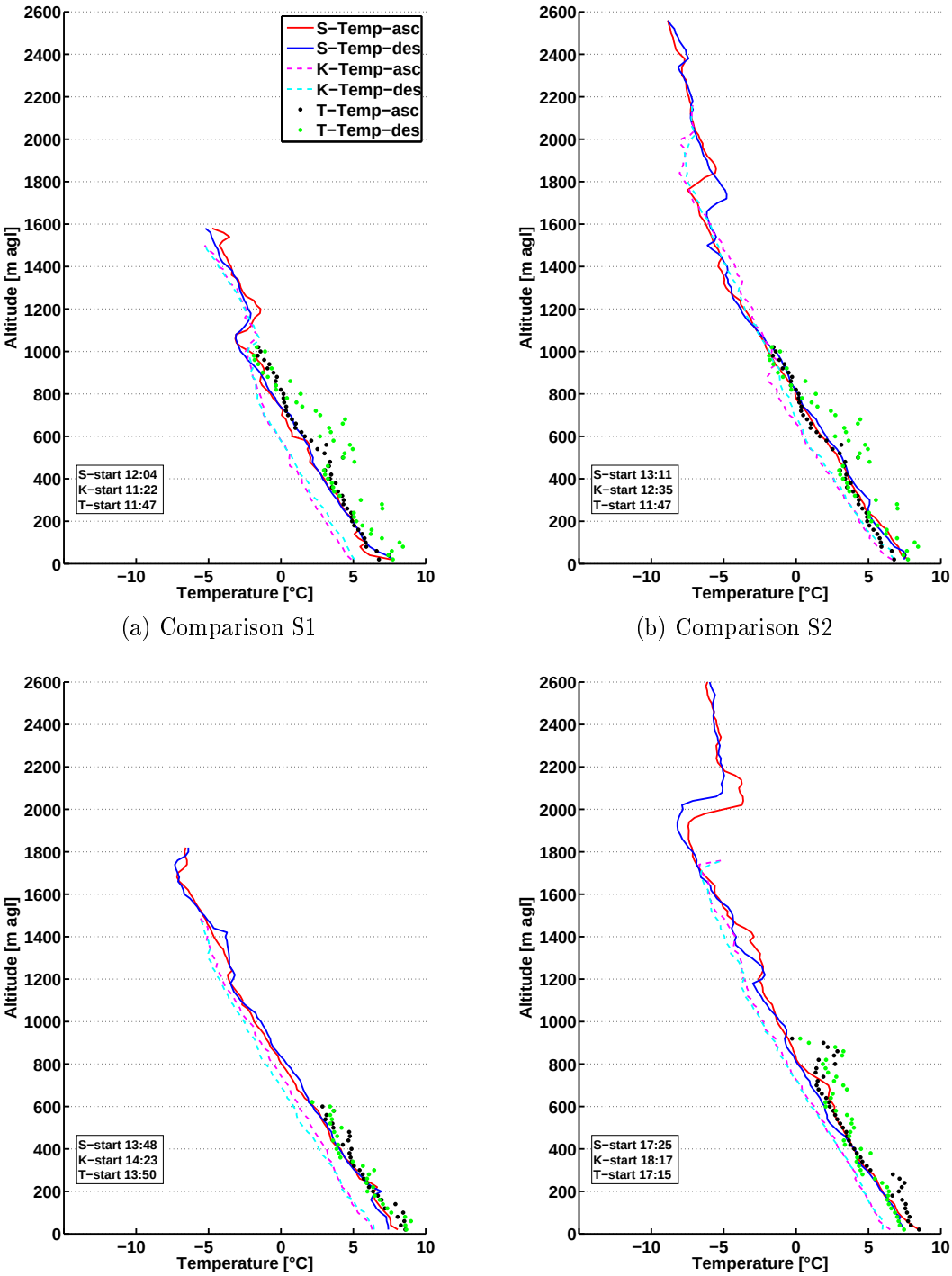

(a) Comparison S1

(b) Comparison S2

(c) Comparison S3

(d) Comparison S4

Figure 4.12: *SUMO, KALI and tethersonde temperature profiles of comparison S1-4, 13.08.2007, South of Hofsjökull.*

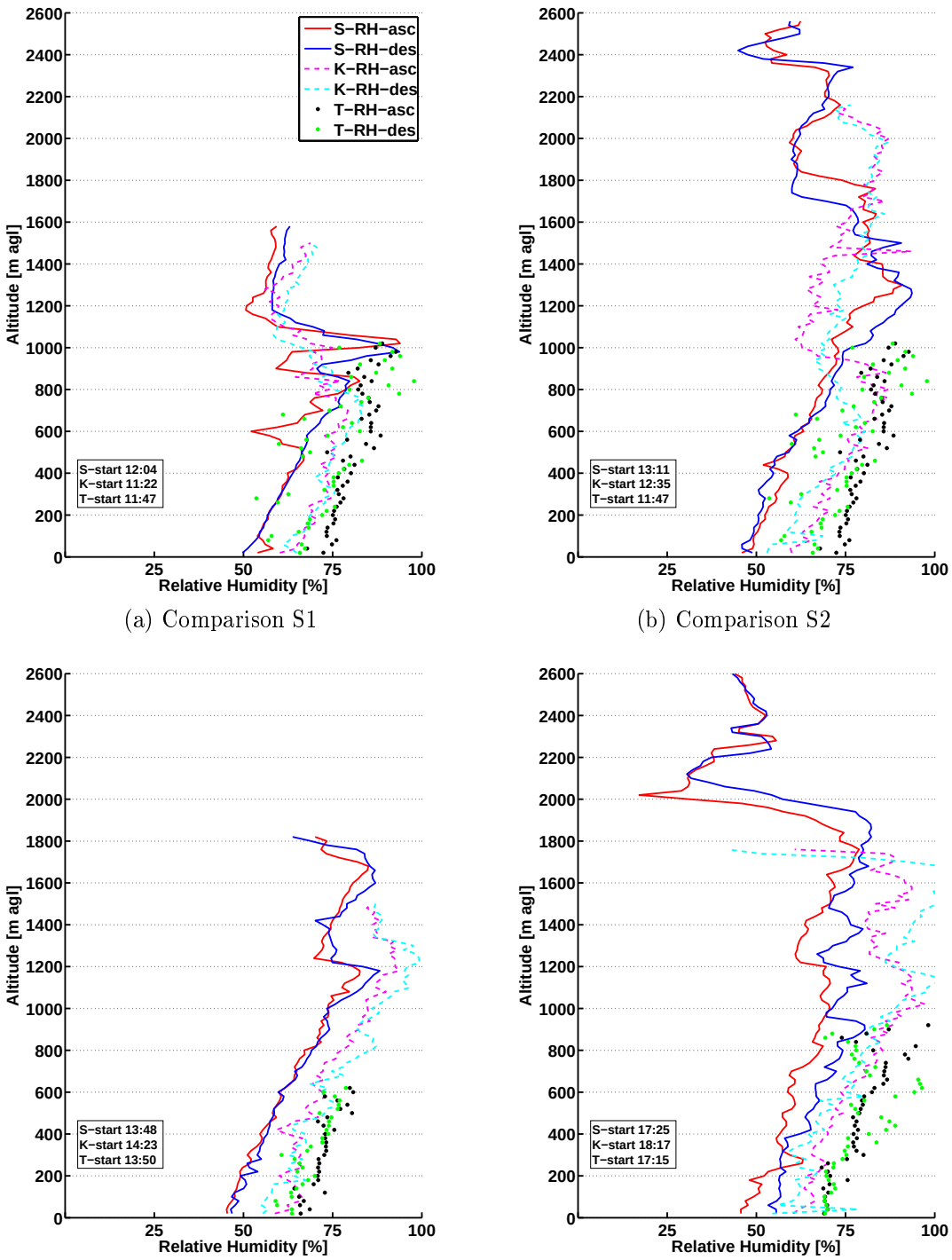

(a) Comparison S1

(b) Comparison S2

(c) Comparison S3

(d) Comparison S4

Figure 4.13: *As in Figure 4.12, but for relative humidity.*

14.08.2007, Kerlingar 2

This day's meaurements were planned to take place at the same site as the 13th, but due to a broken car tire, they had to be performed at a site slightly further to the West. The synoptic situation was comparable to the 13th, only with a slightly more northerly flow, stronger pressure gradient and corresponding wind speed increase. This coincides with the observed wind direction and the wind speed was estimated to around 10-15 m/s. However, in contrast to the day before, this high wind speed reached all the way down to the ground. Moreover, also this day's sky was dominated by wave indicating clouds.

The temperature and relative humidity profiles are presented in Figure 4.14. Due to a technical problem, the KALI descent data are incomplete, and thus only ascent data will be considered here.

In spite of the relative low number of matching profiles, the overall trend is clear and the similarities with the results of the day before are several. Both SUMO profiles have differing inversion heights when compared to the matched KALI profiles. Also differences between the SUMO ascent and descent profiles exist. These are especially evident in S6 where the SUMO ascent profile agrees closer with the KALI profile than the descent profile. In addition, the inversions in both the KALI and SUMO profiles show rather complex vertical structures.

In average, the height difference between the inversion bottoms of the KALI and SUMO profiles are in the order of 150-200 m. The corresponding temperature and relative humidity differences are between 2-3 K and 30-40 %. As for the 13th, these disagreements are clearly visible in both the temperature and the relative humidity data.

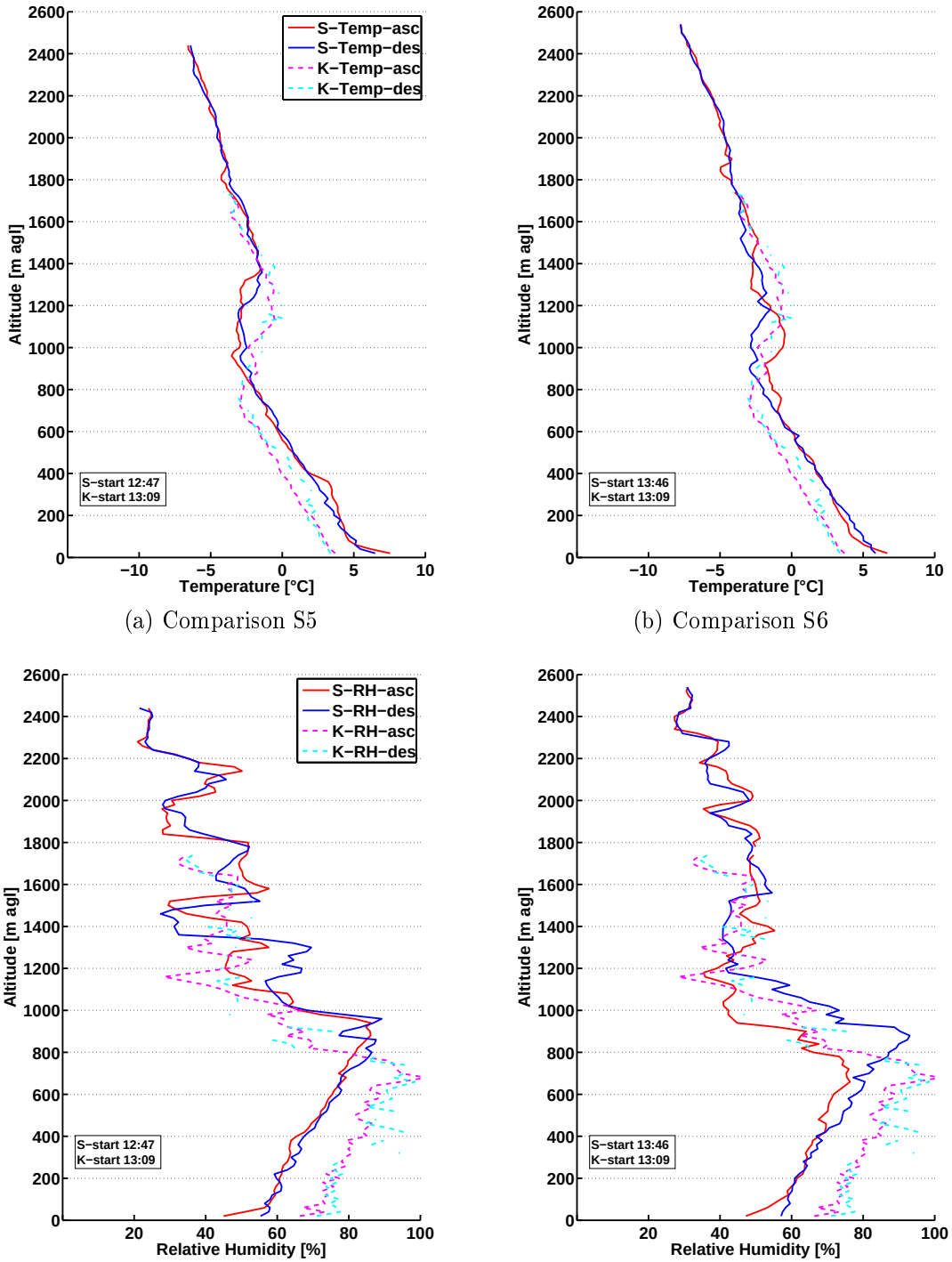

(a) Comparison S5

(b) Comparison S6

(c) Comparison S5

(d) Comparison S6

Figure 4.14: *SUMO and KALI temperature (a and b) and relative humidity (c and d) profiles of comparison S5-6, 14.08.2007, South of Hofsjökull.*

4.2.5 Discussion and interpretation

In comparison to the KALI data, SUMO performs very well for the measurements North of Hofsjökull. The average differences are for these days less than 0.5 K for temperature and around 5-10 % for relative humidity. The largest differences are found in connection to inversions such as in N7, where an ABL height difference of 150-200 m is estimated. In addition, notable differences of 1-2 K and 25 % are found in the lower parts of these platforms' profiles in N1.

Compared to the ground measurements, all airborne platforms of the northern comparisons report in average 0-1.5 K higher temperatures. The relative humidity values are correspondingly drier (appr. 5 %), where SUMO has the closer agreement for most comparisons. There are at least two likely reasons for these discrepanices. Firstly, the airborne platforms were landed/taken down at a site 50-100 meter from the AWS. This horizontal difference might be enough for the observed, relatively small discrepancies to occur. Secondly, these platforms travel through the lower surface layer relatively fast. It is therefore not unlikely that the platforms do not appropriately report values for an eventual super adiabatic surface layer.

The results from the southern sites (Kerlingar 1 and 2) however, are quite different from those of the northern site. The observed differences have a multi faceted character. One part of these is seen as a more or less constant deviation between the platforms' measured profiles.

A second, more interesting difference, is the observed disagreement between almost all inversion heights. In this respect, comparison S2 is an extreme example where the heights of both the higher and the less evident lower inversion disagree by as much as 200 m. Additionally, these height shifts have different signs, indicating no constant offset in the platforms' altitude estimations as otherwise could be suspected. Furthermore, SUMO ascent/descent profile pairs show similar disagreements in inversion heights. Examples are found for 13th of August in S2 and S4 as well as in S6 for the 14th of August. As between the SUMO and KALI inversions, also some of these height shifts have different signs.

A third type of difference is observed in S3, where the lapse rates of the corresponding KALI and SUMO profiles differ, KALI having the steeper.

In general, the same probable reasons for the described disparities between these platforms' soundings exist as for those of the latter section. To summarize, these are related to 1) the platforms themselves, 2) the instrumentation of these and 3) spatial and temporal atmospheric variability.

The platforms of the intercomparison and their instrumentation

From an initial point of view, the tethersonde was in this comparative study expected to provide the better reference data. However, as it turned out, its measurement were dominated by an irregular warm/dry bias and therefore hard to compare with the other platforms. The magnitude of the temperature bias was in some cases over +5 K, which is e.g. about twice as much as can be expected due to rising thermals. After an inspection of the raw data, the most probable reason was found to be solar radiation. It was e.g. found a distinct warm/dry bias at altitude levels where the tethersonde was stopped for several minutes. Though, no clear connection between the solar azimuth angle and the instrument orientation was found as for SUMO in Chapter 3. Another factor is the age of the tethersonde instrumentation. This is now close to 15 years (Tor de Lange, personal communication) and age is e.g. a known quality deteriorating factor for radiosonde instrumentation (M04).

Another instrumentation related factor, is offset due to calibration errors. For the northern sites, more or less constant differences of 0.5 K and 5-10 % between SUMO and KALI are found. A similar trend is also seen for the tethersonde data. For the southern sites, the observed offsets are larger. Still, their systematic character strongly suggests a relation to calibration errors. In this context, the change of SUMO aircraft and belonging instrumentation might play a role in the observed increase in differences.

The observed height shifts of inversions however, are probably not platform or sensor related as there is no systematic deviation which would be expected in that case. The reason for both these and the observed difference in lapse rates are therefore most probably related to atmospheric temporal and spatial variability. An extensive data base of meteorological information from the FLOHOF campaign is available. In addition to the previously mentioned data (e.g. observations, AWS and PiBal), also WRF model simulations for the SUMO measurement days are available (PhD work of Stephanie Mayer, May 2008). The corresponding model setup is described in Chapter 5 (Section 5.1.1). Together, these meteorological data form the basis for the following discussion on atmospheric variability as a probable cause of the observed disparities.

Atmospheric temporal and spatial variability

There are in general two main reasons for such variability to occur, either mechanical effects (e.g. waves/shear) or thermal/convective activity (Stull, 1988).

The measurements North of Hofsjökull are discussed firstly.

Only weak winds (< 5 m/s throughout the lower troposphere) were observed during the northern measurement days. Thus, eventual mechanical effects are not believed to be of a significiant magnitude to cause the observed disparities. However, there was observed convective activity in the form of a Stratocumulus cloud cover in the evening of both the 17th and the 18th of August. Furthermore, when considering temperature

and relative humidity curves from the AWS nearby Ingfolfsskáli (N3b), a typical diurnal signal is found (Figure A.9 and A.10, Appendix A). In addition, soundings from WRF model simulations, as e.g. presented for the 18th of August in Chapter 5 (Figure 5.1), show a convective ABL depth growth. This growth is in the same order as observed between the SUMO and KALI soundings of N7 (150 m, 10-11:00 UTC) and probably explains the difference observed there. The second prominent difference between SUMO and KALI was found in N1. Also in this comparison, the soundings were performed with almost an hour apart. The slightly more stable KALI profile in this example might e.g. suggest the presence of a decaying nocturnal boundary layer. Moreover, for N2, the differences in both start times (1 min) and inversion heights were negligible. These factors strongly suggest temporal atmospheric variability as the main cause of the observed disparities.

A potentially difference enhancing factor is spatial variability. As for the radiosonde intercomparison, also the platforms of this intercomparison were operated at slightly different locations. Between SUMO and KALI, the typical horizontal difference was around 2-3 km. It is therefore not unlikely that flights over e.g. the river nearby or factors such as katabatic drainage flow can have influenced the KALI measurements and caused them to be colder /more humid at lower levels.

For the southern days, significantly larger deviations are found between the platform soundings. Firstly, the southern days did have more sun and therefore possibly also stronger convective activity. Strong thermals are known to cause high temporal and spatial variability in ABL depth (e.g. Stull, 1988; Banta and White, 2003). Furthermore, variability in boundary layer height can also be expected in regions dominated by complex topography. Such variability is potentially enhanced by large scale flow. Lieman (1993) found in a model/in-situ experiment in Israel that "a significant horizontal shift in the maximum PBL height relative to the mountains, is induced by a corresponding displacement of the thermal ridge due to the mountains, in the presence of large scale flow". The measurement locations of this intercomparison were indeed situated in complex terrain, especially the southern sites. The days of the southern locations did also have a significant, prevailing synoptic flow from North East, which coincided with the direction of Hofsjökull and thereby with the potential of creating gravity waves on the lee side. Indications of waves in the atmosphere were observed at site the 13th and 14th in the form of Altocumulus lenticularis clouds.

To further assess the presence of atmospheric variability as a potential uncertainty factor, vertical sections and horizontal fields from the 1 km WRF model simulations were investigated. Representative results from these simulations are presented in Figure 4.15. These do of course not necessarily show the physical truth, but should have the potential of revealing atmospheric flow patterns of relevance to the above mentioned measurement uncertainty. The results can be summarized as follows.

- Hofsjökull North, 17-18.08.2007: A relatively stable meteorological situation, calm wind conditions in the area on and around Hofsjökull. A generally well mixed ABL.

- Hofsjökull South, 13-14.08.2007: A lee-side wake is evident in the horizontal fields and vertical sections the 13th and 14th of August. The wake is located at, around and to the South West of the measurement position of the 13th. A slight shift of the wake to the East, and a corresponding move in measurement location to the West, brought the measurements' ground location out of this wake on the 14th. The position of this wake coincides with experienced wind conditions at the measurement sites. Upstream winds were observed by PiBal soundings and estimated to around 10 m/s at the same days. Moreover, a stable layer is evident in vertical sections close to the heighest point on Hofsjökull. A wind speed decrease with height is observed at the downstream side. There are also signs of downslope wind acceleration on the South West side of Hofsjökull during these southern days. Winds up to 15 m/s on 14th were observed by the AWS HS15, some kilometers South West of the mountain top. These factors indicate gravity waves in the atmosphere, probably also breaking at the downstream side of Hofsjökull on the 13th and 14th. Furthermore, the relatively steep slope of the isentropes on the downstream side indicates a hydraulic jump. Clouds with shapes witnessing about this phenomenon were observed on the 13th. (e.g. Figure A.5, Appendix A).

The model simulations shown in Figure 4.15 further confirms the impression gained by the above stated discussion. Far more dynamical atmospheric conditions are observed for the southern than for the northern measurement locations. It is therefore reasonable to suggest the described temporal and spatial atmospheric variability as the main reason for the contrasting results from the measurements North and South of Hofsjökull.

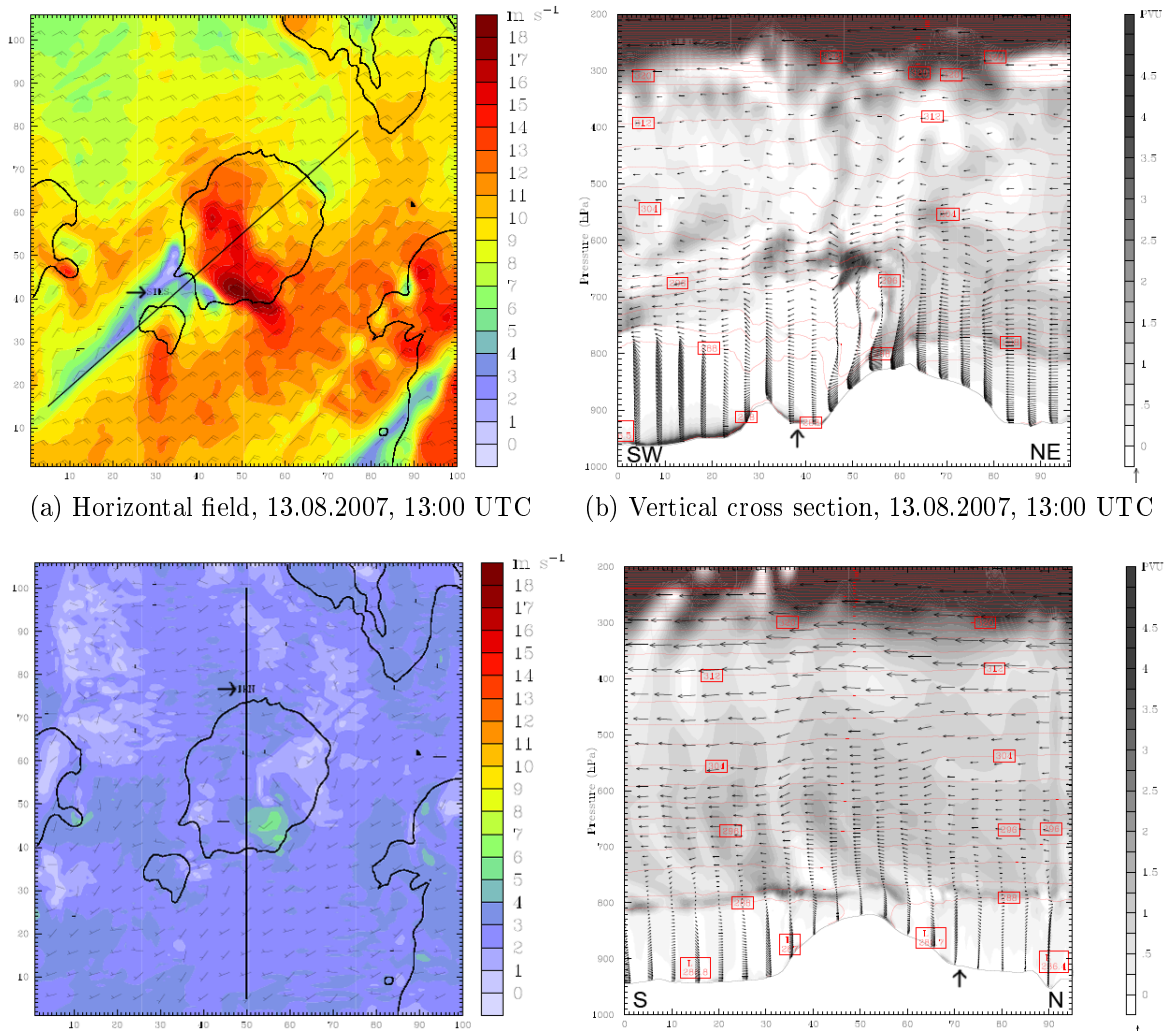

(a) Horizontal field, 13.08.2007, 13:00 UTC

(b) Vertical cross section, 13.08.2007, 13:00 UTC

(c) Horizontal field, 18.08.2007, 13:00 UTC

(d) Vertical cross section, 18.08.2007, 13:00 UTC

Figure 4.15: *WRF model simulations 13:00 UTC of 13th and 18th of August. Horizontal fields (a) and (c) show wind speed and direction at 50 m above ground. Vertical cross sections (b) and (d) for the black lines indicated in the horizontal fields show topography, wind vectors, potential vorticity (grey shaded contours) and isentropes (contour interval; 2K, red lines). The x and y axis of the horizontal fields are given in km units. Similar for the vertical sections, but the y axis is atmospheric pressure in hPa. The measurement locations are indicated by black arrows and Hofsjökull is seen as the central element in all figures.*

4.2.6 Summary

When performing in-situ intercomparison studies as here reported, the meteorological situation plays an important role. The highly dynamical conditions observed and also simulated for the southern part of this experiment showed out to be very interesting, but unfavourable for intercomparison purposes. The results from the northern site however, are very promising for the measurements of SUMO. A very close agreement is seen between the temperature and relative humidity profiles from the well established KALI UAV system and those of SUMO. The existing, smaller differences can mainly be attributed to the inevitable atmospheric temporal and spatial variability. These factors are also likely to be the main cause of disparity between the ground data and the profiles from the airborne platforms. Also the platforms themselves and their instrumentation are potential sources of uncertainty. The tethersonde was in this latter experiment expected to provide the better reference data. However, as is turned out, these data were affected by a warm/ dry bias and were therefore unfortunately of a very limited value for the experiment.

Both comparative studies of this chapter have shown very promising results for the quality of the SUMO data. The improvement gained by correcting for the time-lag error is also clearified, especially for the low temperatures experienced during the Svalbard campaign. In the future, more comparative studies will be performed. An on going project on Northwest-Iceland (the Gufuskalar project), where a 412 m high mast is equipped with meteorological instrumentation, can provide such possibilities. In addition, a new tethersonde system is now available at the Geophysical Institute. This system has the capability of performing measurements at 6 different altitude levels and an intercomparison with this system could form the basis for a corresponding future experiment. There are also plans on a cooperative project with the Norwegian Navy, where an abandoned military base can be used for an intercomparison with radiosondes and tethersondes.

Chapter 5

Potential meteorological applications in the future

The intention of this chapter is to sketch the potential of the SUMO system for future applications. Some of these require a further improvement of the system while others are already within the reach of its current state. An example in the latter category is the validation of boundary layer simulations by numerical forecast models. The corresponding study of this chapter was made possible through the PhD work of Stephanie Mayer where the Weather Research and Forecasting (WRF) model is run for the SUMO measurement days under FLOHOF. The corresponding model data are available since May, 2008. Consequently, only a brief and preliminary discussion will be given here. The main focus of this study will be set on the model's ability to predict the boundary layer growth and structure. This is pursued by an intercomparison of model soundings with real, measured SUMO soundings. In the first part of this chapter, the WRF model and the setup used for the numerical simulations are shortly described. Thereafter, central results will be presented and shortly discussed. At the end of the chapter, additional potential applications are presented together with a short scientific background and corresponding future technical development of SUMO.

5.1 Validation of a numerical model's boundary layer profiles

5.1.1 The WRF simulations

The numerical data used in this study are obtained using the Weather Research and Forecasting (WRF) model (Wang et al., 2008). The simulations are performed in real mode for the SUMO measurement days under FLOHOF. Reanalysis data from the European Centre for Medium-Range Weather Forecasts (ECMWF) are used to initialize

and force the model at its boundaries every 6 hours. For topography, 30 second data are used. There are three interactively nested model domains (9 km, 3 km and 1 km), with the finest one covering the Hofsjökull area and the 3 km domain covering most of Iceland. 60 vertical layers are used with the lower one at approximately 15 m above ground. The simulations include radiative processes and parameterizations for the boundary layer[1] but exclude cloud physics.

The presented soundings are obtained every 30 minute using the 1 km resolution data at the gridpoint closest to the coordinates of each measurement site (Ingolfsskáli and Kerlingar 1, Figure 4.5). The vertical layers' distribution is illustrated by the red dots in the 07:00 sounding of Figure 5.1.

5.1.2 Results

Only the corrected descent profiles from SUMO are used in this study since these are in general found to be less biased than the ascent profiles. The SUMO profiles are matched to the closest 30 min. WRF sounding. Since the main interest here is to compare the development of the boundary layer structure, no absolute values of temperature or relative humidity will be discussed. The presented profiles are therefore plotted with an offset of 2 K and 20 % between each 30 minute sounding. In addition, the x-axis of the associated figures are adapted to the profiles' start times. This implies that the difference between two temperature profiles is equal to 2 K in addition to/minus eventual heating or cooling of the atmosphere.

Data from the nearby AWS (N3b) will be used as reference to estimate the accuracy of the two's measurements/calculations of the lowest level temperature and relative humidity values. The AWS ground data are averaged over a 10 minute interval around each half an hour. All time information referred to in this study is given in UTC.

5.1.3 18.08.2007, Ingolfsskáli

Temperature

In general, the WRF profiles this day show a typical growth of a convective boundary layer as described by e.g. Stull (1988). Before 08:30, the lower 250 m of the WRF profiles are nearly isothermal, indicating the remainder of a stable nocturnal boundary layer. By 09:00, this layer is no longer evident and a neutral, mixed layer (ML) starts to form. At the same time, also a super adiabatic surface layer in the lower 20 meters starts evolving. Thereafter, a rapid ABL growth occurs which lasts until 15-16:00 where a stable ABL height of around 1400 m is reached. The next stage is a decay in ABL height and a sharpening of the capping inversion is seen between 18 and 19:00. A

[1] more details on the corresponding schemes are given in Appendix C

corresponding narrowing of the entrainment zone between the stable, free atmosphere (FA) above, and the ML below, is observed in this latter period of time.

Compared to the SUMO profiles, the model is in general seen to predict the temperature lapse rates ($\frac{dT}{dz}$) very accurately. Both the profiles of the ML below the capping inversion, and the FA above, are in close agreement. However, there are also some disagreements. These are mainly seen for the 8:30 and 9:00 SUMO profiles where there is no capping inversion in the corresponding WRF profiles. In the 10:00 profiles however, the agreement between the two is within the instrument accuracy of SUMO as far as up to 2400 m above ground level. Over this height, a more complex structure is seen for the three first SUMO profiles than in the corresponding WRF profiles. The most prominent difference is observed around the ABL height in the 18:00 profiles. In these profiles, the inversion gradient, the corresponding temperature increase and the ABL height itself are of larger magnitudes in the SUMO profile. A possible explanation for this disparity could be an underestimation of the energy input in the model (e.g. radiation).

Considering the ground temperature data, the model is in general seen to predict these very well. The larger offsets are found during morning and late in the afternoon. It is interesting to see that both SUMO and WRF differ from the ground data at 18:00. An interpretation could be an underestimation of a super adiabatic surface layer, or simply spatial variability.

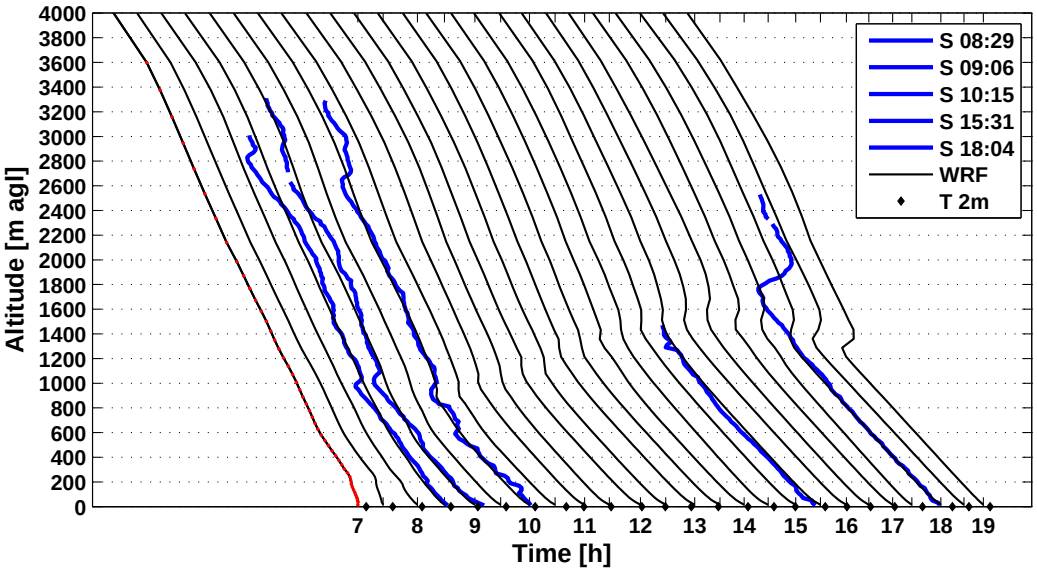

Figure 5.1: *SUMO and WRF temperature profiles, 18.08.2007 Ingolfsskáli. Corresponding ground data are given by black dots. The vertical layers in the model are indicated by red dots on the 07:00 profile.*

Relative humidity

As could be expected, the profiles of relative humidity show more variability between SUMO and WRF than those of temperature. The general trends though, are largely the same as a fairly close agreement is seen for the respective vertical gradients. However, in contrast to the temperature inversion seen at 18:00, the corresponding relative humidity gradient is in the same order for both the SUMO and the WRF profiles. Still, a certain height shift is seen also in these profiles.

As for temperature, the WRF simulations predict the ground relative humidity data very accurately. The larger differences are also here found during morning and late in the afternoon. However, in contrast to what was the case for temperature, both the SUMO and WRF profiles match the 18:00 ground value perfectly.

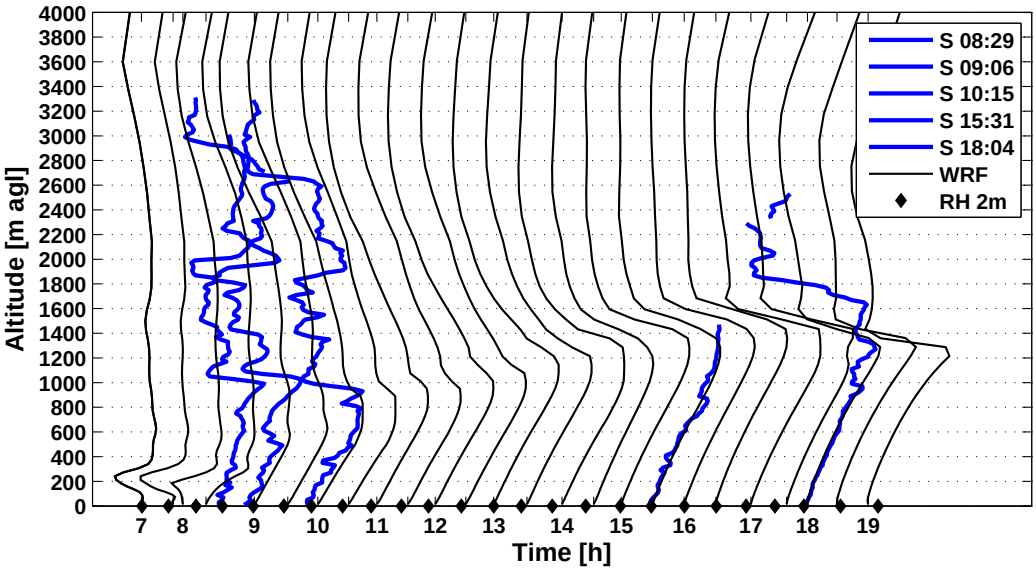

Figure 5.2: *As in Figure 5.1, but for relative humidity.*

5.1.4 13.08.2007, Kerlingar 1

Temperature

As discussed in Chapter 4, the soundings this day were dominated by a highly dynamical boundary layer. In the profiles presented here, this fact is reflected by far more complicated vertical structures than for the 18th. The upper parts of these profiles are dominated by an inversion, probably originating from subsidence (starting at appr. 2800 m). A corresponding inversion is seen in the radiosonde sounding from Keflavik.

Similar to the profiles of the 18th, there are signs of a convective growing ABL, at least until 15:00 where the ABL top is found around 1400 m. After this timestamp however, the lapse rate is seen to vary from every half an hour and also the capping ABL inversion disappears. In addition, an increase in stability with height is found around the altitude at where the capping inversion previously was located. A physical interpretation of this latter finding could be entrainment of more stable air masses from the FA above. Eventual breaking of gravity waves (as discussed in Chapter 4) is in this context likely to be a contributing factor to the associated turbulent mixing.

When considering the SUMO profiles however, the capping inversion is still visible at this later stage of the day. Still, a slight increase in stability with height is seen, also in the SUMO profile.

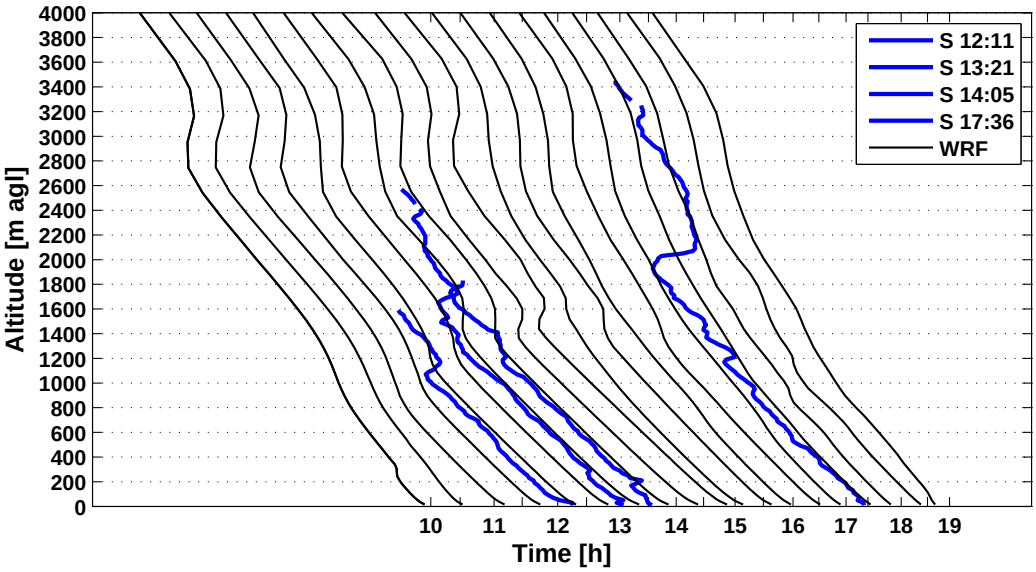

Figure 5.3: *SUMO and WRF temperature profiles, 13.08.2007.*

Relative Humidity

When examining the relative humidity profiles this day, the trend is similar as for temperature. A far more complicated vertical structure is seen in these profiles than for the 18th.

In general, the model profiles agree very well with the SUMO profiles, at least until 14:00. Similar to the temperature profiles, also in the relative humidity profiles there are signs of a transition in the profile trends at around 15:00. The corresponding decrease in relative humdity may also be explained by entrainment of FA air from above.

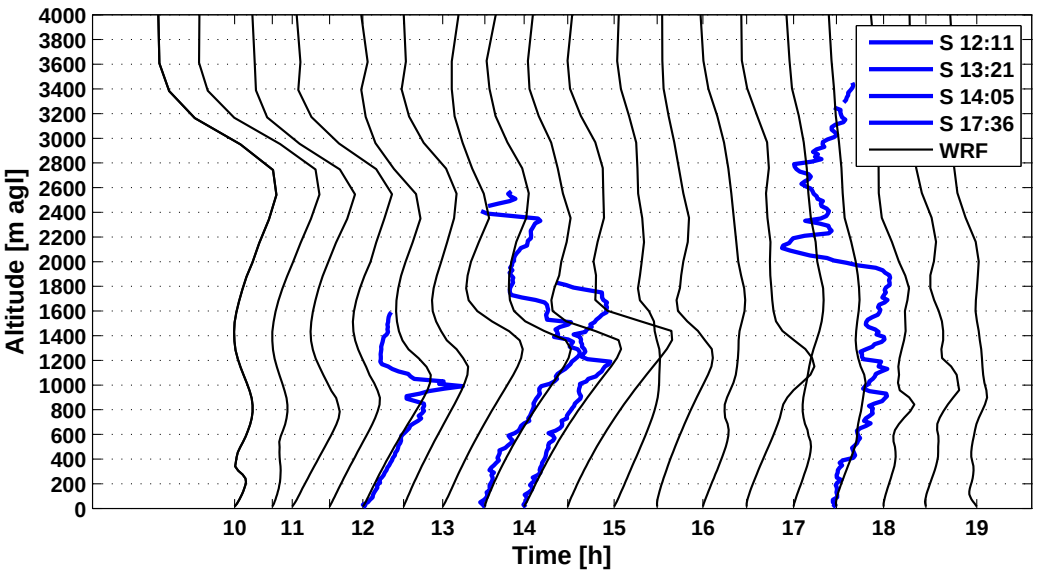

Figure 5.4: *As in Figure 5.3, but for relative humidity.*

5.1.5 Future corresponding applications

For future corresponding model validation tasks, it is desirable to perform more frequent soundings at e.g. 15 or 30 minute intervals. This way, it will be possible to obtain a higher temporal resolution. This would be especially important for measurements of highly dynamical atmospheric boundary layers as here discussed for the 13th of August.

An important atmospheric feature in this respect is the entrainment zone between the FA and the ML (e.g. for dispersion of pollution (Hanna and Yang, 2001)). This highly fluctuating and thin atmospheric layer, dominated by large spatial and temporal variability, is in general hard to assess by conventional measurement systems such as full size aircrafts. These aircrafts are e.g. not capable of performing the described measurements without disturbing the studied phenomenon by their own presence. In addition, radiosondes, that are often used for corresponding boundary layer research (e.g. Hennemuth and Lammert, 2006; Joffre et al., 2001), are only able to penetrate this layer at a single point. Furthermore, no horizontal measurements can be done by radiosondes.

A solution is the utilization of several UAVs at the same time, also referred to as "swarms" or "flocks" (Buschmann et al., 2004). UAVs are able to penetrate this highly fluctuating layer at several points in space with a minimum of influence to the measurements.

A simultaneous operation of several aircrafts for meteorological measurements have not yet been perfomed by SUMO. However, as described in Chapter 2, the potential lays within the system and will be investigated in near future.

5.2 Future scientific applications

In this section, additionally scientific applications, in which SUMO can make a central contribution in the future, are described.

5.2.1 Energy exchange over leads, polynyas and in the marginal ice zone

Leads and polynyas are characterized by large, but not exactly quantified heat fluxes. Up to 1000 W/m^2 have been reported from single measurements and determined by model calculations. Such open water areas are thus estimated to account for up to one half of the overall heat exchange between the Arctic ocean and the atmosphere above (Wadhams, 2000). The associated air-sea-ice interactions have a crucial role in the global climate system (e.g. Andreas and Cash, 1999). The understanding of the related heat and moisture fluxes and the improvement of the corresponding numerical parameterization schemes, necessitate in-situ measurements (Tjernström et al., 2005),

especially with respect to temperature and humidity profiles over the areas in question. The availability of such empirical observations however, is greatly limited by the lack of infrastructure and the harsh conditions prevailing in the polar region. In addition, heavy cloud cover often limits the use of satellites (Inoue and Curry, 2004) and manned aircraft operations are often considered too expensive or dangerous in the area. Hence, there is a need for a small, cost efficient and recoverable platform such as the SUMO UAV capable of performing the needed measurements.

During the Spitsbergen campaign, SUMO proved its viability for measurements under rough Arctic conditions with temperatures down to -20 ^{o}C and winds up to 15 m/s. The system also showed its high flexibility as it was operated from the relatively narrow area of a vessel's helicopter deck. As vessels are the main means of transportation in the representative region, this is a key property of the system and its potential in corresponding future applications should be large.

A technical improvement of direct importance to such applications is protection against icing. No corresponding problems were encountered during the Svalbard campaign, but operations in the humid air over e.g. leads and polynyas might cause icing on the airframe. For the small aircrafts intended for SUMO, only passive systems are possible to integrate. In this context, appropriate fuselage and wing coating, as discussed for the Aerosonde (Curry et al., 2004), could be an alternate.

5.2.2 The stable (nocturnal) boundary layer (SBL)

The stable boundary layer is often characterized by complex horizontal and vertical structures, especially with respect to wind (Stull, 1988). A related phenomenon is the nocturnal jet, which may accellerate to supergeostrophic speeds of over 20 m/s and occurs at heights in the order of 200 m. Together with the high stability dominating this lower part of the atmosphere, these two factors form to counteracting forces. The jet tends to generate turbulence (by shear) while the staticly stable layer below tends to suppress it. The result is short bursts of turbulence which potentially cause mixing throughout the SBL. In contrast to the lower part of the SBL, the upper part often exhibits a more complex structure and is also less available for ground based measurements. Thus, UAVs such as SUMO are platforms capable of closing the observational gap in areas where this phenomenon occurs, e.g. during the polar night in the Antarctic where corresponding work is already carried out (Kroonenberg et al., 2007).

5.3 Future technical improvements of the SUMO system

During the operations of SUMO and also in the subsequent study of this thesis, several potentials of technical improvements for the system have been identified. Some of these

can minimize or even eliminate certain discovered measurement errors.

For future applications of SUMO, it is desirable to install an additional altitude sensing device. This could e.g. be in the form of an acoustic sensor as used as parking distance sensors for cars or even a laser altimeter. Such an installation would greatly lower the safety limit for operations near ground. For the meteorological measurements, the value is a potentially drastic reduction of the observed ground heating effect, described in Chapter 3 and Chapter 4, as this effect can presumably be close to eliminated through flying low altitude circles. These circles would also reduce the impact of profile irregularities when switching from autonoumous to manual flight mode. In addition, this extra altitude sensing system will be an important step towards fully autonomous landings.

Also the SUMO airframe might be subject to a future change and/or improvement. The FunJet has proven as a very flexible and also easy-to-handle aircraft. Still, there are some evident limitations in the application of this airframe. The FunJet has e.g. very limited payload capacitites. A future implementation of new instruments for direct wind measurements and also higher capacity batteries allowing for extensive horizontal survey measurements of phenomena such as capping inversions, desire a larger aircraft. For this purpose, the KALI aircraft might be a solution and the possibilities of employing that airframe will be investigated in near future. The KALI is well built and an integration of the Paparazzi autopilot system should be a straight forward task (pers. comm. Martin Müller). In addition to wind sensors, also instrumentation such as ozone sensors, aerosol counters and a hygrometer for the measurement of relative humidity, will be considered. The latter one might reduce the current problems experienced with time-lag in relative humidity measurements.

Alternative battery technology based on lithium iron phosphate is also under testing by Paparazzi members. These have a somewhat lower energy density than the currently used LiPo cells, but should potentially enable operations under even lower temperatures. The implementation of such batteries is therefore potentially important for future missions in the Arctic as described in this chapter.

Several of the measured meteorological profiles have smaller discontinuities owing to short telemetry failures. The planned solution is the implementation of an on-board datalogger corresponding to the memory sticks used in mobile phones and digital cameras. This will also provide with redundancy in case of more severe telemetry problems. In addition, the antenna used for telemetry so far has been the main limitation to the maximum flight ceiling. A stronger gain antenna will therefore be used for future missions.

An update is also underway for the IR sensors used for attitude determination. The future SUMO aircrafts will be using digital versions that can be mounted in the wing-tips. These will most likely lower the minimum temperature contrast (required for attitude stabilization) between ground and sky and will also be more sustainable against damage under rough landings (as were experienced on Svalbard). In the longer run, a

real inertial measurement unit (IMU) should be implemented to provide possibilities of measurements through clouds.

So far, no calibration of the SUMO instrumentation has been performed. For future scientific applications, calibration devices for the sensors will be developed and brought in-field for use before every mission.

In some temperature profiles, signs of an impact of solar radiation are found. In this respect, the associated errors have a less deterministic character than those of time-lag. Their influence is of a significant magnitude and solutions to eliminate them must be found. One such solution could be numerical correction, as proposed by (Luers, 1997) for radiosonde measurements. Another solution could be an improved sensor housing, which also could provide protection against sensor contamination.

Chapter 6

Summary

The SUMO project at the University of Bergen was initiated to create an economical and flexible platform that can be operated as a recoverable radiosonde for boundary layer research. During the 5 week field campaign FLOHOF, July/August 2007, a prototype of the SUMO system successfully performed its first environmental test. Over 30 profiles of temperature, relative humidity and wind were performed up to 3.5 km above ground. Before this campaign, no meteorological measurements had been made and the autopilot system it is based on had only been operated up to 400 m above ground. It is therefore no overstatement to say that the system performed well beyond the initial expectations.

The development of a modern UAV system is a multidisciplinary challenge involving both atmospheric science and aircraft engineering and technology. The key to the success of SUMO has been the close cooperation between the Experimental Meteorology group at the Geophysical Insitute and Paparazzi. Through their provision of a turn-key, open source autopilot system, and extensive competence in the area of micro UAVs, it has been possible to develop a fully operable meteorological UAV system within a relatively short period of time and at a very favourable price.

The main advantages of the Paparazzi based SUMO system is its ease of use and unique flexibility. Under a second field campaign, on and around Spitsbergen, spring 2008, the SUMO ground station was operated exclusively by scientists rather than UAV specialists. This demonstrates a user-friendliness which by far exceeds that of larger UAV systems and which makes it suitable for use by e.g. smaller university groups. Furthermore, the system also demonstrated its great flexibility as it was operated from the relatively narrow area of a vessel's helicopter deck. The system also proved to be operable in temperatures down to -20 ^{o}C and winds up to 15 m/s. The Arctic is a key area for intended use of the system and the information gained by this second field-campaign is therefore invaluable to future planning and development of SUMO.

Moreover, the small sized aircraft used for SUMO also sets limitations to the on-board, meteorological instrumentation. As a consequece, a compromise between weight, power consumption and technical properties had to be made when the corresponding sen-

sors were selected. Both combined temperature and relative humidity sensors adapted to the system so far have inherent limitations, where a slow response time is found to be the most prominent one. Due to its deterministic character, the resulting time-lag error has to a large extent been possible to correct for. Also other sources of errors in the form of solar radiation and sensor contamination have been identified. The latter sources of error however, are of a less quantifiable character and further investigations are therefore needed in order to identify appropriate means of avoiding their influence on the measured data.

The error source assessment was the first of two important steps that had to be taken to clear the path for future scientific applications. The second main part of this thesis involved a validation of the SUMO measurements by a comparison with data from corresponding, well established profiling systems. During the FLOHOF campaign, this was made possible through a co-location of measurements by SUMO, a tethersonde and the remotely piloted KALI UAV. The outcome of this intercomparison was largely in the favour of SUMO as its data quality is shown to be on an equal, or even higher level than those of its counterparts. This study also demonstrated the need of ensuring stable meteorological conditions for the validity of such experiments. Moreover, a similar study was made possible by the Svalbard campaign, spring 2008, where SUMO was operated simultaneously with a state of the art Vaisala RS92 radiosonde. The results are promising and suggest a data quality comparable to that of the latest, well established sounding system. SUMO represents a unique measurement system with large potential for novel measurement strategies in boundary layer research. A central future application of SUMO will be the validation of model parameterization schemes by 3D atmospheric measurements with spatial and temporal resolution unreachable by present day systems.

Bibliography

E. L. Andreas and B.A. Cash. Convective heat transfer over wintertime leads and polynyas. *Journal of Geophysical Research*, 104(C11):25,721 25,734, 1999.

F.I. Badgley. Response of radiosonde thermistors. *The Review of Scientific Instruments*, 28(12):1079–1084, 1957.

R. M. Banta and A. B. White. Mixing-height differences between land use types: dependence on wind speed. *Journal of Geophysical Research*, 108(D10):ACL 1–11, 2003.

P. Brisset, A. Drouin, M. Gorraz, P. Huard, and J. Tyler. The Paparazzi Solution, 2006. http://www.recherche.enac.fr/paparazzi/papers_2006/mav06_paparazzi.pdf.

M. Buschmann, J. Bange, and P. Vörsmann. MMAV A Miniature Unmanned Aerial Vehicle (Mini-UAV) for Meteorological Purposes. In *16th Symposium on Boundary Layers and Turbulence*, pages 1–7, Portland/Maine, USA, 2004.

B. H. Connell and D. R. Miller. An Interpretation of Radiosonde Errors in the Atmospheric Boundary Layer. *Journal of Applied Meteorology*, 34:1070–1081, 1995.

J. A. Curry, J. Maslanik, G. Holland, and J. Pinto. Applications of Aerosondes in the Arctic. *Bulletin of the American Meteorological Society*, 85(12):1855–1861, 2004.

J. Egger, S. Bajrachaya, R. Heinrich, P. Kolb, P. Lämmlein, M. Mech, J. Reuder, W. Schäper, P. Shakya, J. Schween, and H. Wendt. Diurnal Winds in the Himalayan Kali Gandaki Valley. Part III: Remotely Piloted Aircraft Soundings. *Monthly Weather Review*, 130(8):2042–2058, 2002.

J. Egger, L. Blacutt, F. Ghezzi, R. Heinrich, P. Kolb, S. Lämmlein, M. Leeb, S. Mayer, E. Palanque, J. Reuder, W. Schäper, J. Schween, R. Torrez, and F. Zaratti. Diurnal Circulation of the Bolivian Altiplano. Part I: Observations. *Monthly Weather Review*, 133(4):911–924, 2005.

F. Guichard, D. Parsons, and E. Miller. Thermodynamic and Radiative Impact of the Correction of Sounding Humidity Bias in the Tropics. *Journal of Climate*, 13(20): 3611–3624, 2000.

S.R. Hanna and R. Yang. Evaluations of Mesoscale Models Simulations of Near-Surface Winds, Temperature Gradients, and Mixing Depths. *Journal of Applied Meteorology*, 40:1095–1104, 2001.

B. Hennemuth and A. Lammert. Determination of the atmospheric boundary layer height from radiosonde and lidar backscatter. *Boundary-Layer Meteorology*, 120:181–200, 2006.

G. J. Holland, T. McGeer, and H. Youngren. Autonomous Aerosondes for Economical Atmospheric Soundings Anywhere on the Globe. *Bulletin of the American Meteorological Society*, 73(12):1987–1998, 1992.

S. R. Hudson, M.S. Town, V.P. Walden, and S.G. Warren. Temperature, Humidity, and Pressure Response of Radiosondes at Low Temperatures. *Journal of Atmospheric and Oceanic Technology*, 21(5):825–836, 2004.

J. Inoue and J.A. Curry. Application of Aerosondes to high-resolution observations of sea surface temperature over Barrow Canyon. *Geophysical Research Letters*, 31(14): L14312, 2004.

Kangas M. Joffre, S. M. and, M. Heikinheimo, and S. A. Kitaigorodskii. Variability Of The Stable And Unstable Atmospheric Boundary-Layer Height And Its Scales Over A Boreal Forest. *Boundary-Layer Meteorology*, 99(3):429–450, 2001.

T.G. Konrad, M.L. Hill, J.R. Rowland, and Meyer J.H. A small, radio-controlled aircraft as a platform for meteorological sensors. *Applied Physics Laboratory Technical Digest*, 11:11–19, 1970.

A.C. van den. Kroonenberg, T. Spiess, M. Buschmann, T. Martin, P.S. Anderson, F. Beyrich, and J. Bange. Boundary layer measurements with the autonomous mini-UAV M2AV. In *DACH Conference on Meteorology*, Hamburg, Germany, 2007.

J. S. Langford and K. A. Emanuel. An Unmanned Aircraft for Dropwindsonde Deployment and Hurricane Reconnaissance. *Bulletin of the American Meteorological Society*, 74(3):367–375, 1993.

U. Leiterer, H. Dier, A. Kats, T. Naebert, D. Nagel, D. Althausen, K. Franke, and F. Wagner. Correction Method for RS80-A Humicap Humidity Profiles and Their Validation by Lidar Backscattering Profiles in Tropical Cirrus Clouds. *Journal of Atmospheric and Oceanic Technology*, 22(1):18–29, 2004.

R. Lieman. Investigation of the planetary boundary layer height variations over complex terrain. *Boundary-Layer Meteorology*, 62(1-4):129–142, 1993.

J. K. Luers. Temperature Error of the Vaisala RS90 Radiosonde. *Journal of Atmospheric and Oceanic Technology*, 14(6):1520–1532, 1997.

A. Mahesh, V.P. Walden, and S.G. Warren. Radiosonde Temperature Measurements in Strong Inversions: Correction for Thermal Lag Based on an Experiment at the South Pole. *Journal of Atmospheric and Oceanic Technology*, 14(1):45–53, 1997.

L. M. Miloshevich, V. Holger, A. Paukkunen, A.J. Heymsfield, and S.J. Oltmans. Characterization and Correction of Relative Humidity Measurements from Vaisala RS80-A Radiosondes at Cold Temperatures. *Journal of Atmospheric and Oceanic Technology*, 18(2):135–156, 2001.

L. M. Miloshevich, A. Paukkunen, H. Vömel, and S. Oltmanns. Development and Validation of a Time-Lag Correction for Vaisala Radiosonde Humidity Measurements. *Journal of Atmospheric and Oceanic Technology*, 21(9):1305–1327, 2004.

L. M. Miloshevich, H. Vömel, D.N. Whiteman, B.M. Lesht, F.J. Schmidlin, and F. Russo. Absolute accuracy of water vapor measurements from six operational radiosonde types launched during AWEX-G and implications for AIRS validation. *Journal of Geophysical Research*, 111(D9), 2006.

Multiplex, 2006. http://www.multiplexusa.com/Support/manuals/Planes.

NORUT, 2008. http://projects.itek.norut.no/UAV/.

J. Reuder, P. Brisset, M. Jonassen, M. Müller, and S. Mayer. SUMO: A Small Unmanned Meteorological Observer for atmospheric boundary layer research. *IOP Conference Series: Earth and Environmental Science*, 1:DOI: 10.1088/1755–1307/1/1/012014, 2008.

B. E. Schwartz and C.A. Doswell. North American Rawinsonde Observations: Problems Concerns, and a Call to Action. *Bulletin of the American Meteorological Society*, 72 (12):1885–1895, 1991.

S. M. Skony, J.D.W. Kahl, and N.A. Zaitseva. Differences between radiosonde and dropsonde temperature profiles over the arctic ocean. *Journal of Atmospheric and Oceanic Technology*, 11(5):1400–1408, 1994.

J. R. Soddell, K. McGuffie, and G. Holland. Intercomparison of Atmospheric Soundings from the Aerosonde and Radiosonde. *Journal of Applied Meteorology*, 43(9):1260–1269, 2004.

R. B. Stull. *An Introduction to Boundary Layer Meteorology*. Kluwer Academic Publishers, 1988.

M. Tjernström, M. Ẑagar, G. Svensson, J. J. Cassano, S. Pfeifer, A. Rinke, K. Wyser, K. Dethloff, C. Jones, T. Semmler, and M. Shaw. Modelling the Arctic Boundary Layer: An Evaluation of Six Arcmip Regional-Scale Models using Data from the Sheba Project. *Boundary-Layer Meteorology*, 117:337–381, 2005.

Vaisala. Vaisala Radiosonde RS92-SGP, 2006. http://www.vaisala.com/weather/products/.

P. Wadhams. *Ice in the ocean.* Gordon and Breach Science Publishers, 2000.

J. Wang. Evaluation of performance of the dropsonde humidity sensor. In *Eighth Symposium on Integrated Observing and Assimilation Systems for Atmosphere, Oceans, and Land Surface*, Seattle, WA, 2004.

J. Wang, H.L. Cole, D.J. Carlson, E.R. Miller, K. Beierle, A. Paukkunen, and T.K. Laine. Corrections of Humidity Measurement Errors from the Vaisala RS80 Radiosonde Application to TOGA COARE Data. *Journal of Atmospheric and Oceanic Technology*, 19(7):981–1002, 2002.

W. Wang, D. Barker, J. Bray, C. Bruyere, Duda, J. M. Dudhia, and J. Michalekes. User's Guide for Advanced Research WRF (ARW) Modeling System Version 2.2. *NCAR Tech. Note*, page 21, 2008.

D. S. Wilks. *Statistical Methods in the Atmospheric Sciences*, volume 91 of *International Geophysics series.* Academic Press, 2. edition, 2005.

Appendix A

Meteorological data, SUMO measurement days

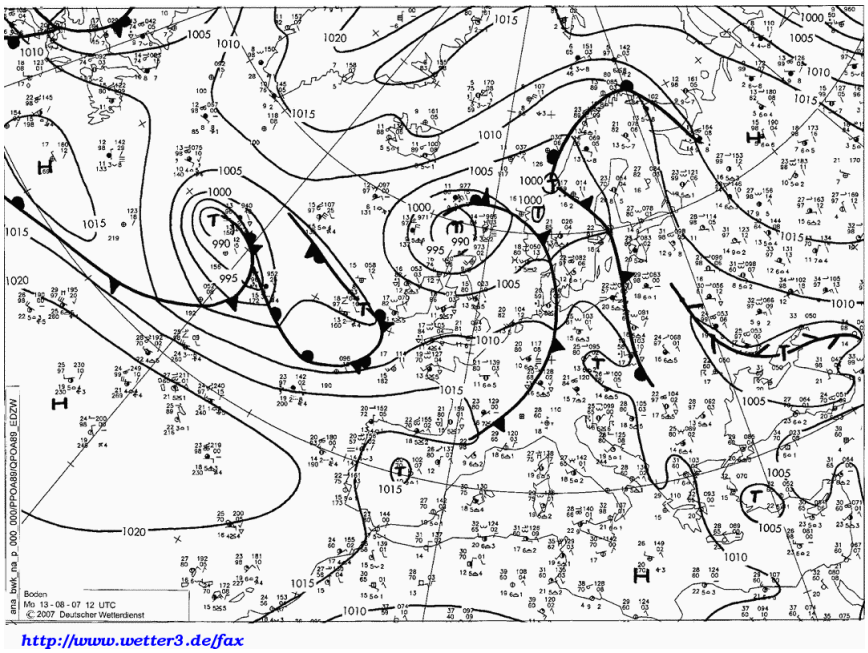

(a)

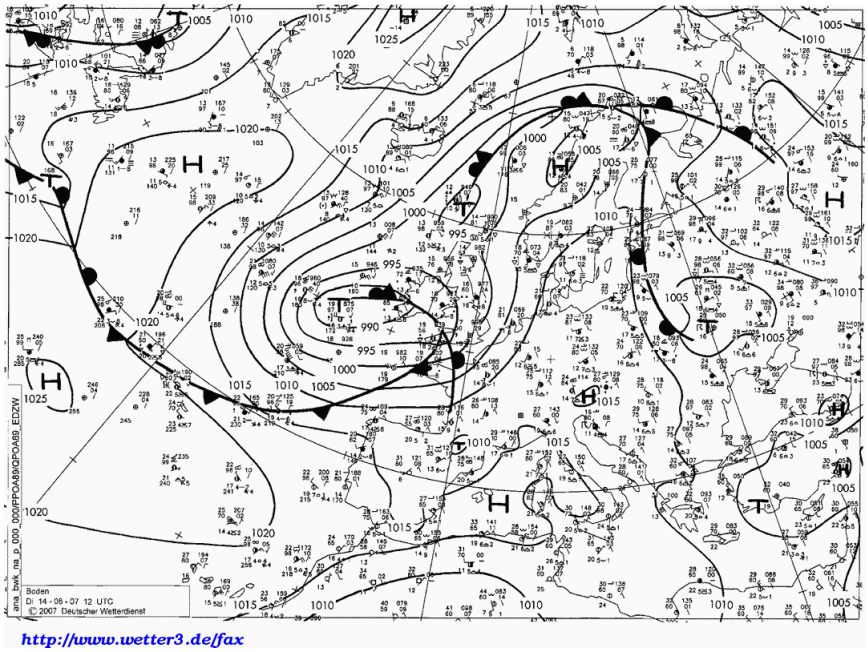

(b)

Figure A.1: *Synoptic charts 13th and 14th of August, valid 12:00 UTC. Aquired from Deutscher Wetterdienst.*

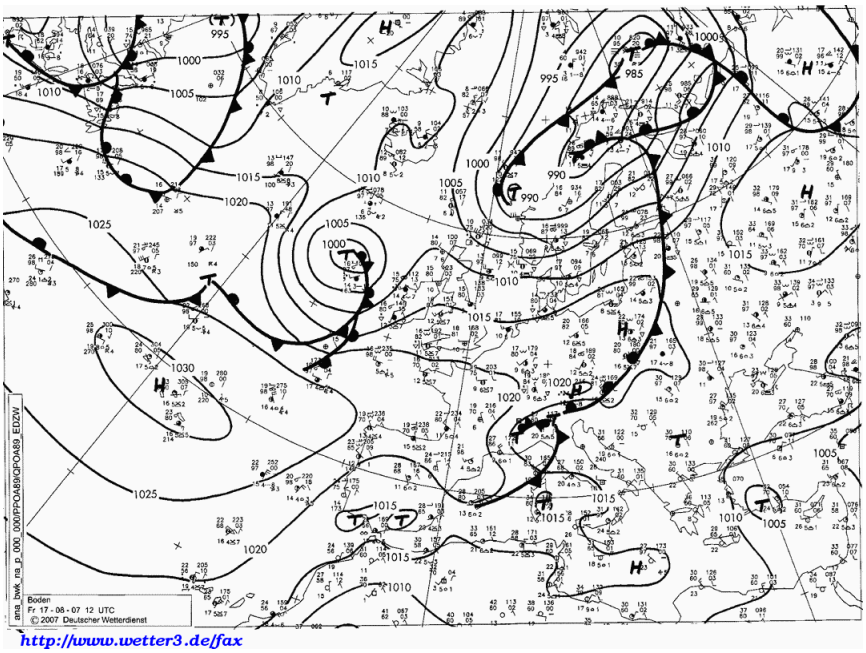

(a)

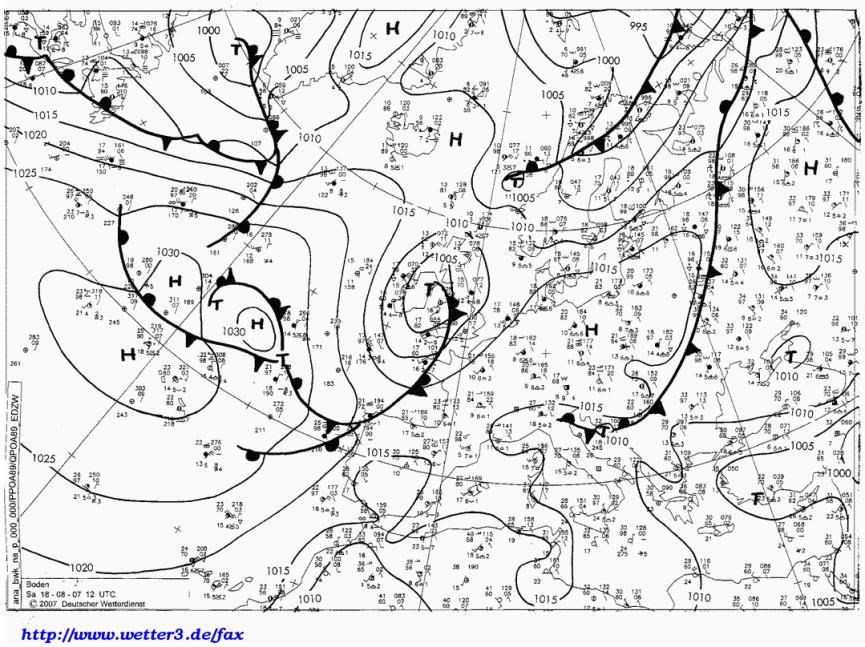

(b)

Figure A.2: *Synoptic charts 17th and 18th of August, valid 12:00 UTC. Aquired from Deutscher Wetterdienst.*

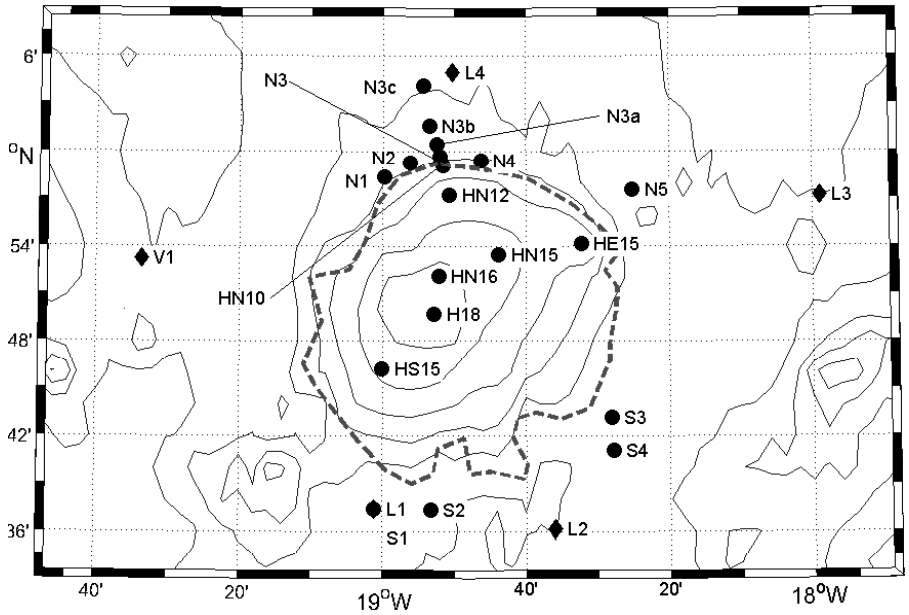

Figure A.3: *Map showing the geographical positions of the FLOHOF automatic weather stations. The glacier edge is indicated by a grey, dashed line (- -).*

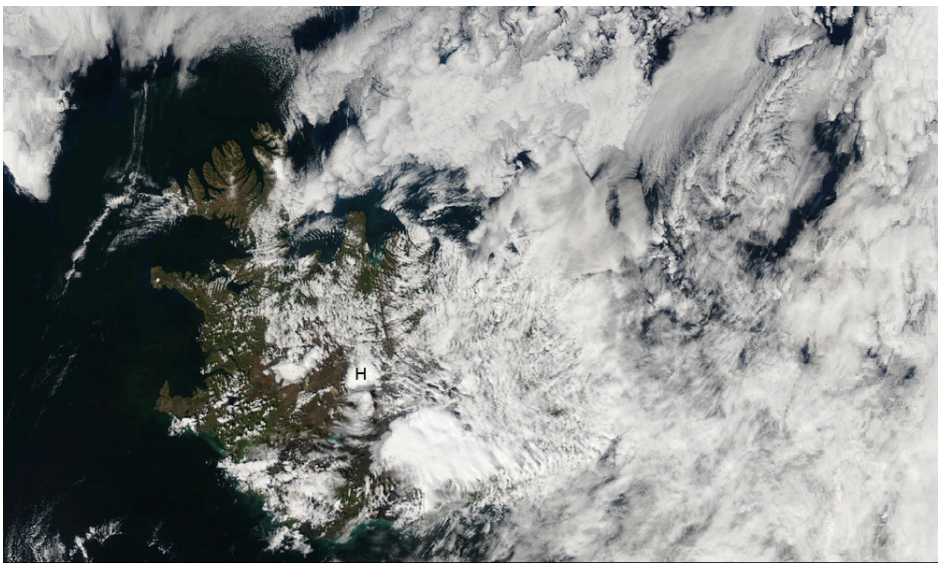

Figure A.4: *Satellite image over Iceland, 13.08.2007, 13:30 UTC. The "H" indicates the position of Hofsjökull. The image is from a NASA Modis satellite, aquired from the Satellite Receiving Station of Dundee University in Scotland.*

Figure A.5: *Picture taken 13.08.2007 of a cloud over Hofsjökull, possibly indicating a hydraulic jump. Courtesy of Joachim Reuder.*

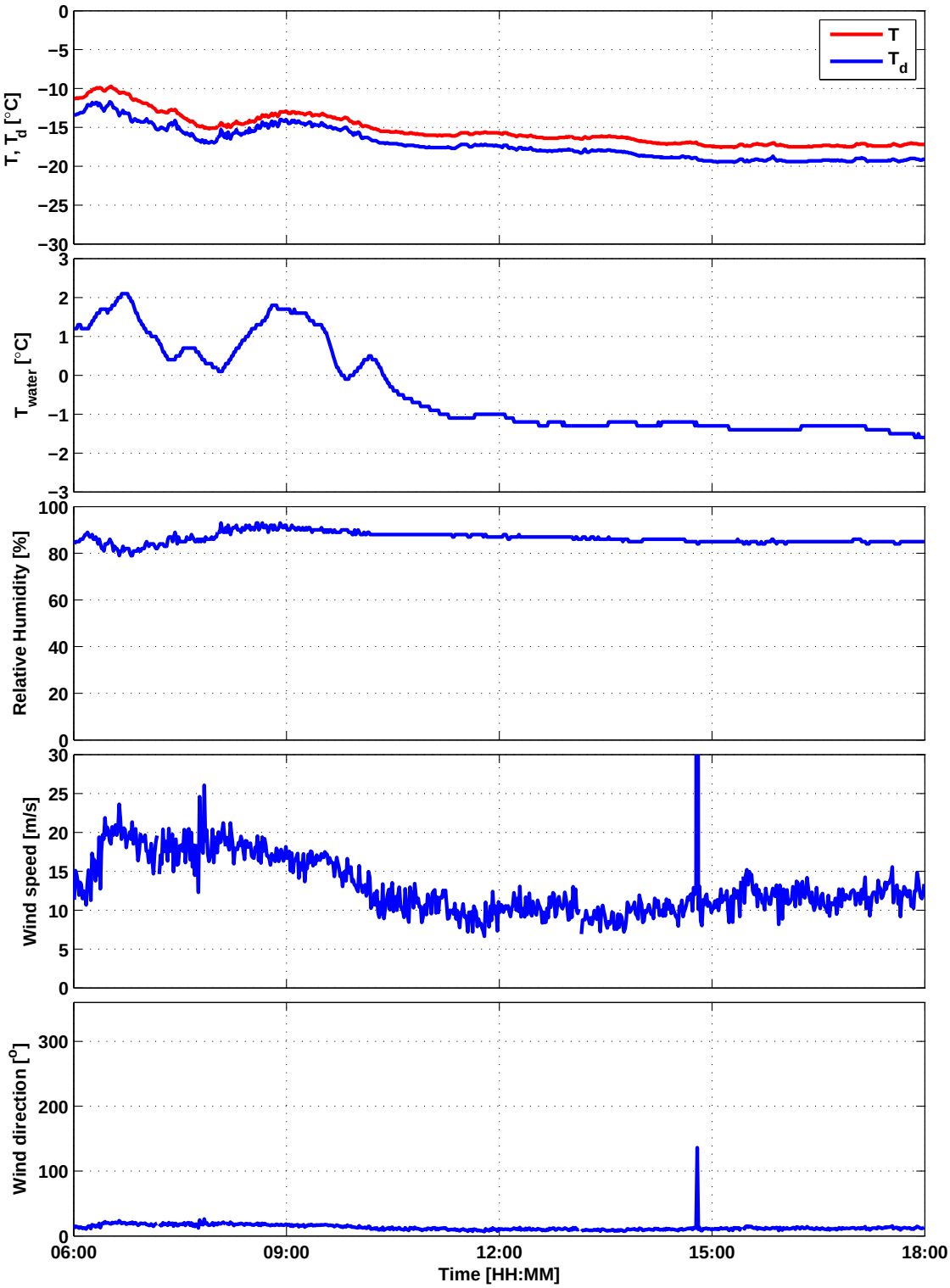

Figure A.6: *Temperature (dry and dew point), sea surface temperature, relative humidity, wind speed and direction, 28.02.2008, East of Spitsbergen. Measured by instrumentation on KV Svalbard.*

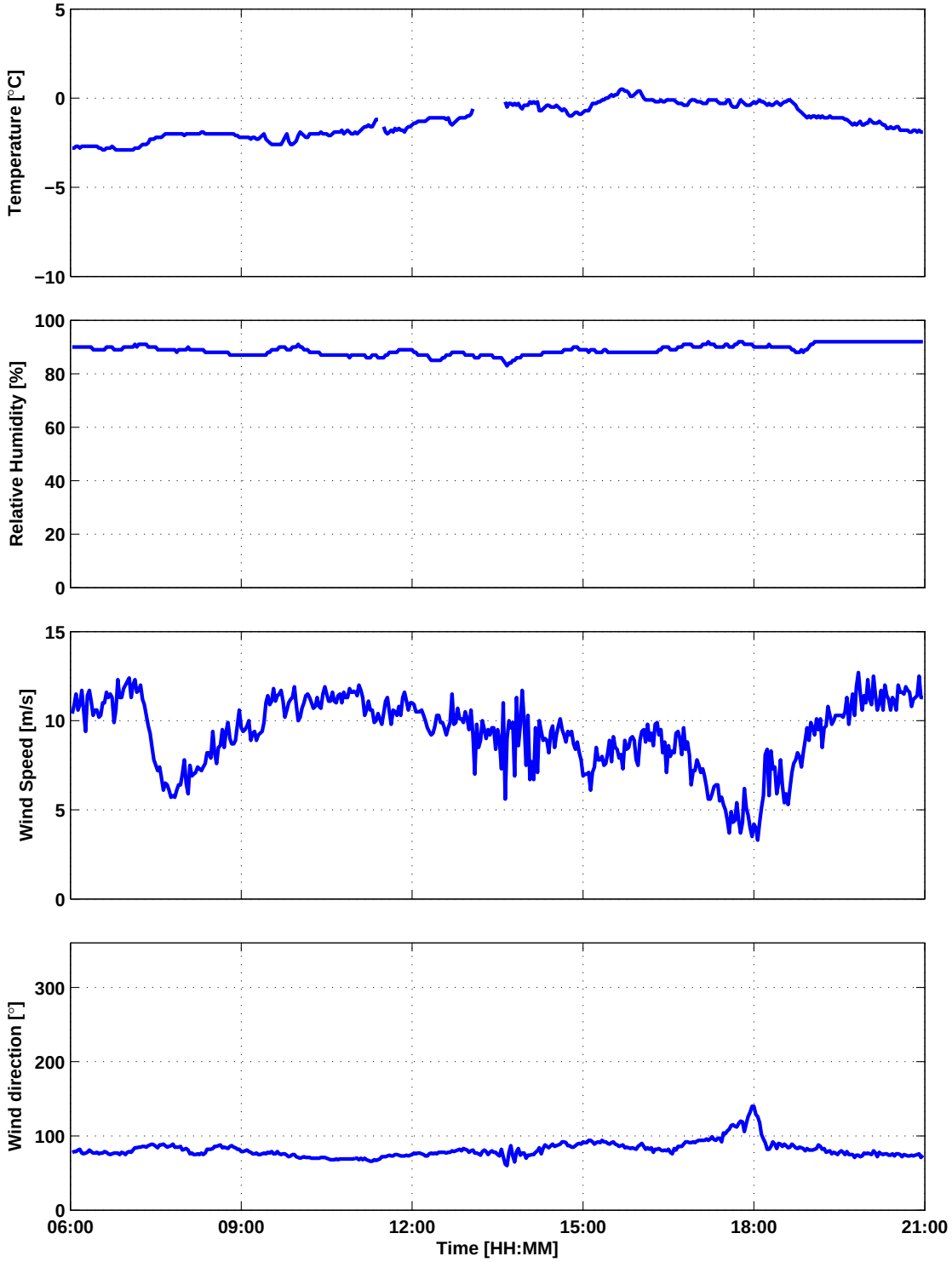

Figure A.7: *Temperature, relative humidity, wind speed and direction, 13.08.2007. Measured by station HS15, Hofsjökull.*

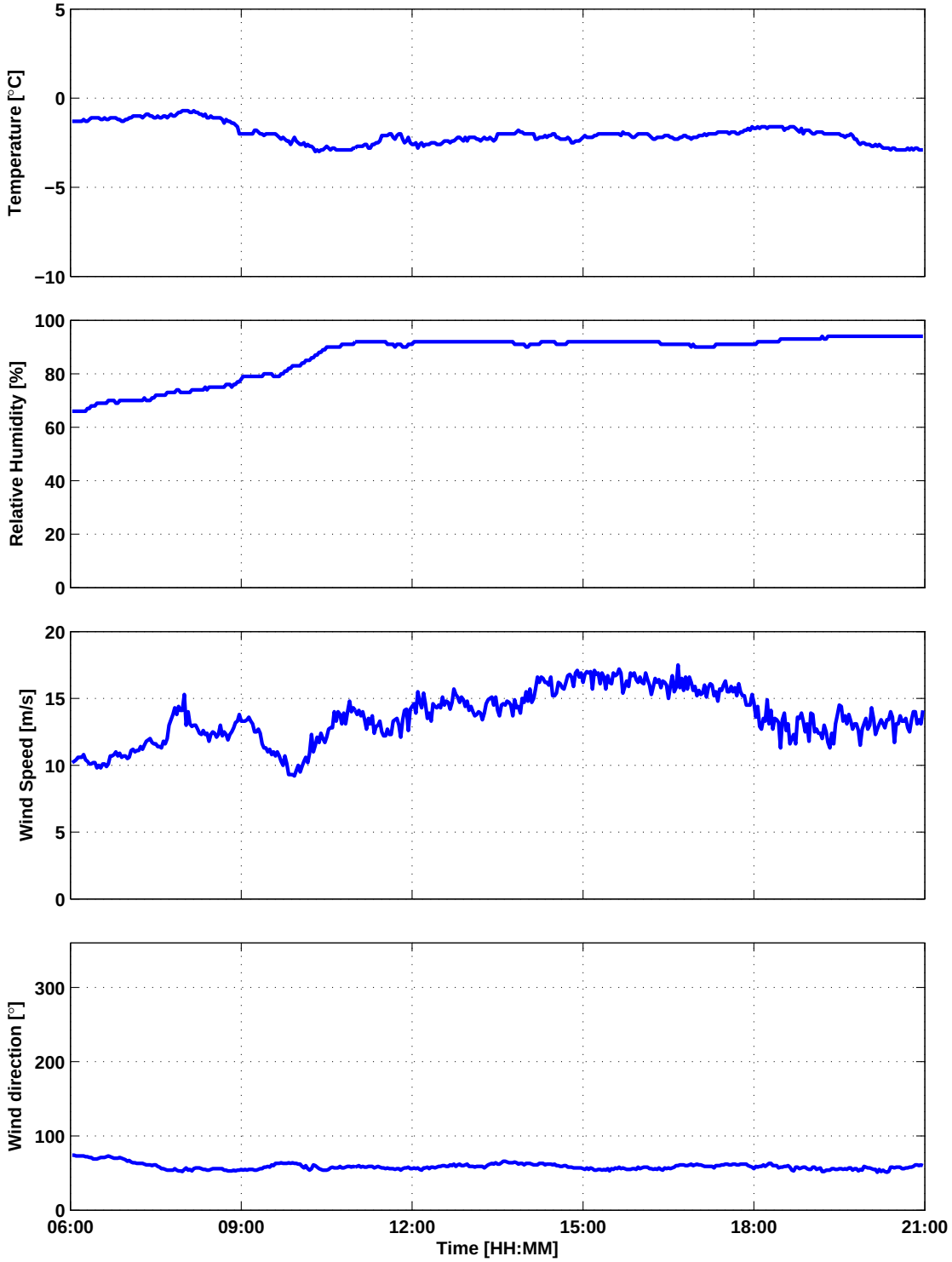

Figure A.8: *Temperature, relative humidity, wind speed and direction, 14.08.2007. Measured by station HS15, Hofsjökull.*

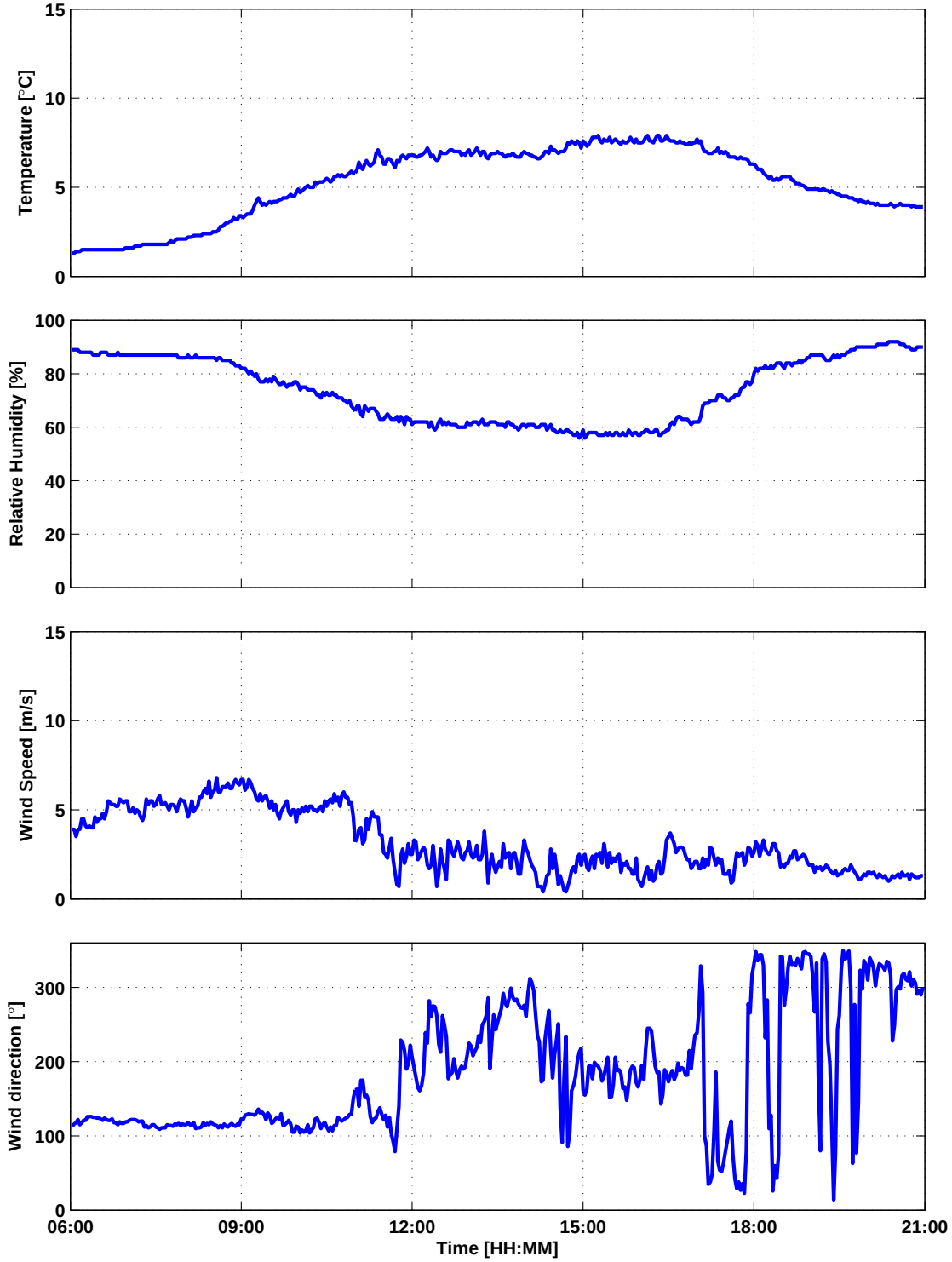

Figure A.9: *Temperature, relative humidity, wind speed and direction, 17.08.2007. Measured by station N3b, at the position of Ingolfsskáli.*

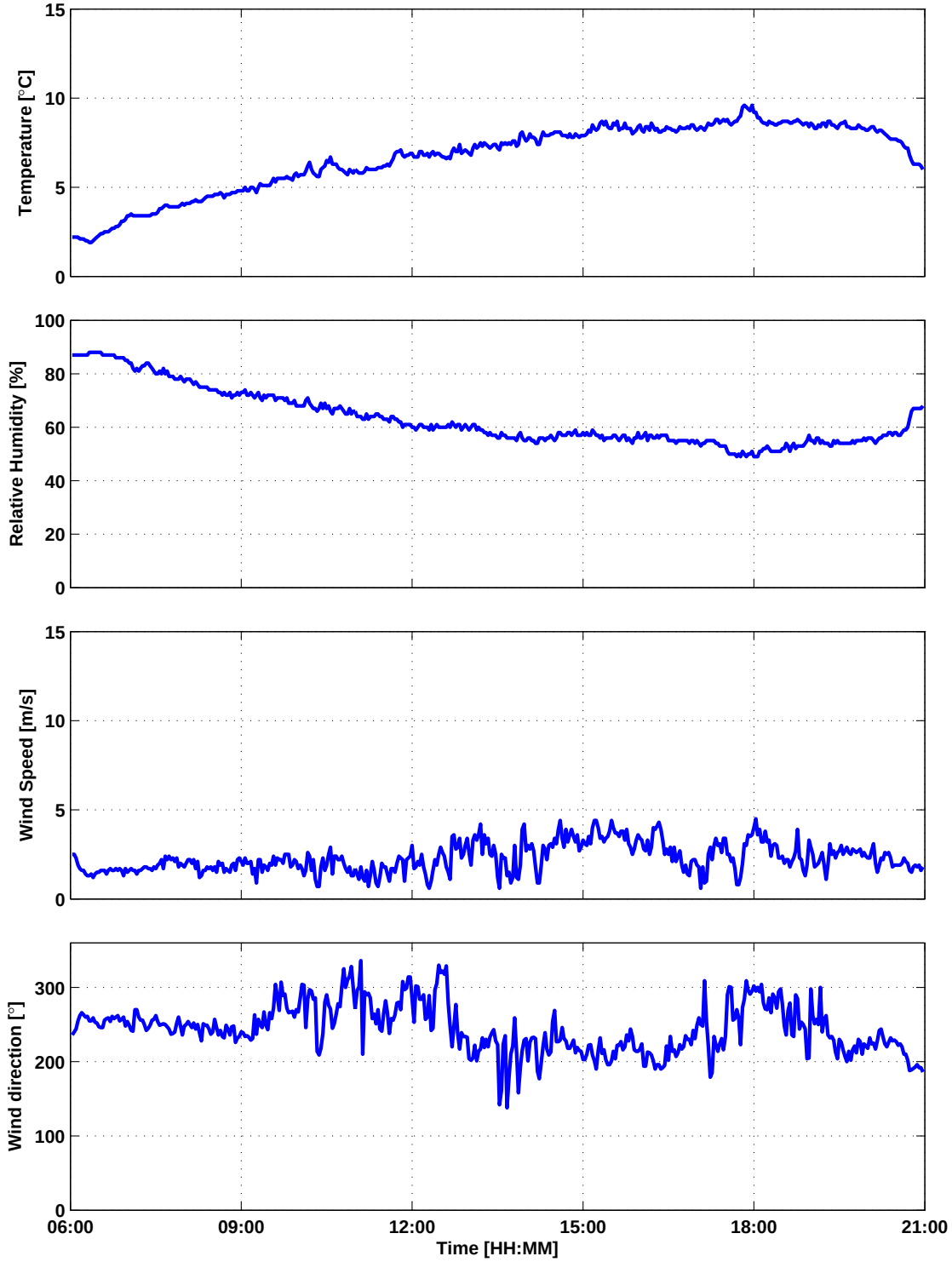

Figure A.10: *Temperature, relative humidity, wind speed and direction, 18.08.2007. Measured by station N3b, at the position of Ingolfsskáli.*

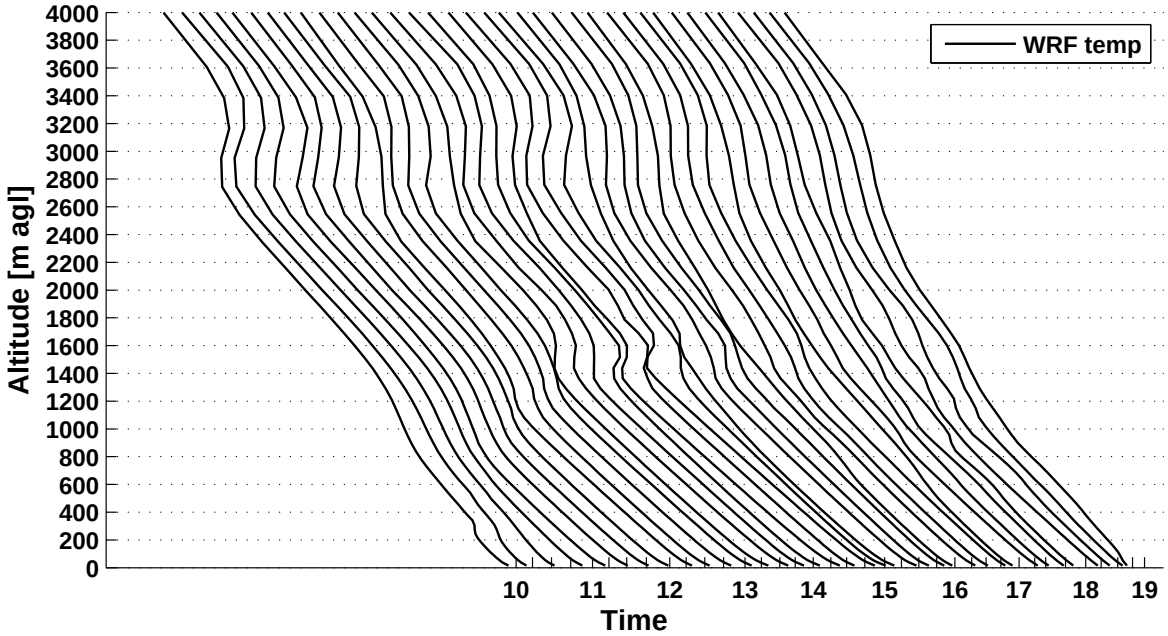

Figure A.11: *WRF temperature profiles,15 min, 13.08.2007 Ingolfsskáli*

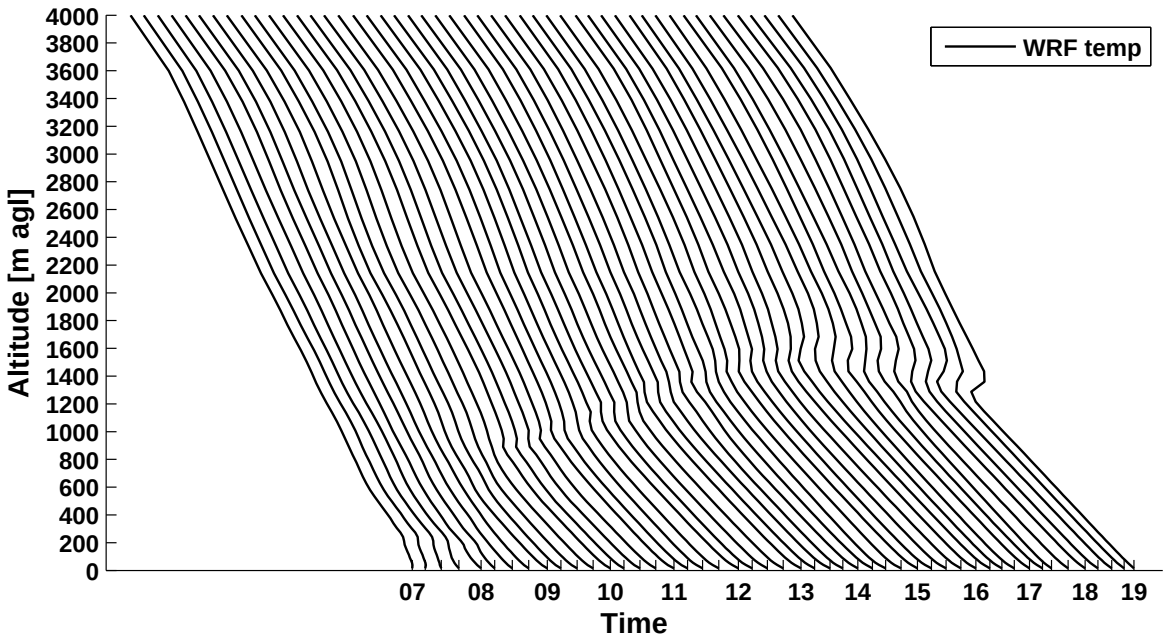

Figure A.12: *WRF temperature profiles, 15 min, 18.08.2007 Kerlingar 1*

Appendix B

Tables

Table B.1: Details on SUMO soundings made under FLOHOF. "Ho." indicates that the flight pattern is made horizontally. Soundings marked "x" are used for the time constant estimation of Chapter 3

ID	Date (local time)	start time (UTC)	end time (UTC)	max height (m agl)	air-craft name	location	comment
1	13.08.2007	11:03	11:36	432	FUN2	Kerlingar 1	-
2	13.08.2007	12:04	12:21	1615	FUN2	Kerlingar 1	x
3	13.08.2007	13:11	13:28	2599	FUN2	Kerlingar 1	x
4	13.08.2007	13:48	14:10	1858	FUN2	Kerlingar 1	x
5	13.08.2007	15:01	15:23	525	FUN2	Kerlingar 1	Ho.
6	13.08.2007	15:52	16:09	432	FUN2	Kerlingar 1	Ho.
7	13.08.2007	16:38	17:04	438	FUN2	Kerlingar 1	Ho.
8	13.08.2007	17:25	17:49	3479	FUN2	Kerlingar 1	x
9	14.08.2007	12:47	13:09	2463	FUN2	Kerlingar 2	x
10	14.08.2007	13:46	14:22	2571	FUN2	Kerlingar 2	x
11	14.08.2007	15:46	16:02	1021	FUN2	Kerlingar 2	-
12	14.08.2007	16:11	16:26	828	FUN2	Kerlingar 2	crash
13	15.08.2007	18:50	19:03	970	FUN3	Ingolfsskáli	-
14	16.08.2007	20:30	20:47	982	FUN3	Ingolfsskáli	x
15	16.08.2007	20:49	21:12	1488	FUN3	Ingolfsskáli	x
16	17.08.2007	09:22	09:52	484	FUN3	Ingolfsskáli	-
17	17.08.2007	09:57	10:19	975	FUN3	Ingolfsskáli	x
18	17.08.2007	11:03	11:28	2395	FUN3	Ingolfsskáli	x
19	17.08.2007	12:09	12:32	1184	FUN3	Ingolfsskáli	x
20	17.08.2007	13:17	13:43	87	FUN3	Ingolfsskáli	test
21	17.08.2007	15:07	15:28	1541	FUN3	Ingolfsskáli	-
22	17.08.2007	15:34	15:58	1271	FUN3	Ingolfsskáli	x
23	18.08.2007	08:16	08:39	3034	FUN3	Ingolfsskáli	x
24	18.08.2007	08:53	09:14	3344	FUN3	Ingolfsskáli	x
25	18.08.2007	10:04	10:27	3321	FUN3	Ingolfsskáli	x
26	18.08.2007	11:27	11:49	994	FUN3	Hofsjökull	x
27	18.08.2007	11:51	12:09	2036	FUN3	Hofsjökull	x
28	18.08.2007	12:11	12:26	337	FUN3	Hofsjökull	-
29	18.08.2007	15:22	15:40	1505	FUN3	Ingolfsskáli	x
30	18.08.2007	17:44	17:56	1022	FUN3	Ingolfsskáli	x
31	18.08.2007	17:56	18:11	2567	FUN3	Ingolfsskáli	x

Table B.2: Details on SUMO soundings made on and around Spitsbergen. Soundings performed in manual flight mode are marked "man."

ID	Date (local time)	start time (UTC)	end time (UTC)	max height (m agl)	air-craft name	location	comment
1	27.02.2008	09:22	09:28	197	FUN3	Van Mijenfj.	test
2	28.02.2008	12:46	12:55	474	FUN3	Storfjorden	-
3	28.02.2008	15:11	15:22	1019	FUN3	Storfjorden	-
4	29.02.2008	08:25	08:39	1428	FUN3	Storfjorden	-
5	29.02.2008	13:32	13:40	384	FUN3	Storfjorden	-
6	29.02.2008	13:57	14:10	1254	FUN3	Storfjorden	-
7	29.02.2008	14:28	14:40	1378	FUN3	Storfjorden	-
8	01.03.2008	07:05	07:12	319	FUN3	Storfjorden	-
9	01.03.2008	10:25	10:35	343	FUN3	Storfjorden	-
10	01.03.2008	10:42	10:50	402	FUN3	Storfjorden	man.
11	01.03.2008	11:20	11:27	348	FUN3	Storfjorden	-
12	04.03.2008	11:34	11:45	512	FUN3	Adventdalen	-
13	05.03.2008	15:19	15:31	309	FUN3	Adventdalen	man.
14	05.03.2008	15:36	15:44	395	FUN3	Adventdalen	man.
15	05.03.2008	15:51	15:59	380	FUN3	Adventdalen	man.
16	06.03.2008	08:25	08:42	1033	FUN3	Adventdalen	-
17	06.03.2008	11:07	11:20	459	FUN3	Adventdalen	man.
18	06.03.2008	11:26	11:42	1361	FUN3	Adventdalen	-
19	06.03.2008	11:49	12:01	1308	FUN3	Adventdalen	-
20	07.03.2008	08:09	08:20	709	FUN3	Adventdalen	man.
21	08.03.2008	06:46	06:52	456	FUN3	Adventdalen	man.
22	08.03.2008	06:53	06:58	431	FUN3	Adventdalen	man.
23	08.03.2008	07:07	07:12	333	FUN1	Adventdalen	man.
24	08.03.2008	07:14	07:17	244	FUN1	Adventdalen	man.
25	08.03.2008	08:07	08:14	639	FUN3	Adventdalen	man.
26	08.03.2008	08:15	08:20	503	FUN3	Adventdalen	man.
27	08.03.2008	08:32	08:38	384	FUN3	Adventdalen	man.
28	08.03.2008	12:41	12:45	440	FUN3	Adventdalen	man.
29	09.03.2008	06:49	07:10	1524	FUN3	Adventdalen	-
30	09.03.2008	07:46	08:02	1172	FUN3	Adventdalen	-

Appendix C

Miscellaneous

C.1 Aeronautics

An aircraft's attitutude is defined by a set of orientational angles. Rotation around the aircraft's longitudinal, lateral and vertical (x, y and z) axes are quantified in terms of these angles which in aeronautics are named roll, pitch and yaw, respectively. The corresponding angles and aircraft-axes are illustrated in Figure C.1.

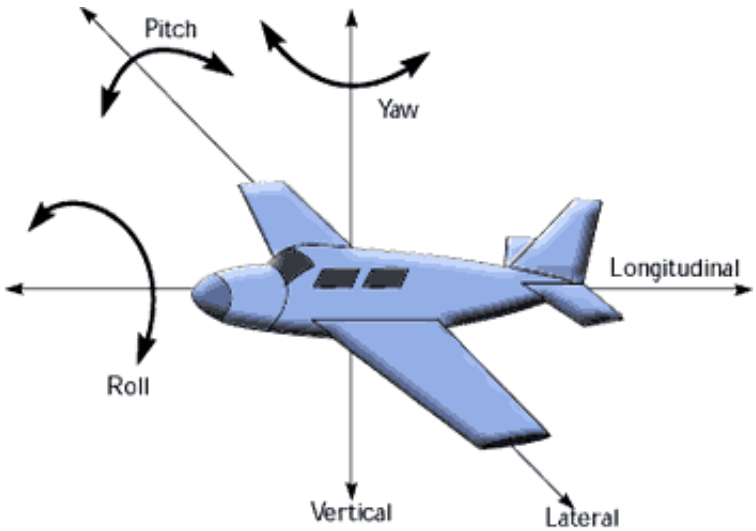

Figure C.1: *Illustration of basic terms within aeronautics. The illustration is found at http://quest.arc.nasa.gov/*

C.2 Statistical methods used in Chapter 3

The definition of the root mean square difference (RMSD) used in the time constant estimation of method 3 is given as (Wilks, 2005):

$$RMSD(x, y) = \sqrt{\frac{1}{n}\sum_{i=1}^{n}(x_i - y_i)^2} \tag{C.1}$$

Where x and y in this study are the 20 meter averaged vectors of SUMO ascent and descent, temperature and relative humidity profiles.

Correspondingly, the mean absolute difference (MAD) is defined as (Wilks, 2005):

$$MAD(x, y) = \frac{1}{n}\sum_{i=1}^{n}|x_i - y_i| \tag{C.2}$$

For the statistics of Figure 3.5 and 3.6, the mean bias difference (MBD) is used and defined as follows (Wilks, 2005):

$$MBD(x, y) = \frac{1}{n}\sum_{i=1}^{n}(x_i - y_i) \tag{C.3}$$

C.3 Parameterization schemes used in the WRF model simulations

- surface layer

  Based on Monin-Obukhov with Carlson-Boland viscous sub-layer and standard similarity functions from look-up tables.

- land surface

  5-layer thermal diffusion. Soil temperature only scheme, using five layers

- planetary boundary layer

  Yonsei University scheme: Non-local K scheme with explicit entrainment layer and parabolic K profile in unstable mixed layer

Appendix D

Paper

The paper "SUMO: A Small Unmanned Meteorological Observer for atmospheric boundary layer research" by J. Reuder, P. Brisset, M. Jonassen, M. Müller, and S. Mayer, is partly based on the results from this master thesis and is therefore attached.

IOP Conf. Series: Earth and Environmental Science **1** (2008) 012014 doi:10.1088/1755-1307/1/1/012014

SUMO: A Small Unmanned Meteorological Observer for atmospheric boundary layer research

J. Reuder[1], P. Brisset[2], M. Jonassen[1], M. Müller[3], and S. Mayer[1]

[1] Geophysical Institute, University of Bergen, Allegaten 70, 5009 Bergen, Norway
[2] Ecole Nationale de l'Aviation Civile (ENAC), 7 avenue Edouard Belin, 31055 Toulouse, France
[3] Orleansstrasse 26a, 31135 Hildesheim, Germany

E-mail:
joachim.reuder@gfi.uib.no
pascal.brisset@enac.fr
marius.jonassen@gfi.uib.no
martin@pfump.org
stephanie.mayer@gfi.uib.no

Abstract. A new system for atmospheric measurements in the lower troposphere has been developed and successfully tested. The presented Small Unmanned Meteorological Observer (SUMO) is based on a light-weighted commercially available model airplane, equipped with an autopilot and meteorological sensors for temperature, humidity and pressure.
During the 5 week field campaign FLOHOF (Flow over and around Hofsjökull) in Central Iceland the system has been successfully tested in July/August 2007. Atmospheric profiles of temperature, humidity, wind speed and wind direction have been determined up to 3500 m above ground. In addition the applicability of SUMO for horizontal surveys up to 4 km away from the launch site has been approved. During a 3 week campaign on and around Spitsbergen in February/March 2008 the SUMO system also proved its functionality under harsh polar conditions, reaching altitudes above 1500 m at ground temperatures of -20 ^{o}C and wind speeds up to 15 m s^{-1}.
With its wingspan of 80 cm, its length of 75 cm and its weight of below 600 g, SUMO is easy to transport and operate even in remote areas. The direct material costs for one SUMO unit, including airplane, autopilot and sensors are below 1200 Euro. Assuming at least several tenths of flights for each airframe, SUMO provides a cost-efficient measurement system with a large potential to close the existing observational gap of reasonable atmospheric measurement systems in between meteorological masts/towers and radiosondes.

1. Introduction

Detailed information on the vertical structure and the horizontal variability of the lower atmosphere, especially with respect to temperature, humidity and wind, is the key for the understanding of exchange processes in the Atmospheric Boundary Layer (ABL). Further improvement of this understanding requires a combination of fine-scale modeling efforts and innovative measurement strategies. Corresponding work is crucial for the validation and improvement of boundary layer parameterization schemes and thus for future progress both in numerical weather prediction and in climate modeling.
Up to now there is a lack of cost efficient measurement systems, applicable for ABL phenomena

© 2008 IOP Publishing Ltd

covering horizontal scales between 100 m up to 10 km. First attempts on the basis of remotely controlled small unmanned aerial vehicles (SUAVs) have already been started some decades ago [1], and the systems have gradually been improved until today. A corresponding profiling system (KALI) has for example been developed at the University of Munich, Germany and has been successfully used during several field campaigns in Nepal, Bolivia and Germany to measure atmospheric profiles of pressure, temperature and humidity up to 3 km above ground (e.g. [2], [3]).
The two main shortcomings of that system are the need of experienced pilots for remote control of the SUAV and the lack of an appropriate wind measurement system. During the last years substantial progress in the field of miniaturization of electronic components has been achieved. As a consequence, miscellaneous autonomous SUAV systems, mainly used as drones for military reconnaissance purposes, have been developed. In addition, smaller, faster and cheaper sensors for meteorological parameters and positioning purposes (e.g. GPS) are available now. Sporadic attempts to use and combine this new technical potential for atmospheric measurements have shown some promising results [4], [5], [6].

2. The SUMO system

The Small Unmanned Meteorological Observer (SUMO) has been developed as a mobile and cost-efficient platform for the determination of the vertical distribution of temperature, humidity, wind speed and wind direction in the ABL and can be operated as "recoverable radiosonde" for boundary layer research. In its recent version, it is based on a commercially available model plane construction kit equipped with an autopilot system and meteorological sensors for the measurement of temperature, humidity and pressure. Figure 1 shows the aircraft and the laptop used as ground control station during SUMO operation.

Figure 1. The SUMO airframe based on the model airplane FunJet by Multiplex and the laptop used as ground control unit.

2.1. Airframe

The construction kit FunJet manufactured by Multiplex is used as airframe of the presented prototype of SUMO. It is a delta-wing pusher prop jet composed of lightweight foam material

EPP (expanded polypropylen), electrically powered by a brushless motor (AXI 2212/26) driving a 9"x 6" propeller. A lithium polymer (LiPo) battery pack with a capacity of 2100 mAh enables a flight endurance of around 20-30 minutes. Due to its size and weight, the SUMO system is highly mobile and easy to operate, even in remote areas and under harsh environmental conditions. The technical details are summarized in table 1.

Table 1. Technical details of the FunJet airframe used as SUMO platform.

length	75 cm
wingspan	80 cm
weight	580 g
average air speed	12-18 m s^{-1}
maximum air speed	35 m s^{-1}
average ascent rate	7-10 m s^{-1}
maximum ascent rate	15 m s^{-1}
maximum altitude above ground	3.5 km
endurance	up to 30 min

The FunJet airframe is quite robust and rather inexpensive (below 100 Euro). Its light weight and the corresponding low speed during landing minimize the risk of structural damage. Additionally EPP can be repaired by instant glue and activator spray within seconds if fractures of the fuselage or wings should occur.

2.2. Paparazzi autopilot system

Paparazzi is an open source autopilot system oriented toward inexpensive autonomous aircraft operation. The system has been designed to be easily adapted to any type of airframe and is currently used in both fixed and rotary wing systems.
It basically consists of:

- the airborne processor board with its required sensors for the determination of the aircrafts attitude (mainly GPS for position and speed and a set of infrared sensors for the horizontal alignment)
- the airborne autopilot software
- the ground control station
- the online communication hardware and communication protocols
- a standard remote control (RC) transmitter as safety link option

The main components of the system are schematically depicted in figure 2. A comprehensive overview of hard- and software setup and configuration as well as the basic principles of operation of the Paparazzi solution can be found in [7] and [8] or on the corresponding home page of the Paparazzi project (http://paparazzi.enac.fr/wiki/index.php/Main_Page).

A powerful flight plan language allows the operator to define complex autonomous missions and create a logical tree of autonomous decisions for the system to make while in flight to perform any task or adapt to any scenario. The ground station operator can also manually navigate the aircraft at any time using video (not installed on SUMO), real-time GPS data, and/or visual contact while relying on the autopilot to perform only the flight stabilization. The ground control station utilizes a powerful and flexible client/server architecture which allows the operator to

Figure 2. The main components of the SUMO system based on the Paparazzi autopilot solution.

control one or more aircraft from a single location or from multiple locations.
As mentioned above, Paparazzi is an open source project. Source code, hardware schematics and thorough documentation are released under the GNU Public License and are freely available for anyone to download from the project website mentioned above.

2.3. Meteorological sensors

SUMO is equipped with sensors for the measurement of pressure, temperature and relative humidity. The pressure sensor is mounted inside the fuselage, while the sensors for temperature and humidity are attached to the fuselage under the wings to provide good ventilation and to minimize heating by solar radiation. Pressure is measured by the miniaturized (diameter 6.1 mm, height 1.7 mm) SCP1000 Absolute Pressure Sensor from VTI Technologies. Its measurement range covers 300 to 1200 hPa with a resolution of 0.015 hPa and an absolute pressure accuracy of 1.5 hPa in the range 600-1200 hPa. The relative pressure accuracy relevant for atmospheric profiling is 0.5 hPa. The pressure sensor is equipped with an onboard temperature sensor that provides in-flight temperature inside the aircraft, an important information for the estimation of battery capacity especially under cold environmental conditions. Temperature and humidity is measured by the sensor DigiPicco I2C manufactured by IST. It combines a PT1000 temperature element with the capacitative humidity sensor P14 SMD. During operation it turned out that the temperature sensor shows a distinctly slower response than the humidity sensor, most likely due to its location on the circuit board behind the humidity sensor. Therefore a second, independent and faster sensor combination (SHT75 by Sensirion) has been additionally mounted in autumn 2007 for the latest measurements. The main specifications of the temperature and humidity sensors are summarized in table 2.

2.4. Operation of SUMO for atmospheric profiling

In general the SUMO system requires two persons for operation. One is preparing and controlling the autonomous mission on the ground control station (GCS), while the other is operating the standard remote control (RC) transmitter and acting as safety pilot during the flight. Take-off and landing are usually performed in manual mode, even though autonomous start is generally unproblematic and autonomous landing is possible at least in flat terrain and under weak wind conditions.

Table 2. Specifications of the temperature and humidity sensors used on.

sensor	DigiPicco		SHT 75	
parameter	RH	T	RH	T
resolution	0.003 %	0.005 K	0.03 %	0.01 K
range	0-100 %	-40 - 50 ^{o}C	0-100 %	-40 - 124 ^{o}C
abs. Accuracy	< 3 %	±0.5 K	±1.8 %	±0.5 K
rel. Accuracy	N/A	N/A	±0.1 %	±0.1 K
response time	5 s	N/A	6 s	5 s

The following favorable mode of operation has been developed during numerous meteorological ascents. SUMO is started manually and flown to a safe altitude of around 100 m above ground. Then the pilot switches control from the RC transmitter to the GCS for autonomous flight. The aircraft is first sent in a standby mode, i.e. flying circles around a defined home point at a given altitude of 150 m. This enables a check of proper aircraft functionality and allows for the adjustment of the temperature and humidity sensors to the environmental conditions. The next step of the flight plan is an upward profile to a user-defined altitude that can be changed in-flight. For that purpose, the airplane is operated with constant throttle and constant pitch angle, the autopilot uses variations of the roll angle to keep the aircraft on its circular upward spiraling track. After reaching the defined maximum altitude, the engine is switched off and the pitch angle set to a constant negative value. From that point the aircraft is gliding down on a spiral track until reaching the safety altitude of 150 m. From there, the pilot is taking control for manual landing. Fig. 3 shows an example of a typical helical flight pattern for boundary layer profiling, where different colors are used for ascent and descent. Typical ascent and descent rates of the SUMO aircraft are in the order of 7-10 m s^{-1}. The x and y values show the relative distance of SUMO to the launch site with respect to height above ground. The maximum height of this flight was 2567 m at an overall flight duration of 16 minutes. Especially at higher altitudes there are some data gaps in the track due to loss of telemetry connection for a few seconds.

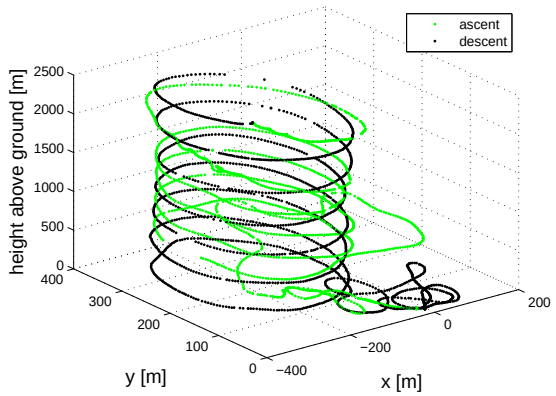

Figure 3. An example of a typical flight pattern during the FLOHOF campaign on Iceland. The ascent starts at 17:56 UTC on 18.08.2007.

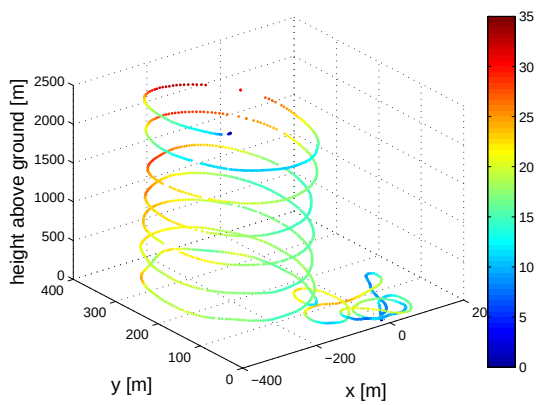

Figure 4. As in fig. 3, but only descent. The colors indicate the ground speed of the aircraft given in m s^{-1}.

Figure 4 shows the instant ground speed from on-board GPS at each position of the track by color code. In one section, the ground speed is decelerated by headwind, indicated by blueish and greenish colors, while it is accelerated by tailwind in the opposite section of the spiral, indicated by yellowish and reddish colors. Assuming constant true air speed, these ground speed differences can be used to determine the horizontal wind speed and direction. Operating the aircraft with constant throttle (zero during descent) and constant pitch angle, this assumption is fulfilled in good approximation. Wind speed can be determined from the difference between minimum and maximum ground speed over a full circle, the corresponding wind direction from the position of minimum and maximum along the track.

3. Measurements

SUMO has been extensively tested during two measurement campaigns. The first one, FLOHOF (FLOw over and around HOFsjokull) took place in July/August 2007 in Central Iceland and was mainly dedicated to the investigation of non-stationary gravity waves (for details see www.flohof.uib.no). During a 3 week campaign on and around Spitsbergen in February/March 2008 the system has been operated for the first time in polar environment to investigate the arctic ABL. Measurement flights have been performed from land near Longyearbyen, from sea ice, and from deck of the ice-breaking Norwegian coast guard vessel KV Svalbard. During both campaigns a total number of more than 70 meteorological profiling ascents have been performed with one airframe. Several ascents of the FLOHOF campaign on Iceland reached altitudes of above 3000 m. Under arctic conditions on and around Spitsbergen, with surface temperatures around -20 ^{o}C and boundary layer wind speeds of 10-15 m s^{-1} maximum altitudes of above 1500 m could be reached. The following section will exemplary present temperature, humidity and wind profiles, measured by the SUMO system.

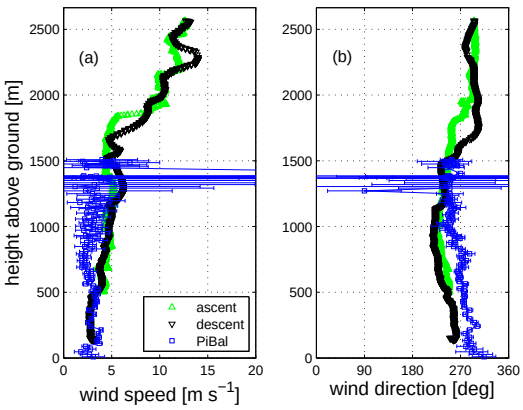

Figure 5. Profiles of wind speed (a) and wind direction (b) measured during the FLOHOF campaign on 18.08.2007. SUMO started at 17:56 UTC, the PiBal ascent at 18:54 UTC.

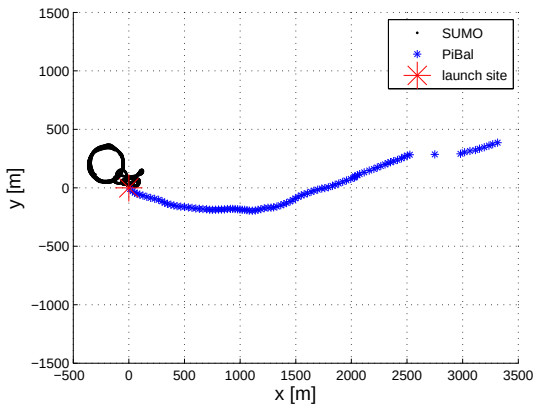

Figure 6. Projection of the SUMO and PiBal tracks to the horizontal x-y plane for the intercomparison presented in figure 5.

3.1. Wind profiles

Figure 5 presents an example of the profiles of wind speed and wind direction derived by the method described above. In accordance with the corresponding temperature and humidity profiles, showing a distinct capping inversion (figure 7), the ascent represents a well developed

boundary layer with rather week and constant wind speed of 3-5 m s^{-1} up to 1600 m above ground. The wind direction near the ground is W, slightly turning to the left with height. At the inversion the wind speed starts to increase to values above 10 m s^{-1}, while the wind direction changes to WNW.
The SUMO wind profile starts at 500 m above ground for the ascent (green) and ends at 150 m above ground in the descent (black). This is due to the fact that SUMO did not fly in autonomous mode below approximately 250 m. In order to obtain wind information via the optimization algorithm the first (last) circle in the auto mode flight pattern has to be completed in the ascent (descent). Therefore, the wind information has to be corrected with respect to height depending on the flight pattern's helical stretching (not shown).

In order to validate the wind estimation method, SUMO ascents have been compared to Pilot Balloon (PiBal) ascents. This method uses small helium filled ballons that are released and optically tracked with two theodolites (e.g. [9]). The corresponding measurement data and their error estimates are plotted in figure 5 in blue. Compared to SUMO, the PiBal method shows very similar wind profiles - both in speed and direction - between 150 up to 1250 m above ground. The large error bars above about 1300 m in the PiBal ascent show the limitation of this system due to a strong increase in uncertainty with increasing distance of the balloon from the observer [10]. Taking into account the delay of about one hour between SUMO and PiBal ascent and the spatial offset due to the drift of the ballon with the wind (see figure 6), the correspondence between the two measurement methods is quite well and promising.

3.2. Temperature and humidity profiles

Figure 7 shows the temperature and humidity profiles taken at the same time as the wind measurements from FLOHOF discussed in the previous section. It can be seen that the vertical structure of the associated parameters is well resolved. The most prominent feature is a marked inversion ranging from appr. 1800 to 2000 m, indicated by an increase in temperature of about 3 K and a corresponding decrease in humidity from above 80 % down to 25 %.

The ascent and descent profiles show systematic deviations at a given altitude that are in the

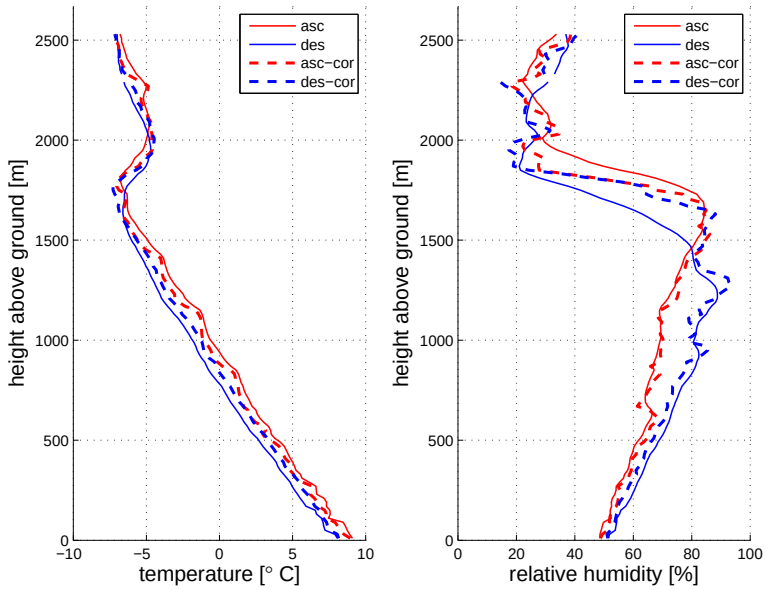

Figure 7. Profiles of temperature and relative humidity, 18.08.2007, start at 17:56 UTC.

order of 1.5 K for temperature and 5-10 % for relative humidity. A closer look reveals that it can be mainly seen as a systematic height displacement, especially evident in humidity around the inversion. This feature has to be attributed to the sensor response time, leading to a general warm bias in the ascent and cold bias in descent. Correspondingly, the humidity has a dry bias during ascent and a wet bias during descent. Due to its deterministic nature, this error can be compensated for to a large extent by the application of a numerical correction scheme. The profiles after application of such a scheme are plotted as dashed lines in figure 7. A main indication of the scheme's effectiveness can be seen by both its ability to bring the profiles closer together and by positioning the inversion heights for relative humidity and temperature to the same level. The remaining deviation in relative humidity has not necessarily to be addressed to sensor problems (e.g. hysteresis). Humidity profiles during the whole FLOHOF campaign, taken by the remotely controlled aircraft KALI and by a tethered balloon, have documented the large spatial and temporal variability of relative humidity in the region.

3.3. Measurements in the Arctic ABL

Figure 8 shows an example of temperature and humidity profiles obtained during the field campaign on and around Spitsbergen in late winter 2008. Here only the results from the descending part of profile are included, because it turned out that the ascent profiles were subject to a distinct warm bias in the lowest levels. This is caused by residual heat due to the large temperature differences between the laboratory for flight preparation (+15 ^{o}C) and the measurement environment itself (-20 ^{o}C). A new feature of the SUMO system during this campaign was the inclusion of an additional, faster sensor for temperature and relative humidity. The results from both sensor sets are presented and compared in figure 8.

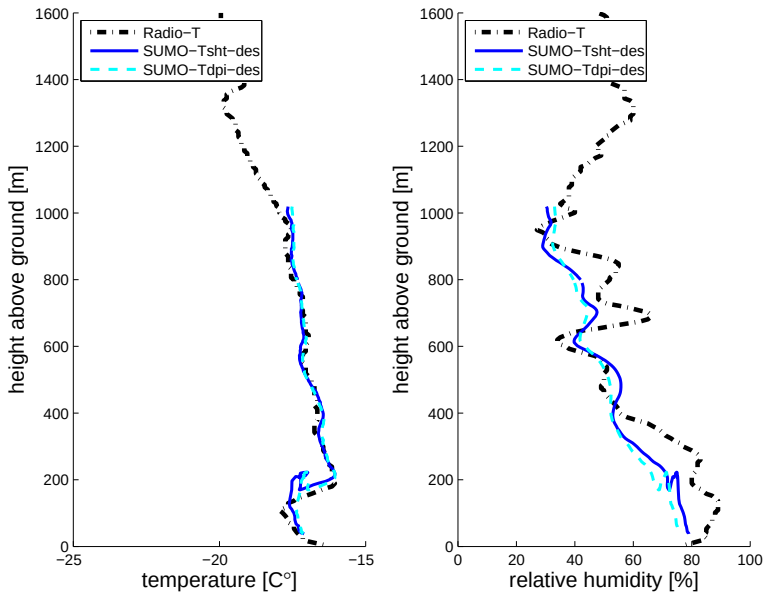

Figure 8. Profiles of temperature and relative humidity taken onboard the Norwegian Coast Guard vessel KV Svalbard at 76.74 ^{o}N and 18.25 ^{o}E in the marginal ice zone on 28.02.2008. (Take-off SUMO: 15:11; launch of radiosonde: 15:15 UTC)

In comparison to most profiles obtained at Iceland, the profiles from the Spitsbergen area, have generally signs of a more complex lower level structure often characterized by multiple

inversions. A central question is how well SUMO is able to resemble the true vertical structure of these fine scale features. The answer was sought through an intercomparison with a radiosonde (Vaisala RS92), which represents a well established and acknowledged measurement platform. SUMO (15:11 UTC) and the radiosonde (15:15) have been launched nearly simultaneously and the ascent rates of both systems are rather similar. It turns out that the temperature profiles of both SUMO sensors and the radiosonde are in excellent agreement of better than 0.5 K from 50 m to the maximum SUMO height of 1000 m during this ascent. The irregularity around 200 m altitude can be explained by a short term ascending motion of the aircraft after switching back from autopilot into manual mode. The relative humidity values have somewhat larger deviations, especially in comparison to the gradients, possibly indicating a generally longer response time for the SUMO instruments than for those of the radiosonde. Furthermore, the measurements from the newest sensor seem to reveal more details than for the old one, indicating a shorter time constant.
Wind profiles of the Spitsbergen campaign are not yet evaluated, but will also be compared to the radiosoundings soon.

4. Summary and outlook

The most important advantage of the SUMO system is its easy-to-hand and cost-efficient performance. During the Spitsbergen campaign, the ground control station was for the first time operated exclusively by scientists rather than aircraft specialists. This proves that the Paparazzi system has now reached a level of user-friendliness that enables operation after rather short training.
The new sensors for temperature and humidity provide the corresponding profiles in an accuracy comparable to that of the latest and well-established radiosonde systems. First validations of the SUMO wind profiles indicate that this information can be obtained at least satisfactory. By keeping strictly to the circling/helical flight pattern, no additional equipment is needed to require information about the horizontal wind. The method uses only modules which are part of the autopilot system anyway. It has to be stressed that the wind estimation method works only for a circling/helical flight pattern which can only be precisely achieved in auto mode. For safety reasons, the auto mode could not be used for heights closer than 150 m above ground during the field campaigns in 2007 and 2008. For the future it is desirable that additional circles in autonomous mode will be flown close to the ground. This will require additional SUMO sensors for continuous monitoring of the distance to the ground. The integration of such sensors will also be one important step toward fully autonomous landing.
The wind estimation method in use has clearly potential for improvements, thus one main focus in the future will be set on corresponding validation and intercomparison with the available parallel radiosonde ascents during the Spitsbergen campaign and by the performance of tailored validation campaigns, e.g. flying SUMO around high meteorological towers. In this context the ongoing Gufuskalar project, equipping a 412 m high mast in Northwest-Iceland with meteorological instrumentation, will be of large importance.

Acknowledgments

The authors are grateful to Christian Lindenberg for his work on the assembly and maintenance of the airplanes and for his assistance as safety pilot during the flights on Iceland and to Michael Kislat acting as safety pilot during the campaign on and around Spitsbergen.
The main financial support for development of SUMO was provided by the Meltzer University Foundation, Bergen, Norway. The comprehensive test of the system on Iceland in August 2007 would not have been possible without the FLOHOF field campaign funded by the German Research Foundation under contract EG 40/25-1. The arctic flights on and around Spitsbergen have been funded by the Norwegian IPY-THORPEX campaign and a personal stipend of

Marius Jonassen (2008-356) provided by the Norwegian Polar Institute. Many thanks to the crew of the Norwegian Coast Guard vessel KV Svalbard for assistance during the research cruise.

References

[1] Konrad T G, Hill M L, Rowland J R and Meyer J H 1970 A small, radio-controlled aircraft as a platform for meteorological sensors *Appl. Phys. Lab. Tech. Digest* 11
[2] Egger J and et al 2002 Diurnal winds in the Himalayan Kali Gandaki valley. Part III: Remotely piloted aircraft soundings *Mon. Wea. Rev.* **130** 2042
[3] Egger J and et al 2005 Diurnal circulation of the Bolivian Altiplano. Part I: Observations *Mon. Wea. Rev.* **133** 911
[4] Holland G J, Webster P J, Curry J A, Tyrell G, Gauntlett D, Brett G, Becker J, Hoag R and Vaglienti W 2001 The Aerosonde robotic aircraft: A new paradigm for environmental observations *BAMS* **82** 889
[5] Ma S, Chen H, Wang G, Pan Y and Li Q 2004 A miniature robotic plane meteorological sounding system *Adv. Atmos. Sci.* **21** 890
[6] Spiess T, Bange J, Buschmann M and Voersmann P 2007 First application of the meteorological Mini-UAV 'M2AV' *Meteorol. Z.* **16** 159
[7] ENAC 2008 Paparazzi user's manual http://paparazzi.enac.fr/wiki_images/Users_manual.pdf
[8] Brisset P 2006 The Paparazzi solution http://www.recherche.enac.fr/paparazzi/papers_2006/mav06_paparazzi.pdf
[9] Thyer N 1961 Double theodolite pibal evaluating by computer *J. Appl. Met.* **1** 66–68
[10] Schaefer J T and III C A D 1978 The inherent position errors in double-theodolite pibal measurements *J. Appl. Met.* **17** 911–915